A Novel Plasma Source for Surface Chemical Patterning and Spatial Control of Cell Adhesion

by

Kristina Louise Parry, B.Eng (Hons)

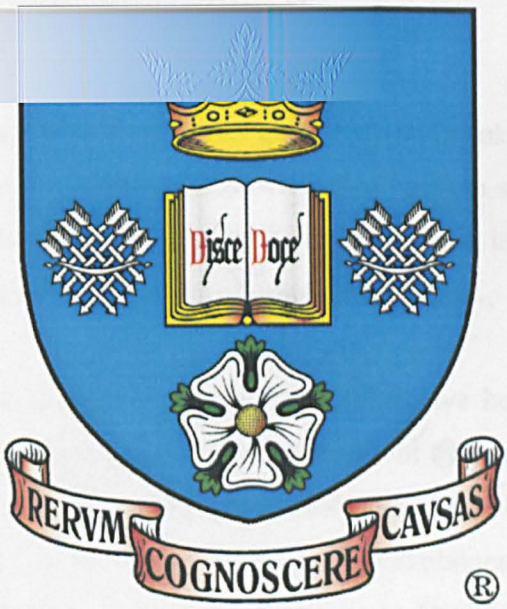

A thesis submitted for the degree of Doctor of Philosophy

Department of Engineering Materials

University of Sheffield

January 2004

Acknowledgements

For their guidance, advice and patience I thank my supervisory team at the University of Sheffield: Professor Robert Short, Dr. Andy Scutt, and Professor Ian Brook. Together we thank our collaborators at the UMIST Plasma Physics Group, Dr. James Bradley and Marshal Dhayal. All of the probe measurements and the vast majority of plasma treatments were performed by Marshal. For funding of the project we thank the EPSRC and the Royal Academy of Engineering for an International Travel Grant award.

I thank Professor Graham Leggett for use of the AFM in the University of Sheffield Department of Chemistry. Thanks to Matthew Montague and Rob Manning for operation of the instrument.

For sharing of technical expertise, thanks go to Patrick Brookes and Nannette Scutt. Pat has helped in many ways with his knowledge of vacuum systems and his general enthusiasm for science. Nannette patiently instructed me in the mysteries of cell culture and has been an endless source of emotional support.

Many members of the Surface Analysis Lab Group have helped me in some way throughout the course of this project. Past and present these are: Alison Beck, Nial Bullett, Stuart Fraser, Jonathan Kelly, Sally McArthur, Anita Mistry, Tracy O'Leary, Alex Shard, Dave Steele, Rosnita Al-Talib, Maria Guadalupe Neira Velázquez (aka Lupita) and Florent Voisin. Special mentions go to David 'Dick' Barton for help with all things concerning plasma physics, and Jason Whittle for knowing at least something about everything to do with science.

Finally, I thank my partner Dan and our furry friend PussyCat for patience, encouragement and hugs as required.

Publications and Presentations

Dhayal, M., Forder, D., Parry, K.L., Short, R.D., Bradley, J.W. (2003). Using an afterglow plasma to modify frequency (RF) polystyrene surfaces in pulsed radio argon discharges. *Surf. Coat. Tech.* **174**, 872-876, presented at the 8th Annual Conference on Plasma Surface Engineering, Garmisch-Partenkirchen, Germany, 2003.

Dhayal, M., Forder, D., Parry, K.L., Short, R.D., Barton, D., Bradley, J.W. (2003). Tailored plasmas for applications in the surface treatment of materials. *Surf. Coat. Tech.* **162**, 294-300.

Parry, K.L., Brook, I.M., Scutt, A.M., Short, R.D. *Plasma Patterning of Polymer Substrates for Cell Shape Engineering*, poster presented at the 17th Annual Conference on Biomaterials, Barcelona, Spain, 2002.

Summary

The aim of this work was to develop and characterise a plasma source, which could be used to modify polymeric surfaces and incorporate well-defined regions of controlled chemistry.

A novel plasma treatment system in which the ion energy and flux at the substrate can be independently controlled was developed. Argon plasma was separated into two regions with stainless steel meshes. The ion energy and flux in the substrate processing region was manipulated by applying an electrical bias to these meshes. This 'tailored' plasma was used to investigate the relative contributions of ions and vacuum ultra-violet (VUV) photons in the plasma treatment of polystyrene (PS). The level of surface modification induced by the plasma treatment was ascertained by X-ray photoelectron spectroscopy (XPS). Isolation of the VUV component by use of the biased mesh system revealed that in this system, these photons were the primary species causing oxygen incorporation into the PS surface.

The modified PS was successfully employed as a culture substrate for bone marrow stromal cells (BMSC). By use of transmission electron microscopy (TEM) grids placed on the PS surface during exposure to the source, micron scale surface chemical patterns were produced. The pattern of hydrophilic and hydrophobic regions was visualised by condensing water onto the surface. On these substrates, bone marrow stromal cells (BMSC) formed patterns with features as small as 5 μm.

The ability to independently control the ion energy and flux at the substrate has enabled the identification of the primary plasma species involved in surface modification of PS in this system. Combined with simple patterning technology, the novel plasma source has been used to produce well-defined micron scale chemical patterns on PS. The biological utility of such patterned substrates has been demonstrated by spatial control over cell attachment and spreading.

Contents

CHAPTER ONE – INTRODUCTION

CHAPTER TWO – PLASMA

CHAPTER FOUR – EXPERIMENTAL METHODS

CHAPTER FIVE – RESULTS I: SURFACE MODIFICATION OF POLYSTYRENE IN A NOVEL PLASMA SOURCE

CHAPTER SIX – RESULTS II: CELL CULTURE SUBSTRATES

CHAPTER SEVEN – CONCLUSIONS AND FURTHER WORK

APPENDICES

Chapter One
Introduction

1.1 Background to this Study

The use of synthetic materials in medical applications such as orthopaedics and vascular surgery is well established and widespread. Many of these materials require some form of surface modification in order to make them perform satisfactorily in the body. In recent years the paradigm shift from the *replacement* of tissues with synthetic materials, to the *regeneration* of tissue by controlled cell growth has further driven the need to engineer tissue culture substrates for use both *in vitro* and *in vivo*. Due to their potential applications in tissue engineering, chemically patterned surfaces are currently the subject of much research (Ohl *et al.*, 1999). Additionally, there is increasing demand for parallel high-throughput screening devices that require spatial control over surface chemistry *e.g.* DNA chips, cellular arrays and microfluidics technologies. As such, chemically patterned polymeric substrates are likely to become a vital component of the post-genomic biologist's "toolkit".

The use of plasma techniques to modify the surfaces of polymers offers many possibilities in the fields of biomaterials and tissue engineering (Ratner *et al.*, 1990). Plasma processing allows the surface properties of the substrate to be modified at low temperature, without altering the bulk properties of the material. This is particularly important in biomaterials and tissue engineering applications, because polymers are often the material of choice in terms of their bulk properties and cost but their surface interactions at biological interfaces are not suitable.

1.2 Aims of this Work

In this work we sought to develop a novel, highly manipulable plasma source in order to generate polymeric substrates with surface chemical patterns of controlled chemistry. To gain further insight into the mechanisms of surface-plasma interactions, a greater degree of control over the plasma processing than achieved in previous studies was desired. The resultant chemically patterned surfaces were used to spatially control the attachment and spreading of bone marrow stromal cells (BMSC). Thus the following aims were set:

- to develop an argon plasma treatment system in which independent control over the ion energy and flux could be achieved
- to use this 'tailored' plasma to investigate the role of ions in the surface modification of polystyrene
- to use plasma processing of PS to create a surface suitable for culture of BMSC
- to create surface chemical patterns on PS using a plasma-based patterning technique
- to employ the surface chemical patterns in a pilot study of the effects of geometric constraint on the attachment, growth and differentiation of BMSC

1.3 Outline of Thesis

This thesis describes the development and characterisation of a novel argon plasma source and it's application in the surface modification of polystyrene. The roles of ions, metastable species and photons in this system are investigated by isolation of their effect on the level of surface modification, as measured by X-ray Photoelectron Spectroscopy (XPS). The use of the novel plasma source to generate chemically patterned surfaces for cell culture is explored, with reference to the effect of geometric constraint on cell behaviour.

A background to plasma and a literature review of plasma modification techniques, with specific reference to argon plasma treatment of polymers, is

provided in Chapter Two. Chapter Three is a brief exploration of the interactions between cells and biomaterials, including a literature review of the effects of surface chemistry on protein adsorption and subsequent cell adhesion pertinent to cellular patterning. The experimental methods employed in this study are outlined in Chapter Four. Chapter Five presents the results and discussion of experiments in the novel plasma reactor designed to exert independent control over the ion energy and ion flux to the substrate, and the effect of these variables on the surface modification of polystyrene. The results and discussion of cell culture experiments conducted on polystyrene modified in the novel plasma reactor follow in Chapter Six. Conclusions and further work are found in Chapter Seven. Finally, descriptions of various techniques used in this study are presented in three appendices (X-ray Photoelectron Spectroscopy, Friction Force Microscopy and Statistical Methods).

Chapter Two

Plasma

2.1 Background to Plasma

Plasma can be defined as 'a quasi-neutral gas of charged and neutral particles characterised by collective behaviour' (Grill, 1993). In terms of particle energy, plasma is the fourth state of matter *i.e.* it is formed when atoms or molecules are supplied with energy sufficient to cause partial ionisation of the gas. Typical values of particle energy, or temperature, and the states of matter in which they are generally found are illustrated schematically in Figure 2.1. The initial ionisation event may be caused by cosmic ray or background radiation ionisation. An applied electromagnetic field is then required to sustain the plasma. Commonly, this field is generated by a direct current, microwave or, as in this work, a radio frequency power source.

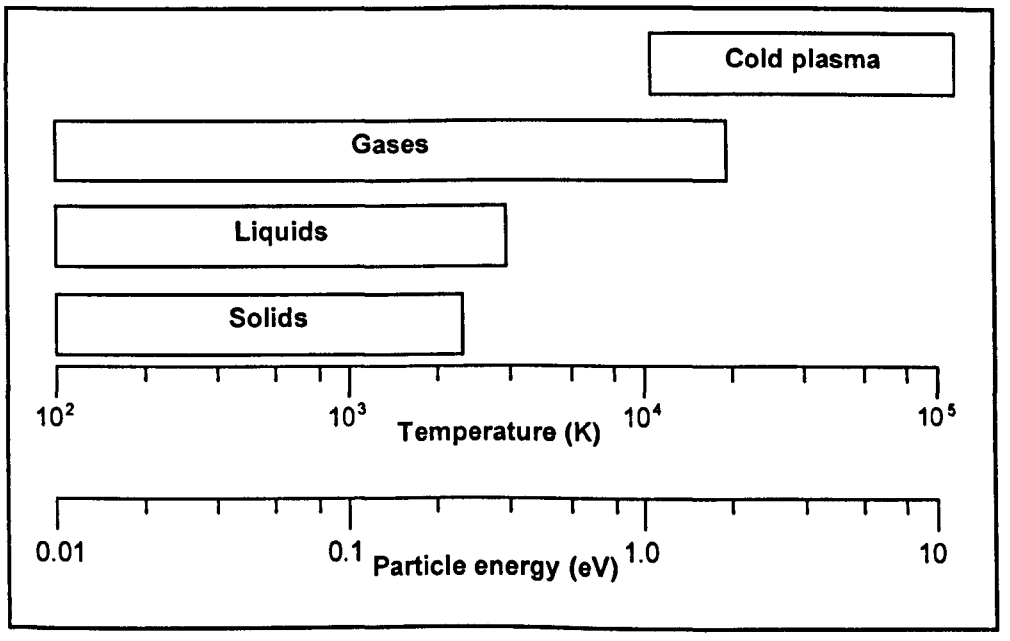

Figure 2.1: Particle temperature ranges for the four states of matter (after Grill, 1993)

The argon plasmas used in this study essentially consist of positive ions (Ar^+) and negative electrons (e^-) in a background of neutral argon atoms (Ar), metastable species (Ar*) and photons. However these species are not in thermodynamic equilibrium. In Figure 2.1, the temperature range for the plasma state refers to the electrons and is generally two orders of magnitude higher than the gas temperature. However, the heavy particles are much more numerous than the electrons, so the overall plasma temperature is approximately room temperature. Such non-equilibrium plasma is referred to as 'cold'. Examples of equilibrium, or 'hot' plasma, where the electron temperature and the molecule temperature are roughly equal, include stars and lightning.

2.1.1 Physics of Plasma

Plasma is characterised by the following basic intrinsic parameters:

- the density of neutral particles,
- the density of ions and electrons,
- the energy distributions of ions, electrons and neutrals

These *intrinsic* parameters are controlled by *extrinsic* parameters such as input power, gas pressure and flow rate.

The term *plasma density* is used to represent the densities of ions and electrons, as they are usually equal in the quasi-neutral state of plasma. The plasma density has implications for the efficiency and reaction rates of plasma processing operations. Derived from these basic parameters are additional physical characteristics, which describe the nature of plasma.

2.1.1.1 Degree of Ionisation

The degree of ionisation of the gas, α, specifies the fraction of the particles that are ionised. It is given by:

$$\alpha = \frac{n_i}{n} \qquad 2.1$$

where n_i is the number of ions per unit volume and n is the number of particles per unit volume. In a 'cold' low-pressure plasma, the degree of ionisation is generally between 10^{-6} and 10^{-3} (Grill, 1993).

2.1.1.2 Electron Temperature

In plasma, the electrons absorb more energy from the applied electric field than the ions. The electrons transfer this energy less efficiently than do ions and neutrals, which lose energy in collisions with other particles and with the chamber walls. The net result is an electron population with an average energy much higher than that of the ions and neutrals. The average *electron temperature*, T_e, is derived from the electron energy distribution function (EEDF). The EEDF can be described to a first approximation by a Maxwell-Boltzmann distribution and thus related to the temperature of the electrons. In low-pressure plasma, a Druyvesteyn distribution is a more suitable approximation as it allows more realistic assumptions than the Maxwell-Boltzmann function, such as:

- the electric field strength is low enough for inelastic collisions to be ignored, but high enough for $T_e >> T_i$,
- the electric field frequency is much lower than the frequency of collisions,
- the collision frequency is independent of the electron energy.

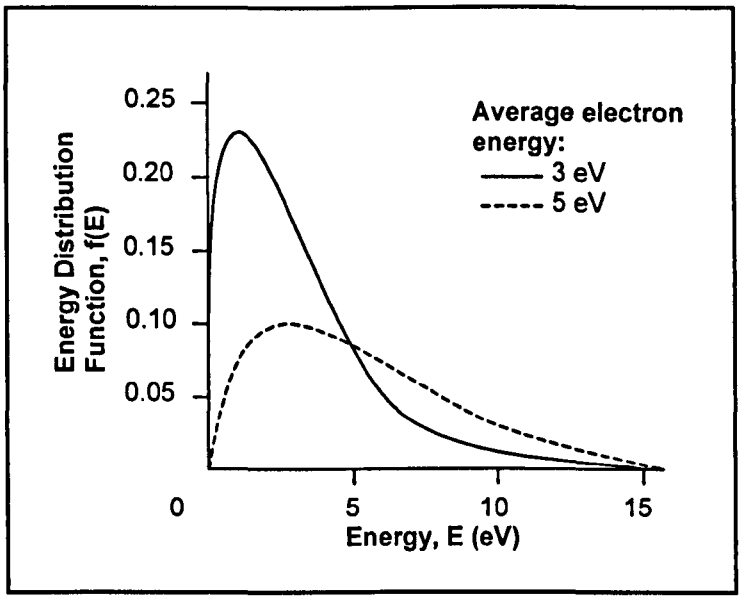

Figure 2.2: Druyvesteyn EEDF (after Grill, 1993)

The Druyvesteyn distribution is characterised by a high-energy tail (Figure 2.2), indicative of a small population of electrons with energy sufficient to have a significant effect on the processing properties of the plasma.

2.1.1.3 Floating, Self-bias and Plasma Potentials

In the applied electric field, the electrons in the plasma have the highest mobility of all the species present, due to their small size. Thus, a surface in contact with the plasma immediately builds a negative charge when the plasma is ignited. The negative charge builds until the repulsion of electrons reduces the electron flux to the surface enough to balance it with the ion flux. The substrate therefore develops a negative "self-bias" potential, V_{sb}, with respect to the plasma. In the case of an insulating or electrically isolated substrate, this potential is called the *floating potential*, V_f (Figure 2.3). Except in regions of perturbation, such as around a substrate, the plasma is equipotential at the *plasma potential*, V_p. Since there is no reference, only the potential difference $V_p - V_f$ is meaningful. Ions are accelerated across this potential energy barrier and can strike the surface, whereas only electrons from the high-energy tail of the EEDF are able to reach the substrate.

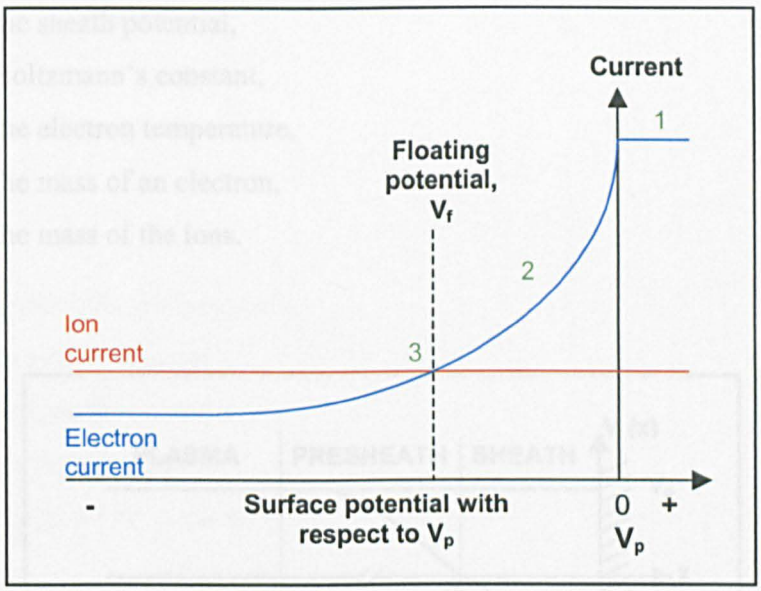

Figure 2.3: Schematic illustrating floating potential. Shortly after ignition of the plasma, the plasma potential, V_p, is established (1). The potential at the surface then decreases as negative charge from highly mobile electrons in the plasma builds. As the surface becomes more negatively charged, it repels electrons, decreasing the electron current (2) to the point at which the electron current and ion current to the surface are equal (V_f) (3).

2.1.1.4 Sheath Formation and Debye Length

In the region around an insulating or electrically isolated substrate, local concentrations of negative charge cause a deviation from the plasma potential. In order to maintain quasi-neutrality, the plasma shields itself from this electric field.

Since the action of $V_p - V_f$ is to repel electrons, a region of positive space charge develops around the isolated substrate. This relatively dark region is called the *plasma sheath* and the potential across it, V_s, is equivalent to the maximum ion energy (Figure 2.4). For a planar surface, the energy of the ions is related to the electron temperature, T_e (which is representative of electron energy) by Equation 2.2 below.

$$V_s = \frac{kT_e}{2e} \ln\left(\frac{m_e}{2.3m_i}\right) \qquad 2.2$$

where

V_s = the sheath potential,

k = Boltzmann's constant,

T_e = the electron temperature,

m_e = the mass of an electron,

m_i = the mass of the ions.

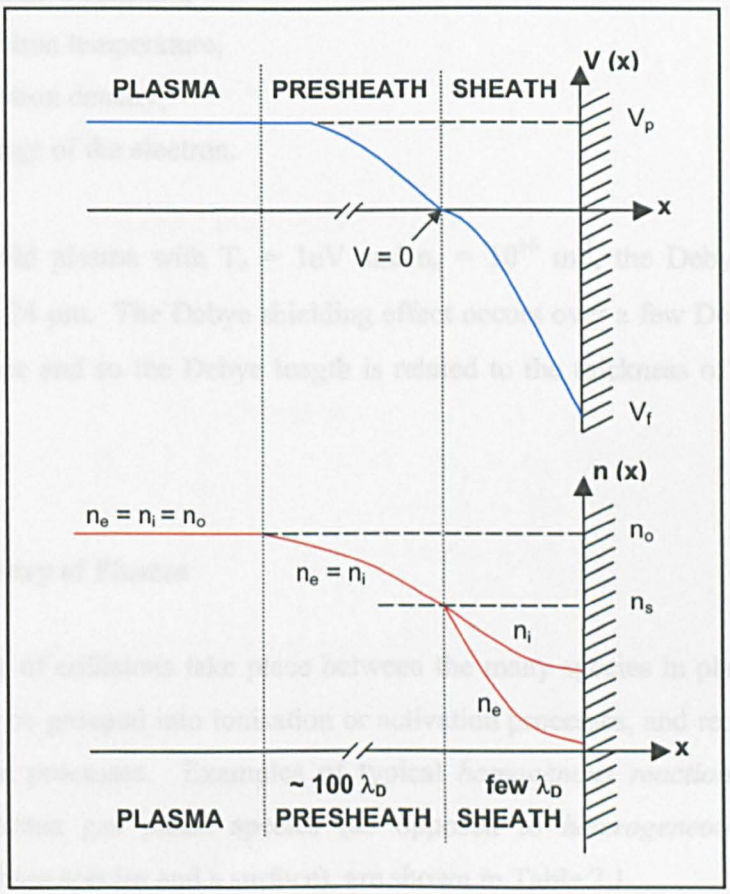

Figure 2.4: Schematic of potential and particle density across plasma presheath and sheath regions in DC plasma (after Roth, 1995). n_e = number density of electrons; n_i = number density of ions; n_o = plasma density; n_s = number density of ions and electrons at sheath boundary.

The response of charged particles to reduce the effect of local electric fields in this manner is called *Debye shielding*. The distance over which these local electric fields operate is limited by the *Debye length*, λ_D, which is defined by:

$$\lambda_D = \left(\frac{\varepsilon_0 k T_e}{n_e e^2} \right)^{1/2} \qquad 2.3$$

where

ε_0 = the permittivity of free space,

k = Boltzmann's constant,

T_e = the electron temperature,

n_e = the electron density,

e = the charge of the electron.

In a typical cold plasma with T_e = 1eV and n_e = 10^{16} m^{-3}, the Debye length is approximately 74 μm. The Debye shielding effect occurs over a few Debye lengths from the surface and so the Debye length is related to the thickness of the plasma sheath.

2.1.2 Chemistry of Plasma

A wide variety of collisions take place between the many species in plasma. They may generally be grouped into ionisation or activation processes, and recombination or deactivation processes. Examples of typical *homogenous reactions i.e.* those occurring between gas phase species (as opposed to *heterogeneous reactions* between gas phase species and a surface), are shown in Table 2.1.

Table 2.1: Examples of typical homogeneous reactions within plasma

Ionisation/Activation	
Ionisation	$e^- + A \rightarrow A^+ + 2e^-$
	$e^- + A_2 \rightarrow A_2^+ + 2e^-$
	$e^- + A_2 \rightarrow A_2^-$
	$e^- + AB \rightarrow A^+ + B + 2e^-$
	$A + B \rightarrow A^+ + B + e^-$
Dissociative attachment	$e^- + A_2 \rightarrow A^- + A$
	$e^- + AB \rightarrow A + B^-$
Dissociative ionisation	$e^- + A_2 \rightarrow A^+ + A + 2e^-$
	$e^- + A_2 \rightarrow A^+ + A^- + e^-$
	$e^- + AB \rightarrow A^+ + B^- + e^-$
Excitation	$e^- + A \rightarrow A^* + e^-$
	$e^- + A_2 \rightarrow A_2^* + e^-$
	$e^- + AB \rightarrow AB^* + e^-$
	$A^+ + B \rightarrow A^+ + B^*$
Penning ionisation	$A^* + B \rightarrow A + B^+ + e^-$
Recombination/deactivation	
Radiative recombination	$e^- + A^+ \rightarrow A + h\nu$
	$e^- + A^* \rightarrow A + h\nu + e^-$
	$A^+ + B^- \rightarrow AB + h\nu$
Dissociative recombination	$e^- + A_2 \rightarrow 2A$

In the case of *charge transfer*, where charge is transferred between an ion and a neutral atom or molecule, the net result is not immediately obvious from the equations:

$$A + A^+ \rightarrow A^+ + A$$
$$A^+ + B \rightarrow A + B^+$$
$$A^+ + B_2 \rightarrow A + B_2^+$$

In fact the process, produces a fast neutral and a slower ion.

The principal sources for the production of atoms, free radicals and negative ions in cold plasma are the processes of dissociative attachment, dissociative ionisation and dissociation (an inelastic collision between an electron and a molecule that causes dissociation without the formation of ions). Penning ionisation is particularly important in plasmas of gases, such as argon, which contain many long-lived metastable species with high cross sections for reaction.

The resultant species of homogeneous reactions may either go on to perpetuate the plasma or if they can cross the sheath, interact in a heterogeneous manner with surfaces in contact with the plasma. The role of specific species in inert gas plasma treatment of polymers is discussed in Section 2.2.3.

2.1.3 Engineering and Material Science Applications

The only widespread use of plasma during 19th century was in electrical arcs for illumination, an application for which plasma remains in use in fluorescent strip lighting. In the 1920's Irving Langmuir introduced the term *plasma*, and research in the field moved gradually forwards. With the advent of microelectronics in the 1970's however, research into plasma and its applications became very popular and moved rapidly to provide methods of deposition and dry etching for the production of components such as integrated circuits.

Cold plasma processing may be applied to most materials including metals, semiconductors and polymers in three ways:

- Etching – the removal of material from the surface
- Plasma polymerisation – deposition of thin films from organic or inorganic monomers onto a surface, which may be of complex geometry

- Surface treatment – modification of material surface properties such as wettability and biocompatibility, without alteration of bulk material properties

In some circumstances a combination of these processes is used. For example, plasma etching may clean a metal surface in order to enhance the adhesion of a plasma polymerised protective thin film (Lin *et al.*, 1997).

In addition to its role as an alternative to many traditional material processing routes, cold plasma processing can perform tasks that can be achieved with no other method. This is due to the multitude of active species generated inside the plasma, which can interact to produce unique surface chemistry. The technique is generally much more environmentally friendly than wet chemical methods and so has gained popular status in industry.

Further to its employment in the microelectronics industry, plasma etching is also used in the automotive and domestic appliance industries as a pre-treatment for metals to improve the adhesion of paint (Chapman, 1980). Plasma polymerised films have found applications as protective coatings for other materials, such as delicate archaeological metallic objects (Favre-Quattropani *et al.*, 2000). They may be used as an interface between two materials that do not readily bond with each other, *e.g.* Teflon® and steel (Inagaki & Yasuda, 1981). Thin films are also used as barrier materials on food and pharmaceuticals packaging, (*e.g.* Ozdemir *et al.*, 1999). The hardness of metals for mechanical tools may be improved with nitrogen plasma surface treatment ("nitriding") (Grill & Itzhak, 1983). Plasma surface treatments are applied particularly to textiles and polymers to improve the adhesion of paint, dye and printing ink. Due to the low reaction temperature involved, plasma surface treatment is widely used to improve the surface properties of polymeric materials. This is discussed in detail in Section 2.2.

In biological applications, a material must not only successfully perform the intended function; it must also do so without inducing any adverse reaction in the biological environment. The use of cold plasma processing to improve the biocompatibility of materials is widespread and actively researched (see reviews by

Chu *et al.*, 2002 and Ratner *et al.*, 1990). Table 2.2 lists some research areas and applications.

Table 2.2: Common research areas and applications of plasma treatment in biomaterials engineering (from Chu *et al.*, 2002)

Blood-compatible surfaces	Vascular grafts, catheters, stents, heart valves, membranes (*e.g.* for haemodialysis), filters (*e.g.* for blood cell separation), biomolecules immobilised on surfaces
Non-fouling surfaces	Intraocular lenses (IOLs), contact lenses, wound healing, catheters, biosensors
Tissue engineering and cell culture	Cell growth, antibody production, assays, vascular grafts
Sterilisation of surgical tools and devices	Surgical cutting tools, tweezers
Biosensors	Biomolecules immobilised on surfaces
Barrier coatings	Drug release, gas exchange membranes, device protection, corrosion protection, reduction of leachables (*e.g.* additives, catalysts, plasticisers, etc.)

The use of surface plasma treatment in the manufacture of cell culture surfaces is explored in Section 3.2.

2.2 Plasma Surface Treatment of Polymers

One of the most attractive aspects of plasma treatment is the ability to alter the surface chemical properties of all polymers at low processing temperature. The resultant surface chemistry is not only dependent on the initial polymer substrate, but also on the treatment gas (which may be reactive, inert or a mixture), and the conditions used (*e.g.* gas pressure, exposure time, input power). In fact, the exact reactor system has a great effect on the outcome of a plasma treatment. Even under nominally identical extrinsic parameters, the intrinsic characteristics of a given plasma are likely to be different in different reactor systems. Caution must therefore be exercised when comparing data obtained by different research groups.

2.2.1 Historical Development

Surface modification of polymers by plasma treatment has become an important industrial technique due to its many advantages over traditional processing routes. In the low temperature plasma environment used during modification, chemical reactions are possible that would usually require high temperatures, or would not occur at all. The process is environmentally friendly and applicable to substrates of complex geometry and is therefore relevant to many manufacturing processes used today.

In 1967, Schonhorn and Hansen stimulated interest in the application of plasma surface treatment specifically to polymeric materials by reporting that the cohesive strength of the bond between epoxy resin and polyethylene (PE) increased when the polymer surface was plasma treated. Westerdahl *et al.* (1974) subsequently extended this result to a range of polymers including polystyrene (PS), cellulosics, fluorinated ethylene propylene copolymer and polycarbonate (PC). The improvement in adhesiveness was attributed to surface crosslinking of the polymer during plasma treatment. The first studies to investigate the coupling mechanism between the plasma and the polymer during crosslinking were by Hudis (Hudis, 1972; Hudis & Prescott, 1972). In these experiments, no physical contact between PE and hydrogen plasma was necessary to produce crosslinking, thus highlighting the significance of

ultraviolet (UV) radiation in the reactor system used. Moreover, in terms of gelation measurements, the crosslinking effect could not be reproduced using a low-pressure mercury-argon UV lamp as the plasma process was far more efficient and surface specific. However, the exact surface chemistry created by the two processes was not examined and compared.

The use of X-ray Photoelectron Spectroscopy (XPS) to examine the surface chemistry of plasma treated polymers is now well established. In the 1970's, a series of papers produced by Clark and Dilks (1977, 1978, 1980) reported the effects of plasma treatment on a range of polymers. The analysis was performed *in situ*, *i.e.* without exposure of the modified polymer surfaces to the atmosphere. These studies, combined with those of Gerenser (1987, 1993) and Yasuda (1977), have been instrumental in elucidation of the processes involved in the plasma surface treatment of polymers, including the roles of the various plasma species.

2.2.2 Reactive Gas Plasma Treatment

Many reactive gases are used to modify polymer surface chemistry, including water (Dai *et al.*, 1997) ammonia (Nakayama *et al.*, 1988), fluorocarbon (Schwarzenbach *et al.*, 2001) and air (Amstein & Hartman, 1975). However, the most commonly employed are oxygen and nitrogen.

2.2.2.1 Oxygen Plasma

Controlled surface oxidisation of polymers is particularly important in improving adhesion, wettability (Westerdahl *et al.*, 1974) and biocompatibility (Chu *et al.*, 2002; Ratner *et al.*, 1990). Conventional chemistry provides many methods of achieving this, but plasma treatment is a one-step, low temperature process requiring no hazardous chemicals. The most common gas used is oxygen, although other oxygen-containing gases *e.g.* water vapour (Youxian *et al.*, 1991) and carbon dioxide (Le *et al.*, 1997) are sometimes used, especially when the incorporation of other elements into the polymer surface is either desired or unimportant. Argon (see Section 2.2.3) and ammonia (Nakayama *et al.*, 1988) plasma treatments also induce

surface oxidation when free radicals generated during treatment are allowed to react with residual oxygen in the reaction vessel or atmospheric oxygen post-plasma.

Oxygen plasma treatment has two principal effects: etching/ablation of surface material by removal of volatile reaction products and the incorporation of oxygen-containing functional groups by reaction of active plasma species with the polymer surface. As demonstrated by Morra *et al.* (1990) with oxygen plasma treatment of poly(tetrafluoroethylene) (PTFE), the two processes occur simultaneously; the balance between them is controlled by plasma parameters such as exposure time and input power. At short treatment times, Morra *et al.* found that surface modification by incorporation of oxygen was the dominant process. After longer treatments however, the chemistry of the surface reverted back to that of unmodified PTFE, suggesting that the etching process had become dominant and removed the modified layers.

The introduction of oxygen to polymer surfaces by oxygen plasma treatment is well documented. Important studies include those of Gerenser (1987, 1993) who used *in situ* XPS to analyse the surface chemistry of polymers treated with oxygen plasma. Survey scans showed a saturation level of approximately 20 at. % oxygen in both PS and PE surfaces after 30 seconds of treatment. Line shape analysis of the C_{1s} envelope revealed three distinct carbon-oxygen functionalities: C – O, C = O and O – C = O. In some cases, these functionalities are used to initiate graft reactions by subsequent conventional chemistry (Kühn *et al.*, 1999; Suzuki *et al.*, 1986). The mechanism by which functional groups are introduced into the polymer surface is a subject of much debate in the literature. It is generally accepted that hydrogen abstraction through the reaction of atomic oxygen occurs (Moss *et al.*, 1986). Subsequent reaction of main chain radicals with molecular oxygen in the plasma produces hydroperoxides, which then decompose into the functional groups. However, the precise mechanisms involved are yet to be confirmed; many authors have reached different conclusions about the roles of molecular ions, atomic ions, radicals and ultraviolet radiation.

The chemical stability of oxygen plasma treated polymers is an important factor to consider in applications where storage may be required (*e.g.* tissue culture dishes). Occhiello *et al.* (1991) explored the tendency for polymer surfaces to rearrange their

structure following oxygen plasma treatment. The study examined the interaction of oxygen plasma treated polypropylene (PP) with air and water after storage. In water, the polar groups remained at the polymer surface. In air however, the modified PP minimised its interfacial energy by macromolecular rearrangement to bury the oxygen-containing groups away from the surface.

2.2.2.2 Nitrogen-containing Plasma

Nitrogen plasma treatment incorporates nitrogen-containing functionalities into polymer surfaces (Foerch *et al.*, 1990; Gerenser, 1987, 1993; Yasuda *et al.*, 1977), although oxygen is also incorporated on exposure to atmosphere when radicals produced during plasma treatment are quenched. Therefore, in the absence of *in situ* XPS, the precise nature of the nitrogen-containing functional groups is difficult to determine as certain carbon-nitrogen functionalities produce very similar chemical shifts to some oxygen-carbon functional groups (Gengenbach *et al.*, 1994; Yasuda *et al.*, 1977). However, *in situ* XPS analysis of nitrogen plasma treated PE, PS and poly(ethylene terephthalate) (PET) revealed amine (C – N) and imine (C = N) groups (Gerenser, 1987, 1993). In addition to these functionalities, the presence of amide (N – C = O) groups in nitrogen plasma treated PE has been reported (Okell *et al.*, 1995).

As with oxygen plasma treatment, the actual mechanisms involved in the formation of these groups, and the specific roles of the plasma species are unclear. XPS and static secondary ion mass spectrometry (SSIMS) studies of NH_3 and N_2 plasma treated PS and PC by Lub *et al.* (1989) indicated that the responsible species might be NH_3^+ or NH_4^+. Moreover, Pringle *et al.* (1996) also proposed NH_3^+ as the dominant ion responsible for modification in ammonia plasma.

2.2.3 Inert Gas Plasma Treatment

The inert gases used in plasma treatment are helium, neon and argon. For reasons of low cost, the most commonly used of these is argon. Inert gases generally produce crosslinking of a polymer surface, and the incorporation of new chemical species into the "activated" surface on exposure to atmosphere. Indeed, argon plasma treatment does not cause oxygen incorporation into a polymer unless exposure to

residual oxygen *during*, or atmospheric oxygen *following* treatment is allowed (Clark & Dilks, 1977; Gerenser, 1987, 1993), suggesting that a radical method is probable. The method by which the radicals are generated is, however, of much debate in the literature.

2.2.3.1 Role of Ions and Metastables

Schonhorn and Hansen (Schonhorn & Hansen, 1967) attributed the increase in adhesive strength of helium plasma treated PE to the formation of a cross-linked surface layer with high cohesive strength. They proposed that the ionic and metastable components of the helium plasma caused loss of hydrogen from the polymer. The observation of radicals in the resulting surface led to the conclusion that the crosslinked layer is formed by subsequent radical reactions. The term CASING (Crosslinking by Activated Species of INert Gases) was applied to this process.

The *in situ* XPS experiments of Clark and Dilks (1977) produced a two-component direct and radiative energy transfer model to explain the differences in surface and bulk modification. They examined the chemical modification of an ethylene-tetrafluoroethylene copolymer that had been exposed to an RF argon plasma at various gas pressures, input powers and treatment times. For all the plasma treated samples, de-fluorination was observed by XPS: a decrease in the fluorine 1s core level (F_{1s}) and the $\underline{C}F_2$ component of the carbon 1s core level (C_{1s}) was accompanied by an increase in the total intensity of the C_{1s}, including an increase in the $\underline{C}F$ component. The ratio of the F_{1s} and F_{2s} peaks was used to ascertain chemical differences between the surface and the subsurface and bulk material. Compared to the untreated copolymer, plasma treated samples showed a decrease in the F_{1s} : F_{2s} peak intensity ratio arising from the lower fluorine content of the surface and subsequent larger mean free path for photoelectrons escaping from the F_{2s} level. Small amounts of oxygen (up to ~10% intensity of the C_{1s} peak) were also observed and attributed to residual oxygen containing species in the reactor system. Through use of a quartz window, it was determined that the ethylene-tetrafluoroethylene copolymer was not chemically modified by photons of wavelength greater than 160 nm.

Clark and Dilks proposed that the outermost monolayer of the polymer surface crosslinks rapidly due to direct energy transfer from argon ions and metastables. The bulk material crosslinks more slowly as a result of indirect radiative energy transfer from vacuum ultraviolet (VUV) radiation in the plasma (see Section 2.2.3.2). Key to this proposal was depth-profiling data gathered by analysing samples at different photoelectron take-off angles (θ) relative to the surface normal. For the untreated copolymer, the ratios $\underline{C}F_2$: $\underline{C}H_2$ and C_{1s}^{TOT} : F_{1s} are independent of θ (*i.e.* they remain unchanged as the sampling depth is increased). However, a sample treated for 25 s in argon plasma at 0.1 Torr and 0.2 W showed marked differences in the ratio $\underline{C}F_2$: $\underline{C}F$: $\underline{C}$ measured at $\theta = 18°$ (deep) and 80° (shallow) (Table 2.3).

Table 2.3: Changes in composition of C_{1s} peak with sampling depth for argon plasma treated ethylene-tetrafluoroethylene copolymer (after Clark and Dilks, 1977)

θ	% of C_{1s}		
	$\underline{C}F_2$	$\underline{C}F$	$\underline{C}$
18°	32.4	7.4	60.2
80°	20.1	17.7	62.2

A substrate/overlayer model was employed to explain these results. The $\underline{C}F_2$ component originates from the "substrate" *i.e.* the unmodified copolymer, whilst the $\underline{C}F$ feature arises from crosslinking in the "overlayer". The relative intensity of $\underline{C}$ is unaffected by θ, as it emanates from CH_2 and CH, which are found in both the "overlayer" and "substrate". The results of subsequent kinetic studies utilising changes in the $\underline{C}F_2$ and F_{1s} levels with respect to treatment time were consistent with the proposal of a two-stage process, with one stage progressing faster than the other. The faster component was attributed to direct energy transfer during surface reactions between the copolymer, and ions and metastables in the plasma. The slower component was ascribed to modification by radiative transfer from photons penetrating into the subsurface and bulk. Thus, the two-component direct and radiative energy transfer model (Figure 2.5) was developed.

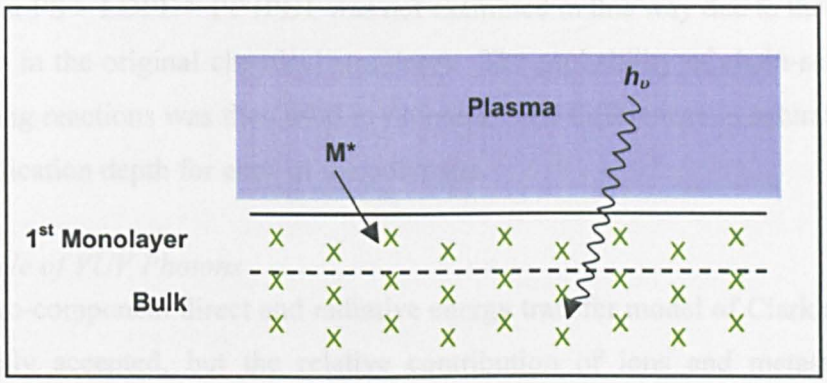

Figure 2.5: Theoretical model of two-component direct and radiative energy transfer. M* is a composite of Ar^*, Ar^+ and e^-; h_υ is a composite of all ultraviolet radiation; X is the type of bond being modified (after Clark and Dilks, 1977).

The incorporation of oxygen into argon plasma treated Teflon® polymers has been linked to the formation of peroxy radicals (Momose *et al.*, 1992). The asymmetric nature of the electron spin resonance (ESR) spectra suggested that the peroxy radicals were associated with two types of oxygen: one bonded to carbon in the crosslinked structures, and the other bonded to carbon arising from main chain scission. As expected from Clark and Dilks' model, the former type of oxygen was localised near the surface (where direct energy transfer applies), whereas the latter was found in the bulk (where radiative energy transfer occurs).

The importance of ions in surface modification was further confirmed by France and Short (1997) with XPS of argon plasma treated PS, low density PE, PP and PET. New carbon – oxygen functionalities were introduced into all the polymers, each exhibiting a 'saturation' level of oxygen incorporation. Following washing with a polymer non-solvent, the saturation level fell to a 'stable' level characterised by high selectivity towards C – O functionalities. The O_{1s} : O_{2s} ratio was used to examine the depth of modification, based on the difference in escape depths for the photoelectrons. This ratio is unity for a homogeneous material. However, plasma treated PS, PE and PP all exhibited an increased ratio, indicative of an oxygen rich surface layer thinner than the XPS sampling depth (5 – 10 nm) arising from direct energy transfer by ions and metastables. The depth of modification was found to increase with treatment time and was dependent on the polymer structure, decreasing

in the order PS > LDPE > PP (PET was not examined in this way due to the presence of oxygen in the original chemical structure). The probability of chain-scission *vs.* crosslinking reactions was then used to rationalise the differences in saturation level and modification depth for each of the polymers.

2.2.3.2 Role of VUV Photons

The two-component direct and radiative energy transfer model of Clark and Dilks is generally accepted, but the relative contribution of ions and metastables *vs.* photons remains unclear. Plasma can be an efficient source of electromagnetic radiation, ranging from soft X-rays to infrared. The region between 100 nm and 200 nm, where radiation is absorbed by air, is referred to as vacuum ultra violet (VUV). The relaxation of excited neutral and singly ionised species in the plasma back down to their ground state results in strong emission lines in the VUV region (Table 2.4). The M I emission line results from transitions between the lowest lying electronically excited state to the ground state (*e.g.* for Ar, $3s^2 3p^5 4s^1 \rightarrow 3s^2 3p^6$). The M II line arises from excited ions *e.g.* Ar^+, $3s^1 3p^6 \rightarrow 3s^2 3p^5$. For both types of line, spin-orbit coupling produces a pair of lines (Hopkins *et al.*, 1996).

Table 2.4: Most intense VUV emission lines for inert gas plasmas (from Hopkins *et al.*, 1996)

Noble gas (M)	M I emission lines/nm	M II emission lines/nm
Ar	104.8, 106.7	92.0, 93.2
Kr	116.5, 123.6	91.7, 96.4
Xe	131.2, 147.0	110.0, 124.5

Radiation of these wavelengths (and from other plasmas such as nitrogen and hydrogen) has great significance in terms of polymer surface chemistry. Organic polymers, such as PE, PP and PS display an intense absorption band below 160 nm due to dissociative electronic excitation of C – C and C – H bonds. Excitation of these bonds initiates homolytic bond scission, which can cause the formation of radicals. These radicals can subsequently react with the atmosphere to which the

treated sample is exposed to incorporate new chemical species (Yasuda *et al.*, 1977) or with other radicals to form a crosslinked structure (Clark & Dilks, 1977).

Materials such as lithium fluoride, magnesium fluoride, calcium fluoride and silica are employed to isolate the VUV component of plasma. Plasma is generated behind a "window" of the material and the polymer placed on the other side. The window is a physical barrier, allowing only electromagnetic radiation down to a certain "cut-off" wavelength to pass through (Table 2.5).

Table 2.5: Cut-off wavelengths for VUV window materials

Material	Cut-off wavelength (nm)
Lithium Fluoride, LiF	104
Magnesium Fluoride, MgF_2	112
Calcium Fluoride, CaF_2	122
Fused Silica (quartz)	160

The first studies to use a window to investigate the coupling mechanism between the plasma and the polymer during crosslinking were by Hudis (Hudis, 1972; Hudis & Prescott, 1972). In these experiments, VUV radiation from hydrogen plasma generated behind a LiF window caused crosslinking of PE. The conclusion of this work demonstrated that in some cases, UV and VUV radiation (rather than ions, metastables, radicals, *etc.*) is the sole or dominant species responsible for surface modification of polymers. Consequently, many studies have identified plasma as a source of VUV radiation that is capable of modifying polymer surfaces. Using fused silica and MgF_2 windows, Corbin *et al.* (1985) found that PE and PS irradiated in a fluorine-containing atmosphere with VUV radiation from a hydrogen plasma incorporated fluorine. Shard and Badyal (1991a, 1991b) compared the surface chemistry of polymers treated with plasma-generated VUV radiation (LiF window) under an oxygen atmosphere with oxygen plasma treated polymers. PE and PS oxidised to a similar level in both types of treatment, leading to the conclusion that VUV induced photochemistry must be one of the dominant processes in oxygen plasma treatment of PE and PS. However, Wilken (1988, 2002) reported the

stability of PS to VUV irradiation through a MgF_2 window, attributed to the distribution of absorbed energy over the aromatic bond system by fluorescence and thermal relaxation.

Holländer *et al.* (1994, 1995) reported on the effects of broad-band radiation from hydrogen plasma on PE, treated under an oxygen atmosphere. The final oxygen concentration and surface chemistry was very similar to that produced by oxygen plasma. Similarly, VUV radiation from Ar, Kr and Xe plasmas was found to induce comparable levels of oxidation in PE (but not in PS) as oxygen plasma treatment (Hopkins *et al.*, 1996). Conversely, Shard (1991a) achieved greater saturation levels of oxidation with the VUV source than with plasma oxidation. This was attributed to the absence of sputtering in the former case. However, compared to plasma treatment, the reaction times were always much longer (typically one hour) for polymers treated only with VUV radiation, as observed by many authors (Corbin *et al.*, 1985; Holländer *et al.*, 1994, 1995; Hopkins *et al.*, 1996; Shard & Badyal, 1991a, 1991b; Wilken *et al.*, 1998, 2002).

Although much of the work discussed above has employed nitrogen and hydrogen plasma as the VUV source, inert gas plasmas (Table 2.3) also have suitable emission characteristics for polymer surface modification and therefore the role of VUV photons should not be dismissed.

2.2.3.3 Summary of the Roles of Plasma Species

In summary, it is very difficult to identify the role of the various plasma species in the surface modification of polymers, and caution must be exercised when comparing data from different reactor systems. Under nominally the same reactor configuration and plasma operating conditions, it may be that the intrinsic plasma parameters change such that the relative contributions of ions and photons to surface modification also change. Moreover, variation of extrinsic plasma parameters such as power and gas pressure in the same system can produce different dominant species (Barton *et al.*, 2000). In general, a comprehensive characterisation of each plasma system with the appropriate plasma diagnostics is necessary before any statements can be made regarding the role of species.

2.3 Review of Recent Work

There exists a vast array of literature on the topic of inert gas plasma treatment of polymers. However, the rationale for this present work was developed from the findings of Steele (2000) and Velázquez (2002), whose work on argon plasma treatment of polymers is reviewed below.

Using a simple glass reactor (Figure 2.6), Steele (2000) set out to investigate the intrinsic plasma parameters and their relationships with extrinsic parameters such as power and gas pressure. Measurements from *in situ* plasma diagnostic techniques (gas phase mass spectrometry, Langmuir probe analysis and VUV/UV spectroscopy) were coupled with XPS data from plasma treated polystyrene to generate a better understanding of the interplay between the physical and chemical aspects of the process.

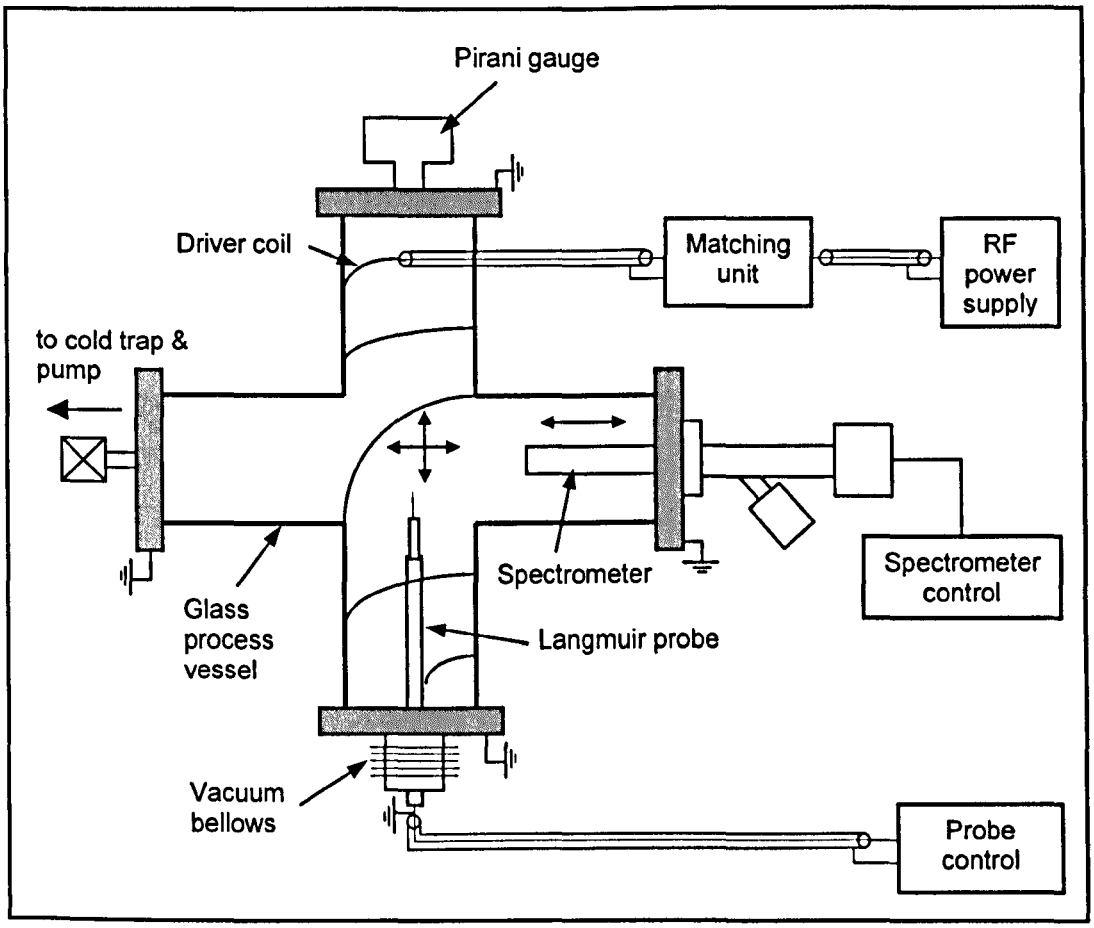

Figure 2.6: Schematic of cruciform reactor used by Steele (2000) and Velázquez (2002)

Using Langmuir probe analysis and absolutely calibrated VUV spectroscopy to determine the ion and photon fluxes respectively, the effect of input power and gas pressure on the relative abundance of species in the plasma was ascertained. Relationships between the ion energy flux to the substrate and the input power and gas pressure were established. Both the ion energy flux and the photon energy flux increased with input power (from 0.5 – 12 W). However, with increase in gas pressure (1 – 100 mTorr), the ion energy flux decreased, whilst the photon energy flux increased (Figure 2.7). Under typical operating conditions of 10 W input power and 10 mTorr pressure, the ion and photon energy fluxes are of the same order of magnitude. However, when the absorption characteristics of VUV photons are taken into account, it can be understood that the effect of VUV on the outer surface of PS is secondary to that of ions, as more than 95 % of the VUV photons penetrate

through the outermost 2 nm of the surface (Barton *et al.*, 1999). This led to the conclusion that in the treatment of PS, ions were most important in terms of energy transfer as the amount of energy they deposit in the outermost layer of the polymer is an order of magnitude greater than that of the photons. However, in polymers with a stronger VUV absorption coefficient, the effect of VUV may be more significant.

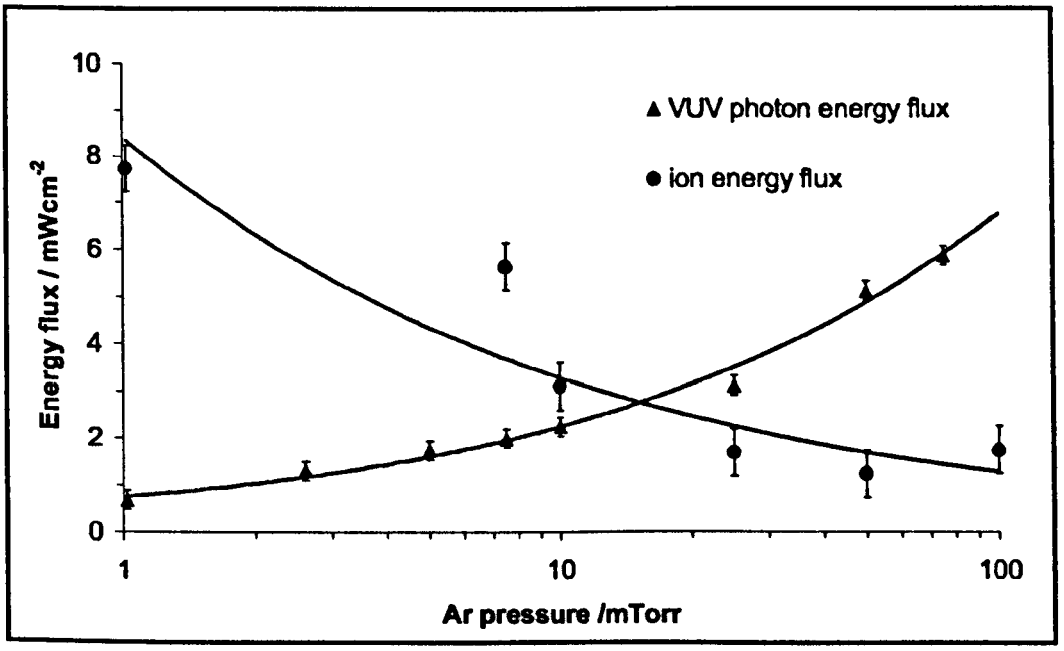

Figure 2.7: Total VUV photon energy flux compared with the ion flux as a function of argon pressure at a generator output of 10W (the curves are a guide to the eye only) (Barton *et al.*, 2000)

Figure 2.7 illustrates how a degree of control over the type and quantity of energy arriving at the substrate can be gained by manipulation of extrinsic parameters. The corresponding effects of such energy flux manipulation on the surface modification of PS (Steele, 2000; Velázquez, 2002), high density polyethylene (HDPE), PP and PET (Velázquez, 2002) were investigated by XPS (not *in situ*). However, these investigations were hampered by impurities in the reactor systems. In the absence of plasma, mass spectrometry of the residual gas in the chamber detected water and residual air. Based upon ideal gas assumptions, it is reasonable to estimate that 1-2% of the species present at operating pressure are impurities. Steele attributed the incorporation of nitrogen into argon plasma treated polystyrene to these species. The

mechanism of oxygen incorporation now becomes difficult to resolve; oxygen could be incorporated from reaction with impurity species *during* plasma treatment, or as a result of radical quenching *after* plasma treatment. Furthermore, Velázquez noted the importance of impurity species in the etching of polymer surfaces during plasma treatment, which in turn affects the level of oxygen incorporation. To proceed with these investigations, a reactor system with less residual species (*i.e.* better base pressure) is required.

2.4 Development of a Novel Plasma Source

The importance of ions having been established by Steele (2000) and Velázquez (2002), the idea of creating a 'tailored plasma', in which ion energies are controlled to target particular bonds within the polymer and thus produce a surface with specific chemistry was developed. Previous studies examining the effect of ion energy on polymer surface modification have generally been conducted using ion beam sources operating in the keV range, rather than tailored at specific bond energies (*e.g.* Wells *et al.*, 1993). The plasma would need to be very cold *i.e.* with ion energies comparable to the bond energies within the polymer. By controlling the electron temperature, it is possible to control to a large extent the floating potential of an isolated substrate, and therefore the mean ion bombarding energy (Liebermann & Lichtenberg, 1994) (Section 2.1.1.3). Control of the electron temperature can be achieved by pulsing the discharge power of the plasma. However this method only takes into account the time-resolved *average* plasma conditions.

In this present work, a reactor system was designed and constructed with the objective of selecting the mode of treatment (*i.e.* ions *vs.* VUV photons) by controlling the species arriving at the polymer surface. To achieve this, control over the ion and photon fluxes, and the ion energy was necessary. We have developed a method of manipulating the EEDF (and thus controlling ion energies) by separating the plasma into two parts by use of one or two DC biased stainless steel meshes (Bai *et al.*, 2001, 2002; Dhayal *et al.*, 2003; Hong *et al.*, 1999; Kato *et al.*, 1994). The first region is the main plasma, which is sustained through electrical excitation. The second region is a diffuse process plasma that is maintained by transport of particles from the main plasma. Independent control of the plasma density (and therefore the ion flux) and the electron temperature (and therefore the ion bombarding energy) in the process chamber is achieved by applying an electrical bias to the separating mesh(es). In the absence of an applied mesh bias, electrons flow through the mesh(es) unimpeded. As an increasing negative bias potential is created, electrons become retarded in the electric field and the density and minimum energy of those reaching the process chamber can be controlled.

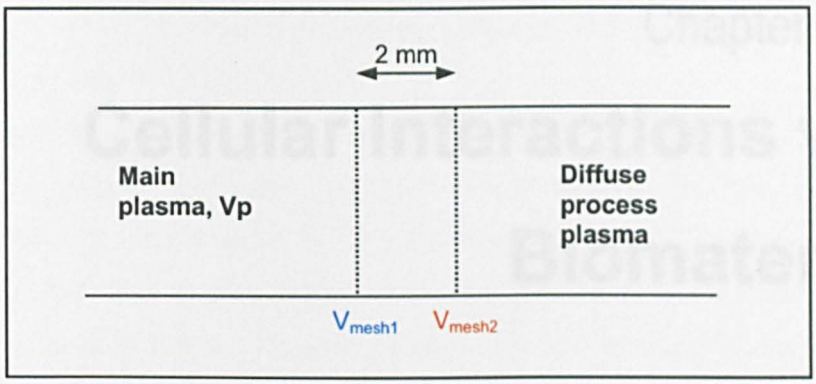

Figure 2.8: Schematic showing separation of plasma by two biased meshes

Figure 2.8 outlines the physical set-up of the plasma regions for the case of the double biased mesh discharge. To penetrate mesh 1, an electron must possess energy equivalent to $V_p - V_{mesh1}$. Thus only a high-energy proportion of the electrons escape the main plasma region and varying V_{mesh1} can alter the density in the process chamber. To penetrate mesh 2, an electron must possess energy equivalent to $V_{mesh2} - V_{mesh1}$. If $V_{mesh2} > V_{mesh1}$, electrons passing through mesh 2 gain energy equivalent to V_{mesh2}. If $V_{mesh2} < V_{mesh1}$, escaping electrons lose energy equivalent to V_{mesh2}. Thus by varying V_{mesh2}, the minimum energy of the electrons escaping into the process region can be selected. Because there is no electrical excitation in the process plasma, the emerging electrons cool through ionisation reactions with the neutral gas. Therefore, we have a very cold process plasma in which the ion flux and ion energy at the substrate can be independently controlled. Simultaneously, simple variation of the distance between the plasma source and the substrate controls the VUV photon flux.

To reduce the impact of impurities, the stainless steel reactor vessel is evacuated with a turbo-molecular pump to base pressures of around 5×10^{-5} Torr, an order of magnitude lower than in the reactors used previously.

Chapter Three

Cellular Interactions with Biomaterials

3.1 Cell Attachment and Spreading

Materials in contact with physiological substances such as blood, serum, urine, tears, *etc.* are rapidly coated with a protein layer. Cell attachment occurs when certain amino acid sequences that act as cell-binding domains are found in this layer. The most important mechanism by which cells adhere to these sites is via cell surface receptors called integrins. The surface chemistry of the substrate influences the composition and conformation of the protein layer, which subsequently directs cell attachment. Once attached, cells must spread out on the surface in order to function normally and proliferate.

3.1.1 Protein Adsorption to Surfaces

Work in the 1970's and early 1980's first suggested that cells adhere to an adsorbed protein layer rather than directly to a substrate surface (Brown & Lackie, 1981; Cassiman *et al.*, 1981; Unhjem & Prydz, 1973). *In vivo*, this layer is derived from the extracellular matrix (ECM), which includes the adhesive glycoproteins fibronectin (Fn), vitronectin (Vn) and, in basal membrane regions, laminin. These are implicated in cell adhesion to artificial substrata and to other extracellular matrix components such as collagen fibres. *In vitro*, the adsorbed layer originates from proteins available in the tissue culture medium, in particular from those found in serum. Indeed, where cell attachment is to be encouraged, foetal calf serum is a common supplement to routine culture media as it provides fibronectin (Grinnell &

Feld, 1982) and vitronectin (Hayman *et al.*, 1985b) in addition to growth factors and hormones (Freshney, 1987).

Proteins are macromolecules, the structure of which can be described by four levels of complexity. The primary structure is determined by the linear sequence of amino acids that copolymerise to form a polypeptide chain. Secondary structure arises from hydrogen bonding within parts of the same chain and/or another chain to form the α-helix or β-sheet. Further interactions within chains of the α-helix or β-sheet produce a globular molecule with tertiary structure. Association of two or more chains creates the quaternary level, which is often the influencing factor in protein adsorption (Chinn, 1995). Distinct domains of polar, ionic and hydrophobic character result from self-association of polar, non-polar and electrically charged amino acid residues. Thus, the protein molecule has a variety of ways to interact with a similarly characterised solid surface, as indicated in Figure 3.1 (Andrade & Hlady, 1986).

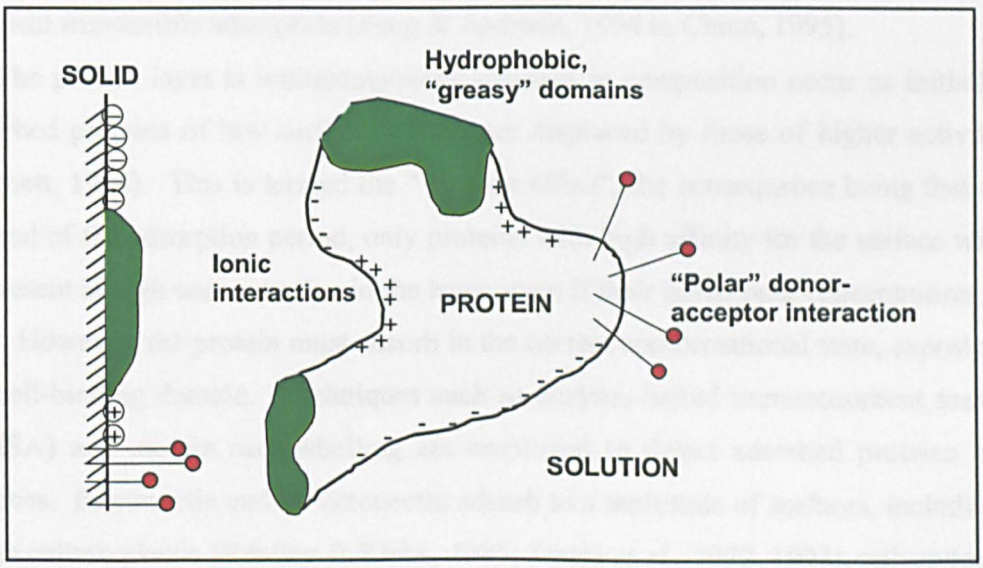

Figure 3.1: Schematic of possible interactions between a protein and a well characterised surface. The protein exhibits domains with hydrophobic, polar and charged character. The solid substrate surface has a similar domain-like character (adapted from Andrade & Hlady, 1986).

Clearly, the chemistry and energy of the solid surface is critical in determination of whether a protein molecule will adsorb and the nature of any adsorption occurring. Vitronectin adsorption, for example, is not strongly influenced by surface wettability, as it adsorbs to both hydrophilic substrates (*e.g.* PTMO-, PEO-polyurethane copolymers) and hydrophobic substrates (*e.g.* polyethylene, silicone rubber) (Fabrizius-Homan & Cooper, 1991). Indeed, after measuring vitronectin adsorption on a range of polystyrene copolymers, Bale *et al.* (1989) postulated that the chemical nature of a surface has more influence on protein adsorption than does its energy. Proteins generally adsorb to hydrophilic substrates in a reversible manner, the process tending to be enthalpy driven. Adsorption to hydrophobic substrates is subject to an entropic driving force and therefore rearrangement on the surface is unlikely (Chinn, 1995). This is due to the ordered nature of water molecules near to a hydrophobic surface, which is disrupted upon adsorption of a protein molecule. Thus, adsorption is favoured on thermodynamic terms and therefore irreversible. In addition, denaturation of the protein molecule may occur as a result of hydrophobic-hydrophobic interactions with the substrate and further augment irreversible adsorption (Feng & Andrade, 1994 in Chinn, 1995).

The protein layer is multicomponent; changes in composition occur as initially adsorbed proteins of low surface activity are displaced by those of higher activity (Horbett, 1984). This is termed the "Vroman effect", the consequence being that at the end of the adsorption period, only proteins with high affinity for the surface will be present at high concentration in the layer, even if their initial bulk concentration is low. However, the protein must adsorb in the correct conformational state, exposing the cell-binding domain. Techniques such as enzyme-linked immunosorbent assay (ELISA) and protein radiolabelling are employed to detect adsorbed proteins on surfaces. Fibronectin and/or vitronectin adsorb to a multitude of surfaces, including tissue culture plastic (Bentley & Klebe, 1985; Steele *et al.*, 1992, 1993), polystyrene copolymeric latexes (Bale *et al.*, 1989), perfluorosulphonate (Steele *et al.*, 1991) and chemically derivatised substrata (*e.g.* Lewandowska *et al.*, 1992), making them capable of supporting cell attachment and growth.

3.1.2 Cell Adhesion Proteins and Peptide Sequences

Fibronectin and vitronectin mediate attachment to differing degrees for a variety of cells on a range of surfaces. Although fibronectin has generally been regarded as the primary cell attachment-promoting protein in serum (Grinnell & Feld, 1982), some authors have reported a critical role for vitronectin. For example, improved endothelial cell attachment is seen in vascular grafts that are pre-coated with fibronectin before cell seeding. However, fibronectin is not necessarily essential for attachment to such a surface, as Steele *et al.* (1991) demonstrated by selectively depleting serum of fibronectin or vitronectin. Vitronectin was found to be vital in this study. However, these results were obtained with the two glycoproteins in isolation and they may behave differently in a mixture (Fabrizius-Homan & Cooper, 1991) and in the presence of other non-adhesive serum components (Steele *et al.*, 1992). Hayman *et al.* (1985b) also proclaimed vitronectin to be "the major adhesive protein in routine cell culture media," although only experimental evidence from fibroblasts was considered in this work and Bale *et al.* (1989) found it to adsorb to a variety of polystyrene copolymers.

In a seminal 1984 paper, Pierschbacher and Ruoslahti used monoclonal antibodies to inhibit cell attachment and hence isolated the domain within fibronectin that enables it to adhere to fibroblast integrins. The primary structure of the domain was determined and the amino acid sequence *Arg-Gly-Asp-Ser* (RGDS) identified as critical in the adhesion mechanism. Subsequently, the RGD sequence was identified in vitronectin (Hayman *et al.*, 1985a), fibrinogen and von Willebrand factor (Ginsberg *et al.*, 1985; Haverstick *et al.*, 1985; Plow *et al.*, 1985), type I collagen (Dedhar *et al.*, 1987) and osteopontin (Oldberg *et al.*, 1986). The RGDS tetrapeptide in fibronectin was originally defined as the cell attachment site because it was the smallest with measurable activity. However, only the tripeptide sequence RGD has to be conserved in order to retain the cell attachment-promoting ability of a peptide or protein; for example, the residue following RGD in vitronectin is valine rather than serine (Ayad *et al.*, 1998).

Despite the apparent importance of fibronectin and vitronectin, cell attachment and spreading is possible in serum free conditions, as reported by Steele *et al.* (1992)

and Curtis *et al.* (1983). Whilst investigating surface chemistry effects on cell attachment, Curtis *et al.* found that the fibroblasts and leukocytes used in the experiment were capable of attaching to hydroxylated surfaces in the absence of serum. The group proposed that cells synthesise wetting agents or proteins as they settle onto the surface and tested this hypothesis by disabling protein synthesis mechanisms with cycloheximide before seeding. The theory was disproved as the cells still attached and spread. Further investigation revealed that in order to form adhesions, cells only required the presence of fibronectin if they had previously been exposed to it (Curtis & McMurray, 1986). However, in a study by Evans & Steele (1997), attachment of corneal epithelial cells in serum free media was not inhibited by the presence of cycloheximide. The authors concluded that these cells employ an alternative method of adhesion, implicating the use of microtubules as disruption of these with demecolcine resulted in decreased attachment.

3.1.3 Integrins

Integrins are cell surface receptors for which the cell-binding sites of the adsorbed adhesion protein function as ligands. They are heterodimic; two non-covalently associated transmembrane glycoprotein subunits, α and β both participate in binding to the protein (Alberts *et al.*, 1994) (Table 3.1). The cytoplasmic domain of the integrin is connected to the cytoskeleton, allowing the cell to be secured to the substrate when ligand-integrin binding occurs. This type of binding is called a *focal contact.* The anchorage is not strong, however; cells may move and spread over the substrate surface, exploring their environment. In fact, weak adhesion occurs in many places on the cell surface, the principle having been compared to that of Velcro (Alberts *et al.*, 1994).

At least twenty integrins have been identified (Ruoslahti, 1996). Some appear to be specific in that they only bind to one type of ligand; others bind to a variety. Furthermore, the same integrin on different cell types binds to different ligands (Ruoslahti & Pierschbacher, 1987). One subfamily of integrins recognises the RGD sequence in many protein molecules, including fibronectin and vitronectin.

Table 3.1: Known integrin subunit combinations and their ligands (taken from The Integrin Page, http://integrins.hypermat.net, December 2003).

β subunit	α subunit	Ligands
β_1	α_1, α_2	Collagens, Laminins
	α_3	Laminins, Fibronectin, Thrombospondin
	α_4	Fibronectin, VCAM
	α_5	Fibronectin
	α_6, α_7	Laminins
	α_8	Fibronectin, Tenascin
	α_9	Tenascin
	α_{10}, α_{11}	Collagens
	α_V	Fibronectin, Vitronectin
β_2	α_L	ICAMs
	α_M	Fibrinogen, ICAMs, iC3b
	α_X	Fibrinogen, ic3B
	α_D	VCAM, ICAMs
β_3	α_{IIb}, α_V	Collagens, Fibronectin, Vitronectin, Fibrinogen, von Willebrand factor, Thrombospondin
β_4	α_6	Laminins
β_5	α_V	Vitronectin
β_6	α_V	Fibronectin, Tenascin
β_7	α_4	Fibronectin, VCAM, MAdCAM
	α_E	E-cadherin
β_8	α_V	Collagens, Laminins, Fibronectin

3.1.4 Cell Spreading

In order to function normally and proliferate, attached cells must spread out to a critical size (Maroudas, 1973) by forming further focal contacts with ligand binding sites (*e.g.* RGD). As outlined above, the availability of binding sites depends upon the conformation of the adsorbed protein, which in turn is dependent upon the chemistry of the surface with which the proteins are in contact. Thus cell spreading is influenced by material surface properties such as wettability, topography and concentration of functional groups. Therefore, on some materials, cells will be able to find enough binding sites to attach, but not enough to spread and will eventually cease to function.

Cell spreading is mediated by the protein filaments of the cytoskeleton, which are:

- actin filaments – cord-like filaments found in bundles or networks, which control cell shape and surface movement (*e.g.* ruffling, lamellipodia)
- microtubules – stiff single structures that provide a transport network for the organelles within the cytoplasm
- intermediate filaments – relatively tough, rope-like structures that afford mechanical stability

The cytoskeleton is a dynamic structure; as the cell spreads more protein subunits polymerise at the leading edge of the cell, extending the filaments. The size and shape of the cytoskeleton plays an important role in determining cell behaviour, as it is a transduction pathway for external signals to the cell nucleus. This is discussed more fully in Section 3.3.2 with specific reference to cell shape engineering *via* cellular patterning.

3.2 Cellular Interactions with Plasma Treated Biomaterials

Due to their convenience, low cost and sterility, disposable plastic materials have largely replaced glass as routine cell culture substrates. However, whilst polystyrene fulfils the requirements of a tissue culture substrate in terms of bulk properties, it is not conducive to the attachment and growth of anchorage dependent cells. For *in vivo* applications, the materials that are most suitable from an engineering and surgical point of view are often not biocompatible. Therefore, plasma modification of the surface chemistry is often employed to improve cell-surface interactions both *in vivo* and *in vitro*.

Much of the literature on the topic of cell-surface interactions appears to be contradictory. Indeed, the literature reviewed in the following sections illustrates two important points regarding the surface chemistry:

a) the response of cells to a given surface chemistry is usually cell-type specific and results achieved with a cell line may not translate to primary cells
b) the collective effect of different functional groups on a cell culture substrate is often difficult to determine, but likely to be important.

Comparisons of data gathered from different cell types on different surfaces are therefore difficult, and the role of model cell culture surfaces such as self-assembled monolayers (SAMs) is increasingly important.

3.2.1 Tissue Culture Polystyrene

Tissue culture polystyrene (TCPS) supports attachment and growth of many cell types due to surface modification by the manufacturer. The FALCON® range of tissue culture products (Becton Dickinson Labware, U.S.A.) is produced by oxygen plasma treatment (LaRocca, 1996). A mixed plasma of oxygen and nitrogen is used to create PRIMARIA™ (Becton Dickinson Labware, U.S.A.), a range of tissue culture products which support the attachment of some cells types that do not attach readily to standard TCPS (*e.g.* some neurons, hepatocytes and endothelial cells)

(LaRocca, 1996). As mentioned previously, Amstein and Hartman (1975) successfully replicated the cell culture properties of TCPS by modifying the surface of polystyrene with air plasma. However, no analysis of the resulting surface chemistry was performed. XPS analysis of several commercial TCPS substrates by Daw (1999) revealed only carbon, oxygen and nitrogen, the relative proportions of which varied from brand to brand. Moreover, the nitrogen content was particularly inconsistent between samples of the same brand. Therefore doubts over the validity of TCPS as a control material for studying the effects of surface chemistry on cells were raised by this work. However, the sensitivity of cells to variations in the adsorbed protein layer determines whether TCPS is a valid control material.

Steele *et al.* (1993) performed an investigation of the adsorption of serum proteins onto TCPS and unmodified PS using ^{125}I labelled Fn and Vn to quantify the amount of adsorption. Both vitronectin and fibronectin adsorbed in greater amounts to TCPS than to PS. Moreover, a higher molecular potency of Vn on TCPS was discovered during cell culture, suggesting that the Vn adsorbed onto PS was in an unfavourable conformation for endothelial cell attachment. However, the authors themselves caution the extrapolation of this result to other cell types, as different subclasses of integrins, which may bind to other adsorbed proteins or binding sites, would undoubtedly be involved.

3.2.2 Other Plasma Treated Biomaterials

The use of materials such as PTFE and PET as medium and large diameter vascular prostheses is a well established surgical technique. Although these materials are the most suitable from an engineering and surgical perspective, they are not biocompatible. Such synthetic surfaces can be thrombogenic: the proteins that adsorb to these surfaces from the blood can make them attractive for platelet adhesion, aggregation and subsequent thrombus formation. This is particularly evident in small bore (<6 mm diameter) grafts, which often fail. Ideally, the inner surface of the graft should be lined with endothelium, just as in natural blood vessels. Therefore, plasma surface treatment is of great potential as a method of modifying the surface chemistry of PTFE and PET to encourage endothelialisation

of the graft. Pigłowski *et al.* (1994) showed that argon plasma treatment of PET did not cause any toxic effect when implanted *in vivo*. Moreover, Mirenghi *et al.* (2000) reported enhanced endothelial cell attachment and growth on PET treated with a mixed nitrogen and hydrogen plasma. The resulting cell culture properties, attributed to the introduction of surface nitrogen-containing groups, were comparable to TCPS and commercially produced Thermanox PET. Alternatively, argon plasma treated PTFE and PET surfaces are capable of binding ECM components, such as collagen (Type IV) and laminin, to which antithrombogenic biomolecules (*e.g.* heparin) can be immobilised. The biomolecules prevent platelet adhesion, whilst the matrix components encourage endothelial cell growth (Chandy *et al.*, 2000).

Plasma surface treatment has also been successful in improving the epithelialisation of materials used for artificial corneas. Latkany *et al.* (1997) identified argon plasma treatment as the optimal process for enhancement of epithelial cell migration and proliferation on a poly(vinylalcohol) (PVA) copolymer hydrogel. Argon plasma has also been used to modify silicon rubber (SR), creating a surface chemistry to which other polymers can be grafted to elicit the desired biological response. Examples include, poly(2-hydroxy ethyl methacrylate) (pHEMA) grafted to peroxide groups in argon treated SR; acrylic acid grafted to plasma treated SR and subsequent linkage of collagen to the carboxylic group (Lee 1996a, 1996b).

Plasma treatment has been employed to improve the performance of a skin substitute material. In the treatment of full thickness burns, a dermal substitute is required to improve the 'take', functional behaviour and cosmetic appearance of grafted cultured epithelial sheets. A biodegradable copolymer of poly(ethylene oxide) (PEO) and poly(butyl terephthalate) (PBT) has been developed with a porous underlayer, suitable for infiltration of dermal fibroblasts and a dense top layer, amenable to the culture of epidermal keratinocytes. The cell culture properties of this material were greatly improved by argon plasma treatment (Beumer *et al.*, 1994).

3.3 Cellular Patterning

The shape and size of animal cells is determined by the availability of binding sites with other cells or with extracellular matrix proteins, such as those adsorbed to a cell culture substrate from serum. By using patterned surfaces to control the spatial distribution of protein adsorption, cells can be forced to adhere from suspension to specific regions, and spread from their initial spherical shape to a restricted shape and size. Regulation of cell shape and size has been shown to control viability, function and differentiation via the cytoskeleton.

3.3.1 Patterning Methods

3.3.1.1 Physical Restriction

Cellular micropatterns may be achieved using patterned substrate topography (Chehroudi *et al.*, 1992; Clark *et al.*, 1990, 1991; Mrksich *et al.*, 1996; Rovensky *et al.*, 1971; Wood, 1988), or by spatially selective protein adsorption to a substrate by means of physical restriction (*e.g.* a stencil) (Chiu *et al.*, 2000; Folch *et al.*, 2000; Folch & Toner, 1998; Ostuni *et al.*, 2000). The former approach is constructive in terms of studying the fundamental cell biology of contact guidance and cell alignment, for example. Patterned topography has been employed *in vivo* to improve the success rate of dental implants by encouraging connective tissue ingrowth and impeding epithelial downgrowth (Chehroudi *et al.*, 1992). However, the technique is strongly cell-type dependent and is hampered by the lack of understanding of the mechanism by which it operates (Singhvi *et al.*, 1994a). Additionally, the processing route of these surfaces is often complex. The latter approach, physical restriction of protein adsorption, is powerful in spreading and migration studies as it can be performed on homogeneous cell culture substrates. In studies of geometric constraint, however, the presence of non-adherent areas is important in order to confine cells to adhesive regions (Chen *et al.*, 1997; Lee *et al.*, 1994).

3.3.1.2 Self-Assembled Monolayers

Micropatterning techniques that utilise surface chemistry modification are suitable for studies investigating the effects geometric constraint on cells. Many

investigations of geometrically selective cell attachment utilise the formation self-assembled monolayers (SAMs) of silanes on silica substrates or thiols on gold substrates. Cellular patterns are produced using photolithography (Cooper *et al.*, 1997; Scotchford *et al.*, 1998; Thomas *et al.*, 1997) or microcontact printing (Kumar & Whitesides, 1993; Zhang *et al.*, 1999) to define areas to which SAMs of contrasting cell adhesiveness adsorb. Such use of SAMs has been successful in controlling the spatial distribution (Cooper *et al.*, 1997; Mrksich *et al.*, 1996) and morphology (Chen *et al.*, 1997; Cooper *et al.*, 1997; Scotchford *et al.*, 1998; Singhvi *et al.*, 1994b) of cultured cells. An alternative patterning system is the combination of photolithography with silane coupling techniques, which enables chemical patterns to be produced in μm dimensions on quartz, glass and silicon. On these surfaces, the method is valuable in *in vitro* studies of cell patterning (Bhatia *et al.*, 1997; Healy *et al.*, 1994, 1996; Kleinfeld *et al.*, 1988) and has potential applications in developmental biology, tissue engineering and implant biology (Bhatia *et al.*, 1997).

3.3.1.3 Plasma Patterning

Although the SAM and silane coupling techniques provide effective routes to micropatterning, integration with *routine* tissue culture and biocompatible materials, such as polymers, is generally restricted by the requirement of a specific substrate. Indeed, the development of surface chemistry patterning techniques that are applicable to polymers would be welcome in other disciplines such as adhesion science, polymer film technology, biotechnology and electronics. Surface chemical patterning by means of plasma processing has several advantages over other techniques, including:

- sterility,
- high throughput,
- applicability to objects of complex geometry (restricted only by the fabrication of suitable a mask),
- suitability to polymeric substrates,
- positive and negative contrast generation,
- possible one step processing.

The resulting pattern has the potential to be used in spatial control of protein adsorption, and hence cell attachment and spreading on the basis of surface chemistry. There is also the possibility of binding short peptide sequences to sites activated by plasma treatment.

Plasma patterning is often used as a processing step in other micropatterning techniques *e.g.* for photoresist removal (Kleinfeld *et al.*, 1988), substrate pre-treatment (Healy *et al.*, 1996) and fabrication of elastomeric and poly(dimethylsiloxane) stamps in microcontact printing (Mrksich *et al.*, 1996; Singhvi *et al.*, 1994b). However, the simplest use of the technique is plasma treatment of a non-biocompatible surface through a mask placed on the substrate surface, thus creating regions of cell adhesiveness in one step. This is the method adopted in this present work, where bacteriological grade PS is argon plasma treated through a transmission electron microscopy (TEM) grid (Figure 3.2). The resulting oxygen incorporation into the exposed regions is sufficient to encourage cell adhesion in a negative pattern to the mask.

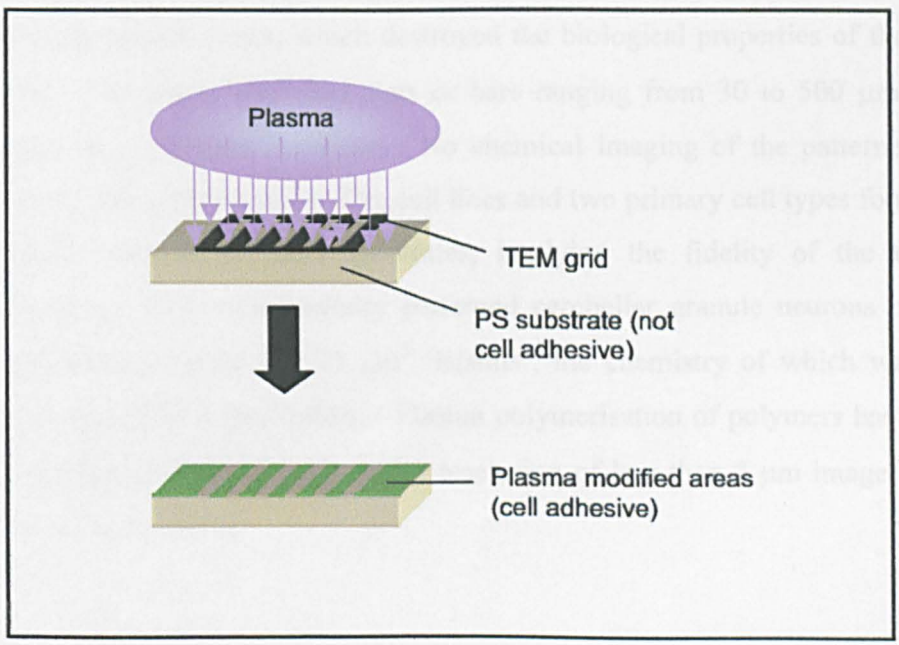

Figure 3.2: Schematic of simple plasma patterning with a TEM grid placed on a PS substrate. The regions exposed to the plasma become cell adhesive, generating a negative pattern of the original TEM grid.

Patterned plasma treated substrates have been used to create cellular micropatterns with varying success (reviewed by Ohl & Schroder, 1999). Vargo *et al.* (1992) were unable to pattern neuroblastoma cells on an aminosilane-coupled fluoropolymer that had been treated through a TEM grid. The TEM grid had 15μm slots and 7 μm bars. However, cells did not adhere to the region masked by the wide grid rim (150 μm). Surface chemical imaging by time of flight static secondary ion mass spectrometry (ToF-SIMS) revealed a high degree of fidelity to the TEM grid, except in small regions where contact between the grid and substrate was not adequate. Thus, the small size of the non-adhesive regions might explain the absence of patterning in the main body of the grid. It should also be noted that the cell line used in this experiment is transformed and so may display markedly different adhesion behaviour to normal cells. Ohl *et al.* (1999) achieved greater success using a plasma etching process. Polystyrene substrates were treated with Ar/NH_3 plasma to incorporate amino groups and hence render them capable of bonding biomolecules. Patterning was achieved by Ar/H_2 plasma treatment through a laser-cut metallic mask, which destroyed the biological properties of the exposed regions. The masks used had slots or bars ranging from 30 to 500 μm in width arranged in a logarithmic pattern. No chemical imaging of the patterned surface chemistry was performed, but five cell lines and two primary cell types formed well-expressed patterns on these substrates, implying the fidelity of the technique. Bullett *et al.* (2001) successfully patterned cerebellar granule neurons on plasma deposited 50 μm bars and 75 μm^2 'islands', the chemistry of which was imaged using both XPS and ToF-SIMS. Plasma polymerisation of polymers has also been used to achieve patterns with spatial resolution of less than 5 μm imaged by AFM (Mitchell *et al.*, 2002).

3.3.2 Cytoskeletal Involvement in Gene Expression and Shape Engineering of Cells

In vivo, cells receive multiple simultaneous stimuli that activate numerous signalling cascades in parallel. Thus, the mechanisms of signal transduction, *i.e.* how an

external signal produces an intracellular response, are highly complex (Ingber, 1998). Both the chemical (Ingber, 1990; Ingber & Folkman, 1989; Ingber *et al.*, 1990) and mechanical (Chen *et al.*, 1997; Huang *et al.*, 1998; Ingber & Folkman, 1989; Singhvi *et al.*, 1994b) context of signal transduction influence cellular response.

In a review of cell shape and gene expression, Ben-Ze'ev (1991) proposes two mechanisms of cytoskeletal involvement in gene regulation; direct signal transduction via focal contacts and sequestration of signalling molecules by microfilaments. Focal contacts formed between cell and ECM are associated with localisation of various regulatory molecules such as kinases, phosphatases, transcription factors and mRNAs. Localisation of a protein kinase, for example, may lead to phosphorylation of an integrin. The introduction of negative charge from phosphate groups causes a change in conformation of the integrin, which may lead to the exposure of different ligand-binding sites to those normally expressed. An example of this occurs during mitosis of cultured cells, when a serine residue on the cytoplasmic tail of a β_1 integrin is phosphorylated, resulting in the inability of the integrin to bind to fibronectin so the cells round up and detach from the substrate (Figure 3.3). Changes in the distribution of focal contacts, induced by forced changes in cell shape, could hence regulate survival, growth, movement, morphology and differentiation.

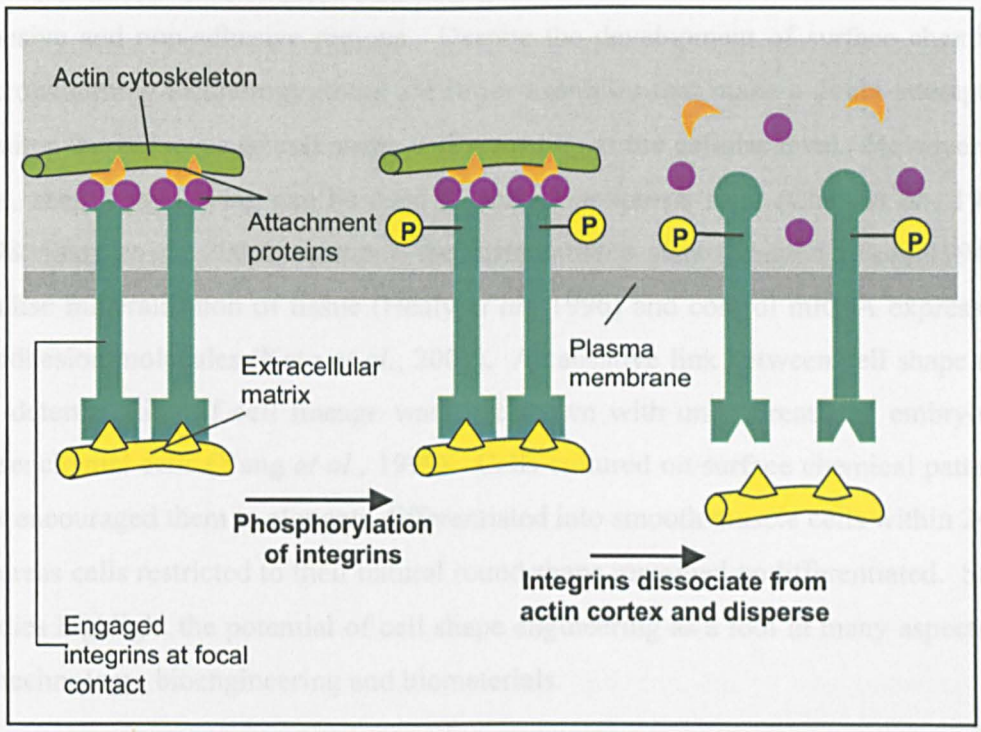

Figure 3.3: Schematic illustration of regulation of cytoskeletal attachment. Phosphorylation of the cytoplasmic tail of the integrins impairs their ability to bind to the actin skeleton. The integrins can then no longer maintain a robust cell-matrix adhesion and their binding to the ECM is released. After Alberts *et al.*, 1994.

Alternatively (or additionally), regulatory molecules can be sequestered by the cytoskeleton. For example, kept in association with microfilaments, nuclear regulators are unavailable to the nucleus. Changes in the microfilament assembly, such as alteration of cell shape, could release the sequestered factors, allowing their translocation to the nucleus. The development of computer simulations based on dynamic Boolean networks has enabled modelling of signal transduction in shape-engineered cells (Huang & Ingber, 2000).

Whatever the mechanism of signal transduction, the use of micropatterned culture substrates in many studies has allowed the demonstration of some of the effects of cell shape engineering. Many studies (as outlined in Section 3.3.1) of cellular patterning achieve control over the spatial distribution of cells and observe cell morphology conforming to the size and geometry of adhesive regions. This is expected when the geometry of the adhesive regions is of dimensions smaller than or

equal to the maximum unconstrained cell area, and there is a boundary between adhesive and non-adhesive regions. Despite the development of surface chemical micropatterning technology, there are fewer examples that make a direct attempt to monitor the influence of cell shape and spreading at the cellular level. However, to date, shape engineering can be used to control apoptosis rates (Chen *et al.*, 1997, 1998; Ferri *et al.*, 2000), maintain the differentiated state (Singhvi *et al.*, 1994b), localise mineralisation of tissue (Healy *et al.*, 1996) and control mRNA expression of adhesion molecules (Kato *et al.*, 2001). A causative link between cell shape and the determination of cell lineage was first shown with undifferentiated embryonic mesenchymal cells (Yang *et al.*, 1999). Cells cultured on surface chemical patterns that encouraged them to elongate differentiated into smooth muscle cells within 24 h, whereas cells restricted to their natural round shape remained undifferentiated. Such studies highlight the potential of cell shape engineering as a tool in many aspects of biotechnology, bioengineering and biomaterials.

3.4 Bone Marrow Stromal Cells

The cells used in this study are rat bone marrow stromal cells; therefore a brief review of the biology of bone and studies relating to *in vitro* culture of these cells is appropriate.

Bone consists of both organic and inorganic components. The organic component includes three cell types:

- Osteoblasts – responsible for the formation of bone
- Osteocytes – mature osteoblasts, which maintain bone
- Osteoclasts – large cells, which resorb bone matrix

Amongst other functions, osteoblasts secrete *osteoid*, an organic substance containing proteoglycans, glycoproteins and collagen fibres that accounts for approximately one third of the ECM. The organic substances, particularly the collagen fibres, impart flexibility and tensile strength to bone. The remaining two thirds of the ECM is made up of hydroxyapatites, most of which are calcium phosphates. These give bone its exceptional hardness.

Bone provides the body with support and protection, allows movement and stores minerals. Some bones also contain red marrow, which is the site of blood cell formation (haematopoiesis).

3.4.1 Origin and Differentiation

Owen (1988) proposed that in addition to haematopoietic stem cells, bone marrow also contains *stromal* cells (also called mesenchymal stem cells), which produce committed progenitors for different mesenchymal cell lines (Figure 3.4). The existence of these cells is now accepted and their mulitpotentiality well demonstrated (Pittenger *et al.*, 1999; Prockop, 1997).

As cells progress along the lineage, their capability for self-renewal decreases. The multipotency of the bone marrow stromal cells (BMSC) suggests an ability to respond to external stimuli, such as chemical signals or mechanical forces.

Considering the link between phenotype and cell shape (Section 3.3.2), BMSC are therefore suitable for studies of the effects of cell shape engineering on cell differentiation.

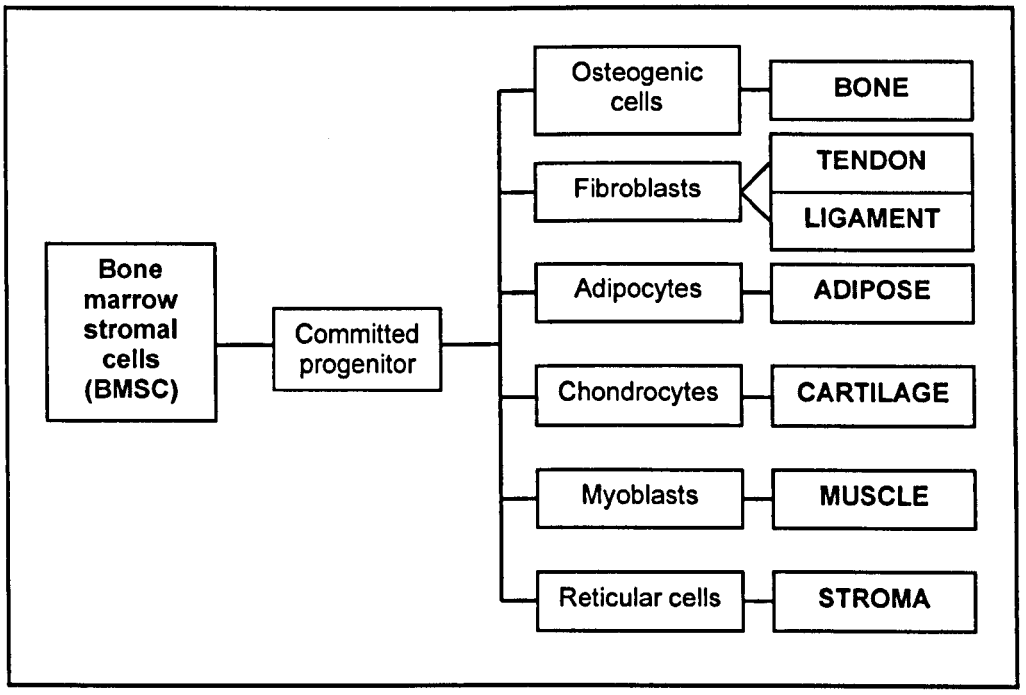

Figure 3.4: Diagram illustrating the mulitlineage potential of BMSC.

BMSCs can be separated from the other cells in bone marrow by their ability to adhere to TCPS (Freidenstein *et al.*, 1976). Culture conditions for differentiating BMSCs are species-dependent and can be influenced by incompletely defined variables such as the batch of foetal calf serum used (Prockop, 1997). However, BMSCs from mouse, rat, rabbit and human origin have been shown to differentiate into osteoblasts, chondrocytes, adipocytes and myoblasts by the addition of various supplements to the culture medium (Table 3.2).

Table 3.2: Examples of culture conditions employed to differentiate BMSCs along specific lineages

Lineage	Culture Conditions	Reference
Adipogenic	• 1-methyl-3-isobutylxanthine, • dexamethasone, • insulin, • indomethacin	Pittenger, 1998
Chondrogenic	• serum free, • transforming growth factor -β3	Barry *et al.*, 2001 Yoo *et al.*, 1998
Myoblastic	• 5-azacytidine, • amphotericin B, or • amphotericin B alone	Wakitani *et al.*, 1995
Osteogenic	• dexamethasone, • β-glycerophosphate, • ascorbate	Pittenger *et al.*, 1999 Peel *et al.*, 1992

When cultured on TCPS, BMSC generally differentiate to acquire an osteoblastic phenotype. Osteoblastic differentiation can also be induced by addition of ascorbic acid, β-glycerophosphate and dexamethasone to the culture medium (*e.g.* Peel *et al.*, 1992; Pittenger *et al.*, 1999). Committed progenitors for the osteogenic lineage (osteoprogenitor cells) subsequently mature into osteoblasts, which proliferate and begin to produce collagenous ECM. After about 9 days, proliferation decreases and mineralisation of the matrix begins. This differentiation stage is characterised by the increased production of the enzyme *alkaline phosphatase*, which causes precipitation of hydroxyapatite. As the matrix matures, mineralised nodules nucleate on the collagenous matrix. Eventually osteoblasts become surrounded by mineralised matrix and differentiate into osteocytes, which maintain and regulate bone formation.

3.4.2 Interactions with Biomaterials

Peel *et al.* (1992) demonstrated the effect of surface chemistry on the phenotype of bone marrow cells. Bacteriological grade (*i.e.* unmodified) PS dishes were treated with concentrated sulphuric acid in selected areas. On these surfaces, primary rat bone marrow cells were cultured in medium supplemented with ascorbic acid, β-glycerophosphate and dexamethasone. Cells colonised both the treated and untreated areas of the plates, but more rapidly on the former. Compared to the untreated areas, production of a continuous, non-collagenous cement-like matrix was accelerated on the treated areas. Although the authors acknowledged the role of surface chemistry in the initial adhesion of cells, this apparent difference in phenotype was attributed to differences cell spreading. Atomic force microscopy, (AFM) showed that the acid treatment had introduced changes in topography on a scale that could potentially affect the organisation of the ECM. Due to the γ-irradiation sterilisation procedure used on the plates, the "untreated" areas almost certainly contained oxygen, as demonstrated with XPS by Callen *et al.* (1993). This latter study found no significant differences in cell behaviour on sulphuric acid treated and γ-irradiated PS, despite XPS analysis revealing different surface chemistries. The combined results of these two studies suggest that primary bone marrow cells are more sensitive to topography than to subtle changes in surface chemistry.

Primary rat bone cells do, however, respond to gross changes in surface chemistry. Daw (1999) examined ECM production from osteogenic cells cultured on octadiene plasma polymers (OD PP) and acrylic acid/octadiene plasma copolymers (PCP). After ten days in culture, cells on the PCP had formed multi-layers and produced small nodules containing calcium and phosphorus, and some fibrous material (observed by scanning electron microscopy). However, on the OD PP only a single cell sheet had formed and the cells appeared relatively inactive. This was confirmed biochemically by Kelly (2001), who used cellular alkaline phosphatase, calcium and collagen as markers of osteoblastic differentiation. BMSC cultured on PCP (COOH/R = 3.8% of C_{1s}) and TCPS (positive control) expressed

similar levels of these differentiation markers, significantly greater than on the OD PP (negative control).

Chapter Four

Experimental Methods

4.1 Substrate Preparation

Polystyrene (PS), with an average molecular weight of 280 000 $gmol^{-1}$ and a polydispersity of 3.0, was obtained from Aldrich Chemical Co., U.K. From a solution of 0.3 g of polystyrene granules in approximately 10 ml of toluene (HPLC grade, Aldrich Chemical Co., U.K.), polystyrene films were spun cast onto clean glass coverslips (Fisher Scientific U.K.).

4.2 Novel Plasma Source

A novel stainless steel reactor system was designed and built at UMIST (Figure 4.1). The chamber was a 5-way tubular cruciform vessel, 15 cm in diameter, pumped to a base pressure in the order of 10^{-5} Torr by a turbomolecular pump backed by a rotary pump. The main plasma production region consisted of a stainless steel cylinder, 8 cm in diameter and 12 cm in length mounted on the inside of one flange. Here the plasma was sustained by RF excitation at 13.56 MHz from a signal generator (Coaxial Power Systems Ltd., U.K.). The driver electrode was a 5 cm diameter stainless steel plate attached to the power supply via a manual impedance matching unit.

The separation of the discharge into a main plasma production region and a diffuse process plasma by the use of biased meshes is described in Section 2.4. The meshes used were of stainless steel (SS304), 6 cm diameter, with wire of diameter 0.05 mm and 165 lines per inch (45 % transmission). They were attached to the end of the main plasma production cylinder via insulators and connected to ground via a

10 μF capacitor to null any RF excitation. The DC potential on the mesh was applied using a ripple-free power supply.

Various electrical probes were used to measure the parameters of both the main plasma and process plasma: a cylindrical probe measured the EEDF and plasma density, n; a double probe was used to measure the effective T_e and give an independent reading of n; an emissive probe measured the plasma potential; and a passively compensated single probe was used to determine T_e and n in the RF plasma discharge. Ion energies to an electrically isolated substrate at various positions within the process plasma were determined using a retarding field analyser (RFA).

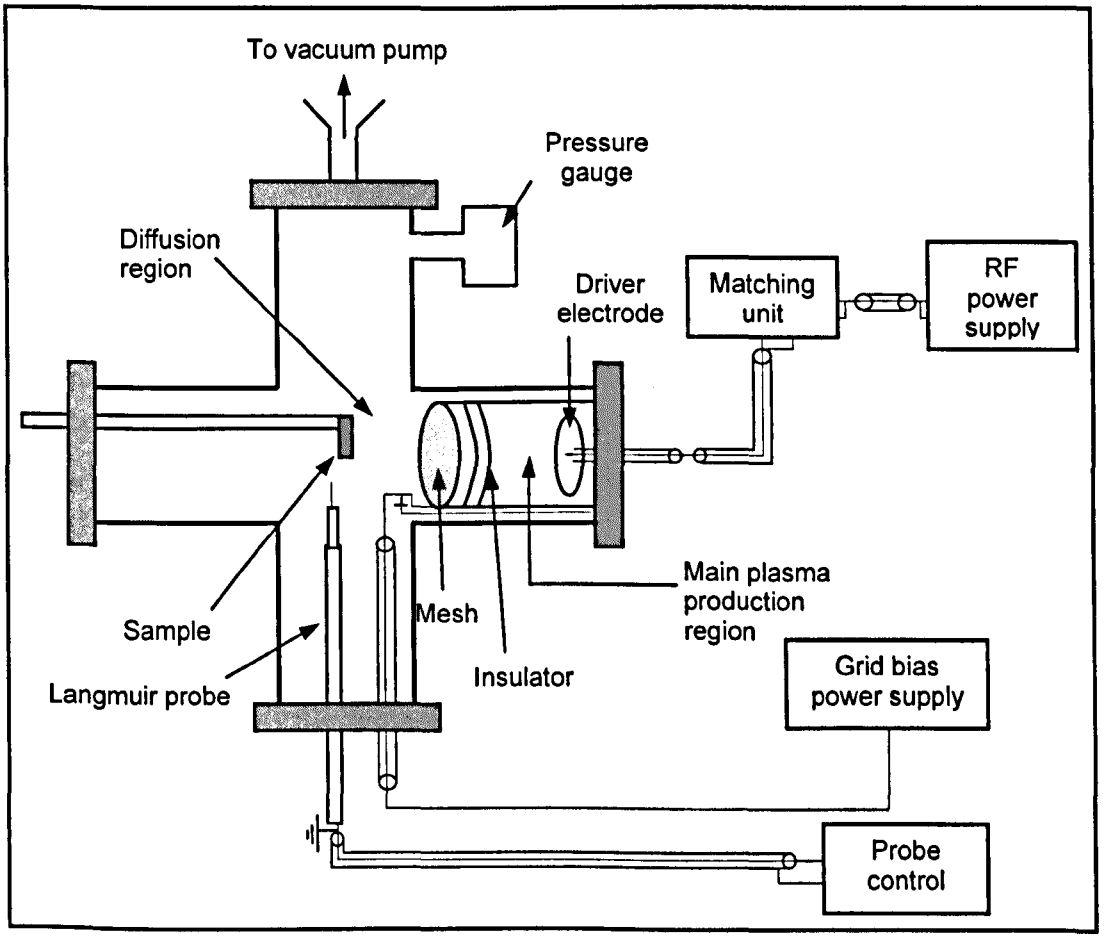

Figure 4.1: Novel plasma reactor system at UMIST.

4.3 Surface Chemical Patterning

To create surface chemical patterns, specially designed copper transmission electron microscopy (TEM) grids, (Agar Scientific Ltd., U.K.) were placed on polystyrene surfaces prior to plasma treatment. Grid #1 (Figure 4.2) was designed to allow demonstration of simple cellular patterns and to examine the fidelity of the pattern with AFM. Slots of various widths (5 μm to 75 μm) are separated by 200 μm bars. Grid #2 (Figure 4.3) was designed specifically to examine the effects of geometric control on cultured cells. The pattern consists of arrays of squares and rectangles, some smaller and some larger than the normal spreading area for BMSC (approximately 10 μm x 30 μm). The grids were removed prior to cell culture on patterned surfaces.

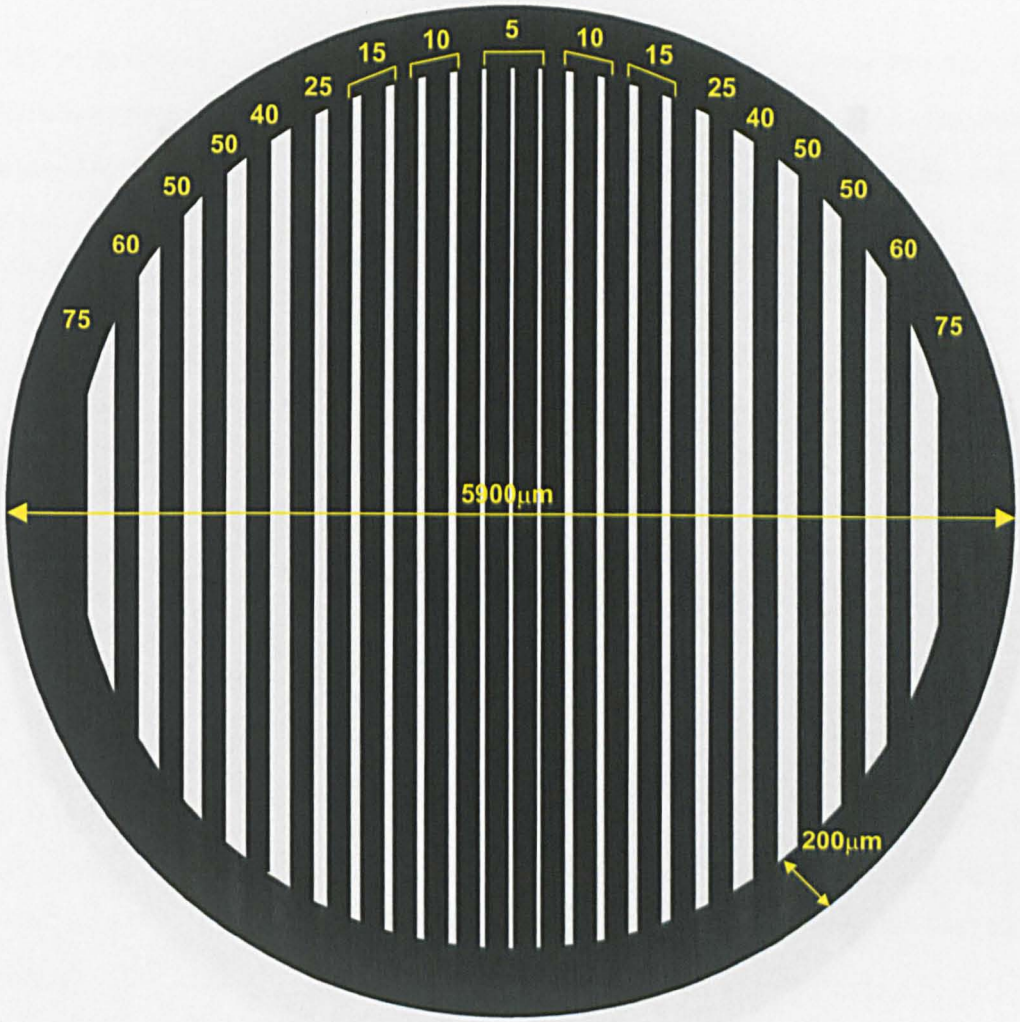

Figure 4.2: Schematic of custom designed copper TEM grid (#1) for patterning of cell culture substrates. Separating bars are 200 μm. All measurements are in microns. The drawing is not to scale.

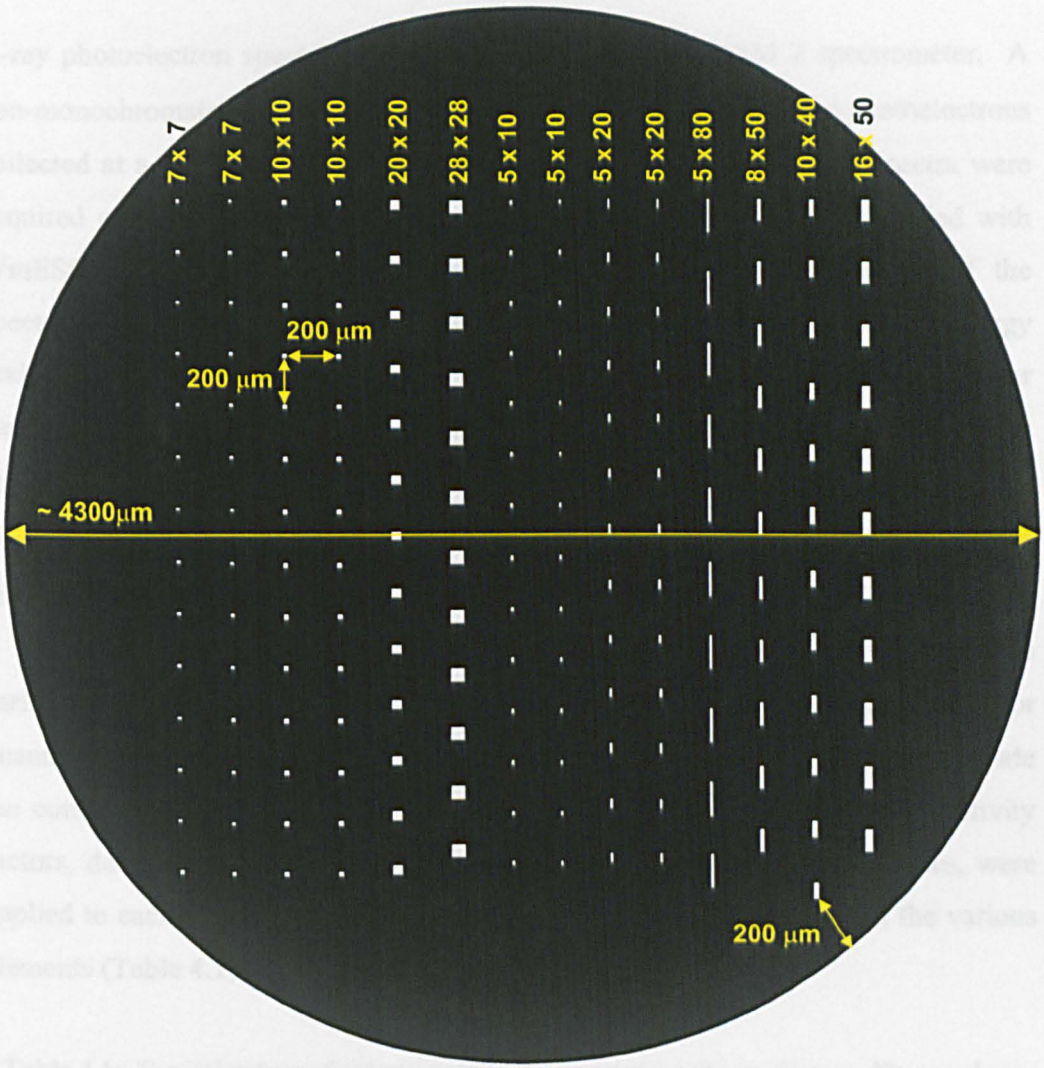

Figure 4.3: Schematic of custom designed copper TEM grid (#2) for patterning of cell culture substrates. All measurements are in microns. The drawing is not to scale.

4.4 Surface Analysis

4.4.1 X-ray Photoelectron Spectroscopy (XPS)

X-ray photoelectron spectra were obtained using a VG CLAM 2 spectrometer. A non-monochromated Mg Kα X-ray source was operated at 100W and photoelectrons collected at a standard take-off angle of 30° relative to the surface. Spectra were acquired on Spectra 6.0 software (R. Unwin Software, U.K.) and quantified with WinESCA software (Scienta Instruments, Sweden). Regular calibration of the spectrometer was performed by analysis of thin gold foil and PTFE. The energy scale was calibrated by scanning the Au $4f_{7/2}$ peak (84.00 eV) at differing analyser pass energies, checking that the peak positions from differing pass energies were convergent to ± 0.1 eV. Linearity of the binding energy scale was monitored by ensuring that the separation of the C_{1s} and F_{1s} peaks from PTFE was 397.19 ± 0.2 eV (Briggs, 1998).

Widescan spectra (binding energy range 0-1100 eV) were used to determine the surface elemental composition (excluding hydrogen). To calculate the peak areas for quantification purposes, a linear background was applied to each peak to eliminate the contribution from inelastically scattered electrons. Relative atomic sensitivity factors, determined experimentally by analysis of standard polymer samples, were applied to each peak to allow for differences in the level of detection of the various elements (Table 4.1).

Table 4.1: Typical values of experimentally determined sensitivity factors. These values are subject to change following each quarterly calibration of the instrument.

Element	Peak	Sensitivity factor
Carbon	C_{1s}	1.00
Oxygen	O_{1s}	2.52
Nitrogen	N_{1s}	1.56

From the peak areas, the percentage of each element is calculated. When considering the total level of surface modification, it is useful to express the result as the ratio of oxygen (plus nitrogen, if present) to carbon.

Narrow scan spectra were acquired for each 1s peak in the widescan. After application of a linear background, the C_{1s} peak was fitted with peaks corresponding to various carbon functionalities. The hydrocarbon peak (C-C/H) was set at 285 eV to correct for sample charging, before peaks representing suitable functionalities were fitted at the relative shifts shown in Table 4.2. Where appropriate, the proportions of the various components of the C_{1s} are reported as percentages.

Table 4.2: Binding energy shifts, relative to the hydrocarbon peak, employed in peak fitting of the C_{1s} core level.

Functionality	Shift (eV)
C-COOH/R	+ 0.7
C-OH/R	+ 1.5
C=O	+ 3.0
COOH/R	+ 4.5
π-π^*	+ 6.6

A description of the principles of XPS and the interpretation of spectra is presented in Appendix One.

4.4.2 Light Microscopy of Patterned Substrates

As a quick and simple method of visualising chemical patterns on substrates, differences in the wettability of the modified and unmodified regions of the pattern were exploited. The patterned samples were exposed to a humid atmosphere and photographed under a light microscope.

4.4.3 Friction Force Microscopy (FFM)

Friction force images of patterned substrates were obtained with a Digital Instruments Nanoscope IIIa Multimode atomic force microscope (Veeco, U.K.). Friction force data was collected using silicon nitride Nanoprobe cantilevers (nominal normal force constants 0.12 Nm^{-1}, Veeco, U.K.). The spring constants of individual cantilevers ranged from 0.10 – 0.14 Nm^{-1} and were determined using a resonance method integrated within the microscope software. Images were processed using SPIP (the Scanning Probe Image Processor, Image Metrology ApS, Denmark). The basic principles of FFM are outlined in Appendix Two.

4.5 Cell Culture and Assays

4.5.1 Preparation of BMSC Cultures

Bone marrow cells were obtained from tibiae and femurs of 125g male Wistar rats. The bones were removed under aseptic conditions and all soft adherent tissue removed. Proximal ends were removed and the bones placed in microfuge tubes supported by small plastic inserts and centrifuged at 2000 rpm for 5 seconds. Repeated pipetting dispersed the resulting cell clump and a single cell suspension was achieved by forcefully expelling the cells through a 21-gauge syringe needle. Microscopic analysis confirmed the single cell nature of the cell suspension. High density secondary BMSC cultures were generated by culturing primary cells at a density of 10^7 cells/cm^2 in T75 culture flasks with DMEM (Dulbecco's modified Eagle's medium) supplemented with 10% foetal calf serum, 1% Ultraglutamine and 1% penicillin/streptomycin, until confluent. The incubation atmosphere was humidified at 37°C, with 95% air and 5% CO_2.

Cell suspensions of 50,000 cells/ml were prepared and seeded on to plasma treated 24-well plates at 0.5ml per well. Tissue culture grade 24-well plates (Corning Incorporated, U.S.A.) and bacteriological grade 24-well plates (Iwaki, Japan) were used as positive and negative controls respectively. Incubation conditions were as above. The culture media was changed on days 2, 5, 7, 9 and 12 of each 15 day experiment.

4.5.2 Cell Morphology Stain

Methylene blue is a general stain for the nucleus and cytoskeleton. The culture medium was removed, cells washed in PBS, fixed in 4% paraformaldehyde solution and rinsed with PBS again. Sufficient methylene blue to completely cover the cells was added to each well and left at room temperature for 5 minutes. Stained cultures were washed with tap water and photographed under a light microscope.

4.5.3 Cell Proliferation/Vitality Assay

Cell proliferation was measured with Alamar Blue, a large molecule that is broken down by mitochondrial enzymes, producing a colour change from blue to pink. Thus, measurement of this colour change indicates the relative number of active mitochondria and hence the quantity and vitality of the cells.

Alamar Blue (Serotec Ltd., U.K.) was added to cell cultures and "blanks" (media only) at a concentration of 10 vol.% (*i.e.* 50 µl) and incubated for 3.5 hours. Triplicate aliquots of 100 µl were then removed from each well and transferred to a 96 well plate. The plate was read with a Dynatech (U.K.) MRX II spectrophotometer at 570 nm. To account for background staining, the intensity of the blanks was removed from the intensity of each measurement.

4.5.4 Alkaline Phosphatase Assay

Alkaline phosphatases are enzymes, which, under alkaline conditions, cleave phosphate groups from molecules in many key biochemical reactions. Quantitative measurement of the alkaline phosphatase level in BMSC cultures was performed with a colorimetric assay using ρ-nitrophenyl phosphate (Sigma 104, Sigma-Aldrich Company Ltd., U.K.) as the (colourless) substrate. Alkaline phosphatase cleaves the phosphate group from the substrate to produce ρ-nitrophenol, which is yellow in colour. Culture media was removed and cells washed with PBS. 0.5 ml of a 1mg/ml solution of Sigma 104 in 20 mM Tris buffer was placed in each well and left at room temperature for 1.5 hours. Triplicate aliquots of 100 µl from each well were transferred to a 96 well plate along with "blanks" (solution only) and read at 405 nm in the spectrophotometer described above.

Histochemical analysis of alkaline phosphatase levels was performed by reaction with α-naphthol AS-BI phosphate (Sigma-Aldrich Company Ltd., U.K.), a colourless substrate, which is broken down to naphthol (also colourless) by alkaline phosphatase. Naphthol is not soluble in the aqueous environment, so precipitates at the site where the enzyme is located. The distribution of alkaline phosphatase is then visualised by coupling a dye, such as Fast Red TR, to the naphthol precipitates.

After the culture media was removed, cells were washed with PBS and briefly fixed (30 seconds) in 4% paraformaldehyde solution. 1 mg/ml of Fast Red (Sigma-Aldrich Company, Ltd. U.K.) was added to a solution of 50 μg/ml α-naphthol AS-BI phosphate in 20 mM Tris buffer. 0.5 ml of this solution was placed in each well and left at room temperature for 1.5 hours. Stained cultures were digitally photographed under a light microscope.

4.5.5 Total Collagen Assay

The total collagen content of BMSC cultures was determined using Sirrius Red (Sigma-Aldrich Company Ltd., U.K.), dissolved at 1 mg/ml in saturated picric acid. The culture media was removed, cells were washed with PBS and then fixed in 4% paraformaldehyde solution. 0.5 ml of Sirrius Red solution was placed in each well and left for 1.5 hours at room temperature. For qualitative analysis, cells were washed thoroughly and photographed under a light microscope. For quantitative analysis, bound Sirrius Red was eluted from washed cells by adding 200 μl of a 50/50 mixture of 0.2 M NaOH and methanol to each well. Triplicate aliquots of 100 μl from each well were transferred to a 96 well plate and read in the spectrophotometer at 570 nm.

4.5.6 Statistical Methods

Quantitative data from the cell vitality/proliferation, alkaline phosphatase and total collagen assays was analysed statistically with one-way analysis of variance (ANOVA) and multiple comparison post hoc tests, performed using SPPS for Windows© version 11.5. A description of the procedure, along with an example illustrating interpretation of the results is provided in Appendix Three.

Chapter Five

Results I: Surface Modification of Polystyrene in a Novel Plasma Source

The aims of this section of work were:

- to develop an argon plasma treatment system in which independent control over the ion energy and flux could be achieved
- to use this 'tailored' plasma to investigate the role of ions in the surface modification of polystyrene

This chapter presents and discusses the results of initial experiments where independent control over the ion flux and ion energy to the substrate was achieved using a single biased mesh to separate the main plasma from the process plasma. In these initial experiments, it was necessary to change multiple variables simultaneously in order to gain such control. Therefore, the novel plasma source was improved by development of a double-meshed discharge, which allowed independent control over the ion energy and flux by changing only the applied mesh biases. This double-meshed discharge was subsequently used to investigate the relative contributions of ions and VUV photons during argon plasma treatment of polystyrene.

5.1 Evaluation of Errors

To assess the error involved in chemical quantification and the setting of global plasma parameters (*i.e.* input power, gas pressure, grid bias), five samples of polystyrene were subjected to nominally identical treatments and analysed by XPS. The calculated elemental ratios are presented in Table 5.1. The standard deviation is 0.01, indicating a high level of reproducibility; this value is applied to all the XPS data presented in the next sections and in Chapter 6 (in general, the error bars are not shown on graphs).

Table 5.1: Elemental quantification results for five samples subjected to identical treatments. Gas pressure = 20 mTorr, input power = 20 W, exposure time = 90s, sample position = 15 mm from the mesh. Mean = 0.13; standard deviation = 0.01.

Sample	% O	% C	O/C
1	11.0	89.0	0.12
2	9.9	90.1	0.11
3	11.4	88.6	0.13
4	12.4	87.6	0.14
5	12.3	87.7	0.14

5.2 Treatment in a Single-Meshed Discharge

5.2.1 Characterisation of the Plasma

In order to achieve independent control over the ion flux and ion energy, a single biased mesh was used to separate the main plasma from the process region (see Section 2.4). The ion energy distribution function, plasma potential, plasma density and electron temperature were measured using electrical probes for various applied mesh biases and main plasma input powers. Figure 5.1 illustrates how the electron temperature and electron (plasma) density in the process region are controlled by both the input power to the main plasma and the applied mesh bias. Figure 5.2 shows the spatial variation of the electron temperature and density within the process plasma for various mesh biases. In both figures, the values of T_e and N_e are normalised to the peak values, T_{e0} and N_{e0}.

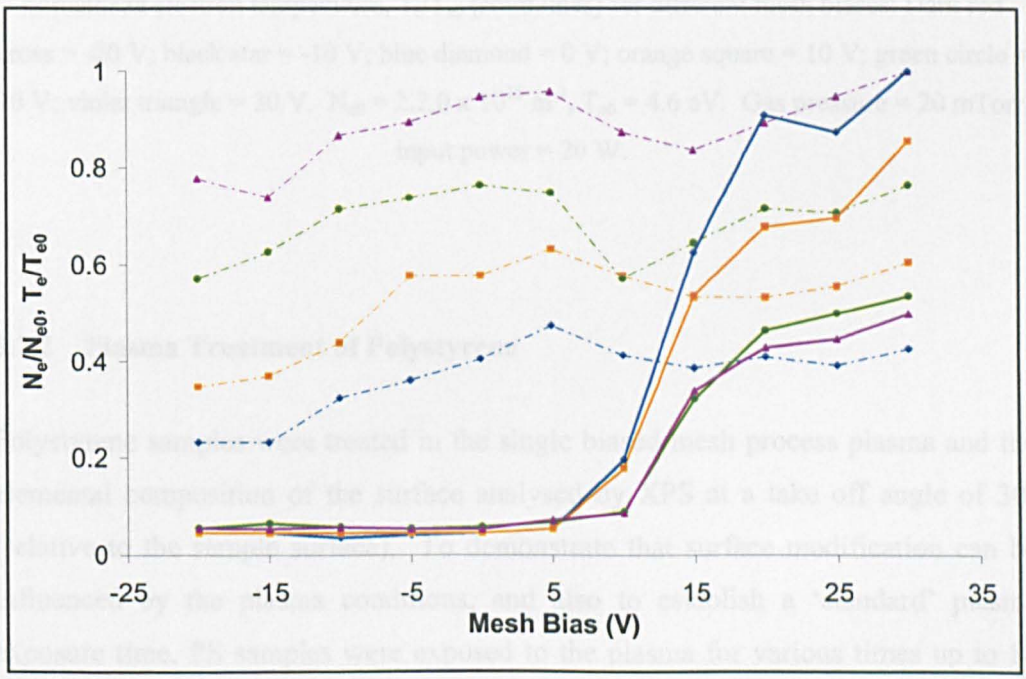

Figure 5.1: Normalised plasma density, N_e/N_{e0} (dotted lines) and normalised electron temperature, T_e/T_{e0} (solid lines) for different input powers: blue diamond = 5 W; orange square = 10 W; green circle = 20 W; violet triangle = 30 W. $N_{e0} = 3.0 \times 10^{15}$ m^{-3}, $T_{e0} = 5.6$ eV. All measurements were recorded at 8 mm from the mesh. Gas pressure = 20 mTorr.

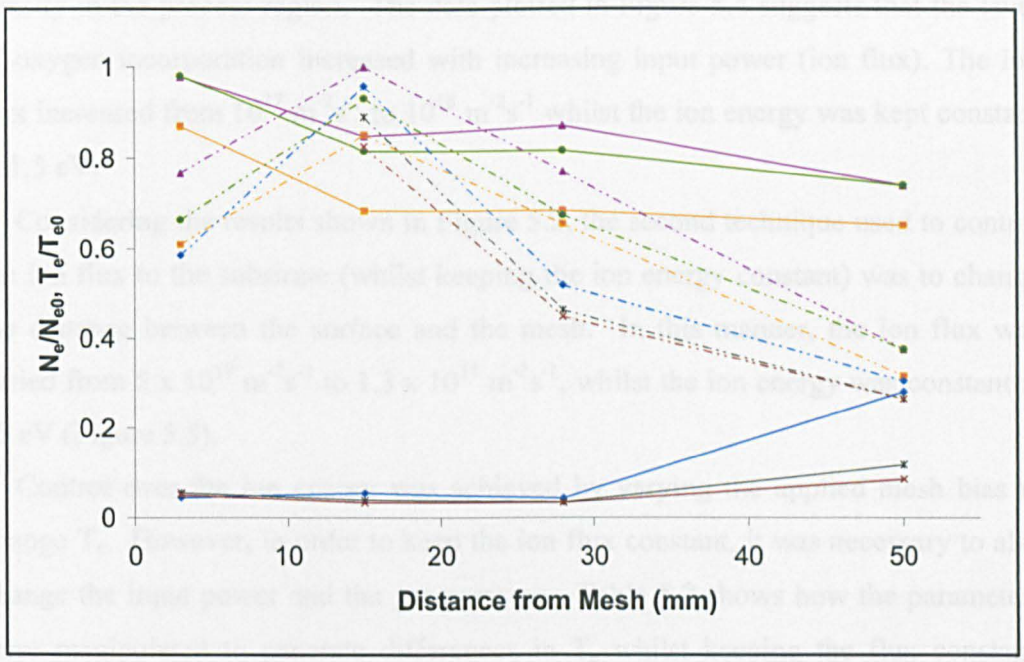

Figure 5.2: Spatial variation of normalised plasma density, N_e/N_{e0} (dotted lines) and normalised electron temperature, T_e/T_{e0} (solid lines) for different mesh biases: Dark red cross = -20 V; black star = -10 V; blue diamond = 0 V; orange square = 10 V; green circle = 20 V; violet triangle = 30 V. N_{e0} = 2.2.0 x 10^{15} m^{-3}, T_{e0} = 4.6 eV. Gas pressure = 20 mTorr, input power = 20 W.

5.2.2 Plasma Treatment of Polystyrene

Polystyrene samples were treated in the single biased mesh process plasma and the elemental composition of the surface analysed by XPS at a take off angle of 30° (relative to the sample surface). To demonstrate that surface modification can be influenced by the plasma conditions, and also to establish a 'standard' plasma exposure time, PS samples were exposed to the plasma for various times up to 80 seconds. The percentage of oxygen introduced into PS surface by plasma treatment increased with exposure time (Figure 5.3). No saturation level was reached within the time frame investigated.

Based on the results shown in Figure 5.1, the first technique used to control the ion flux was to increase the input power to the main plasma, thus varying the plasma

density in the process region. The data plotted in Figure 5.4 suggests that the level of oxygen incorporation increased with increasing input power (ion flux). The ion flux increased from 10^{17} $m^{-2}s^{-1}$ to 10^{18} $m^{-2}s^{-1}$ whilst the ion energy was kept constant at 1.5 eV.

Considering the results shown in Figure 5.2, the second technique used to control the ion flux to the substrate (whilst keeping the ion energy constant) was to change the distance between the surface and the mesh. In this manner, the ion flux was varied from 5 x 10^{18} $m^{-2}s^{-1}$ to 1.3 x 10^{18} $m^{-2}s^{-1}$, whilst the ion energy was constant at 15 eV (Figure 5.5).

Control over the ion energy was achieved by varying the applied mesh bias to change T_e. However, in order to keep the ion flux constant, it was necessary to also change the input power and the gas pressure. Table 5.2 shows how the parameters were manipulated to generate differences in T_e whilst keeping the flux constant. Figure 5.6 would suggest that the increase in ion energy caused a decrease in the level of surface modification of PS.

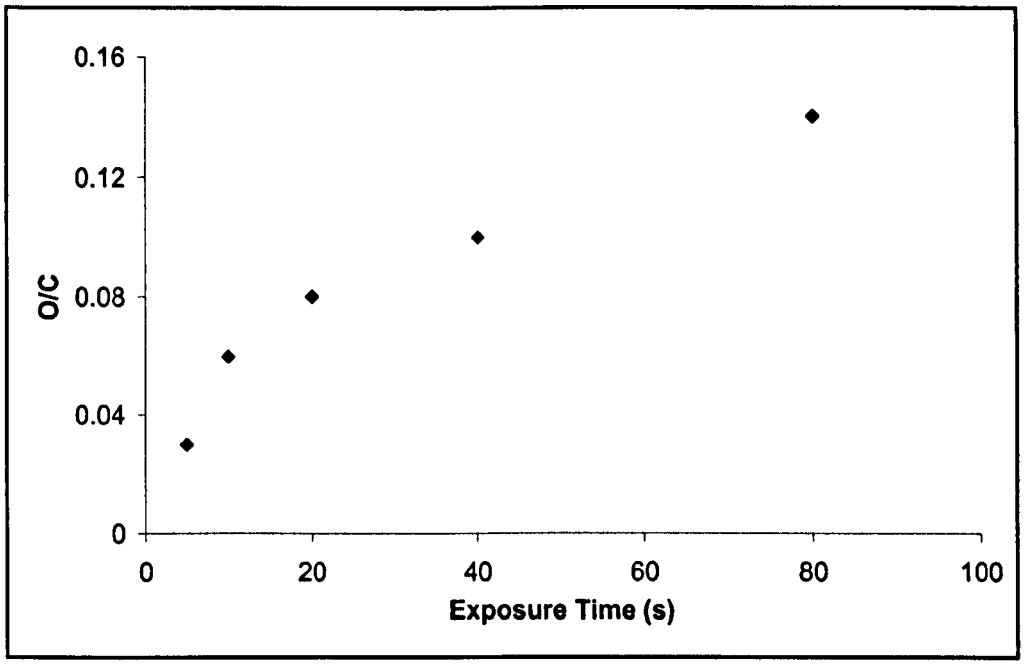

Figure 5.3: Effect of exposure time on the oxygen/carbon ratio of plasma treated polystyrene. The ion energy and flux were kept constant. Gas pressure = 20 mTorr, input power = 20 W, sample position = 15 mm from the mesh, V_{mesh} = 0 V.

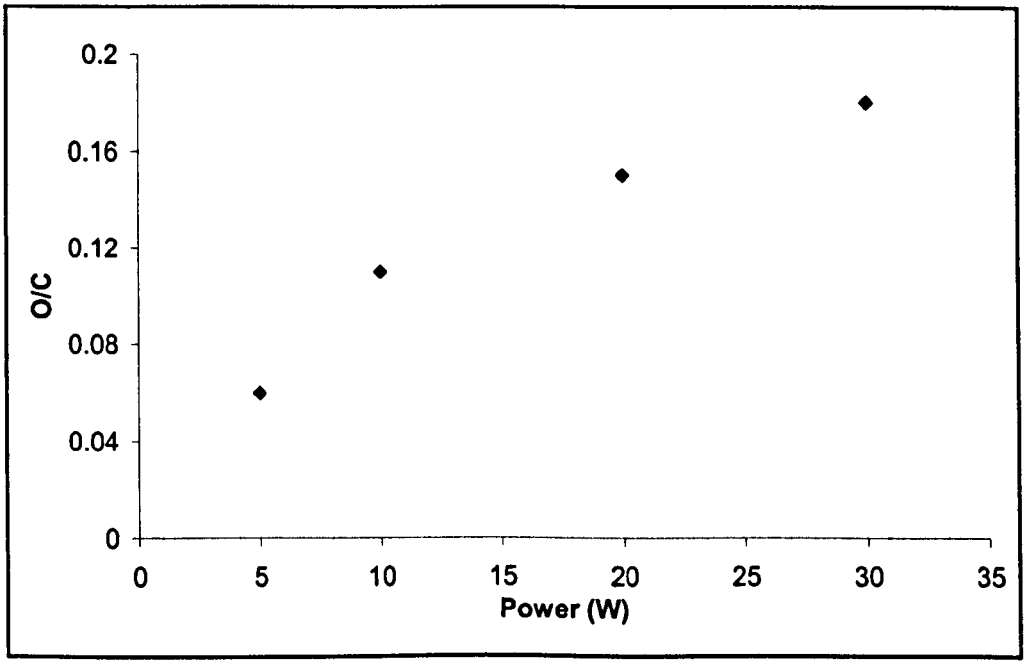

Figure 5.4: Effect of increasing input power on the oxygen/carbon ratio of plasma treated polystyrene. The ion energy was kept constant as the ion flux was varied. Gas pressure = 20 mTorr, exposure time = 30 s, sample position = 15 mm from mesh, V_{mesh} = 5 V.

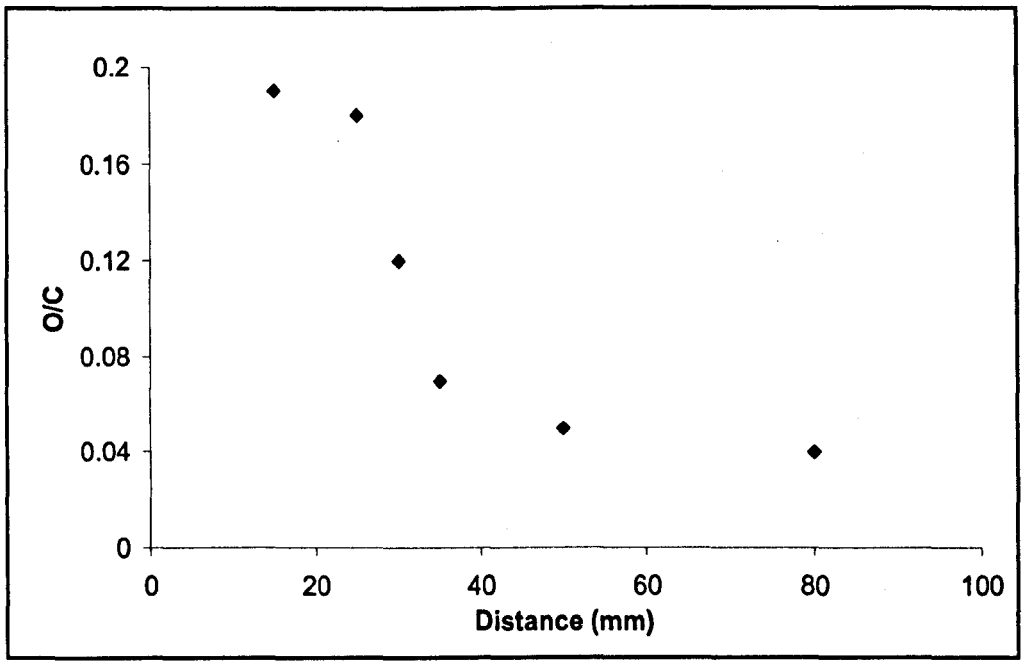

Figure 5.5: Effect of increasing distance from the main plasma source on the oxygen/carbon ratio of plasma treated polystyrene. The ion energy was kept constant whilst the ion flux was varied. Gas pressure = 20 mTorr, input power = 20 W, exposure time = 30 s, V_{mesh} = 10 V.

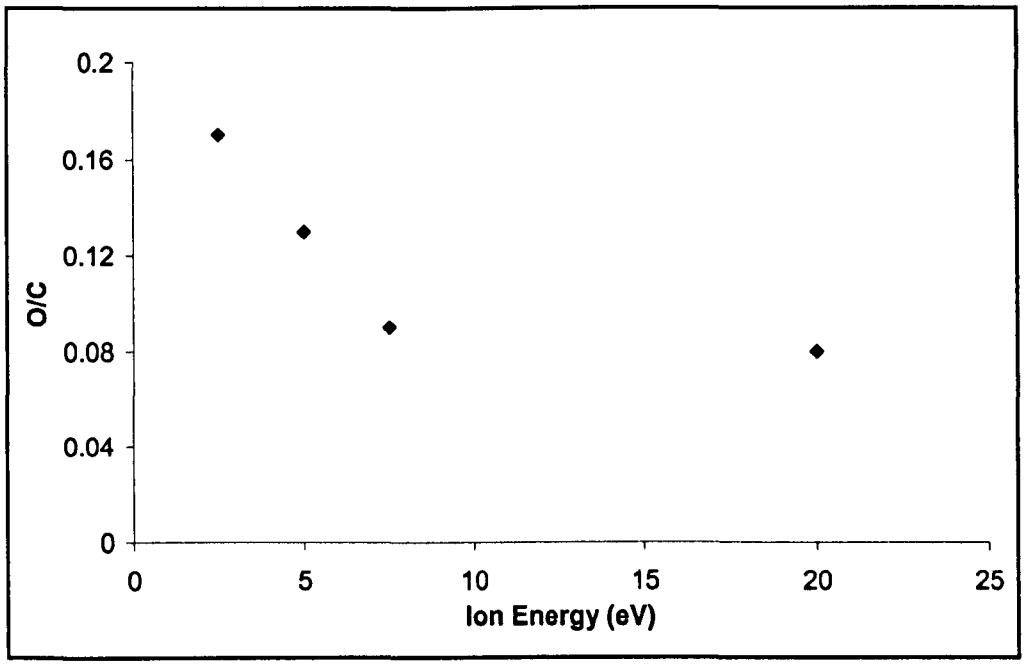

Figure 5.6: Effect of ion energy on the oxygen/carbon ratio of plasma treated polystyrene. The ion energy was varied whilst the ion flux was kept constant by changing the mesh bias, input power and gas pressure (see Table 5.2). Exposure time = 30 s, sample position = 15 mm from mesh.

Table 5.2: Process plasma conditions used to manipulate the electron temperature and the corresponding oxygen/carbon ratio for polystyrene treated in the plasma.

Power (W)	Gas Pressure (mTorr)	Mesh Bias (V)	T_e (eV)	O/C
5	30	25	3.8	0.08
10	30	10	1.5	0.09
10	20	10	1.0	0.13
30	20	5	0.4	0.17

5.2.3 Discussion

A single biased mesh has been used to separate an electrically excited main argon plasma from a diffuse process plasma. The application of a DC bias to the mesh influenced the proportion of the electron energy distribution that was able to penetrate from the main plasma into the polymer processing discharge. Thus, the electron temperature and electron density in the process plasma were controlled. As stated in Section 2.1.1.4, the electron temperature and sheath potential are related by Equation 2.2:

$$V_s = \frac{kT_e}{2e} \ln\left(\frac{m_e}{2.3m_i}\right) \qquad 2.2$$

where

V_s = the sheath potential,

k = Boltzmann's constant,

T_e = the electron temperature,

m_e = the mass of an electron,

m_i = the mass of the ions.

Thus, control over the electron temperature in the process plasma results in control over the sheath bias at the substrate and hence the maximum ion energy arriving at the surface. Moreover, Equation 5.1 relates the electron temperature and the plasma density to the ion flux, Γ:

$$\Gamma = \exp^{-\frac{1}{2}} n_e \left(\frac{kT_e}{m_i}\right)^{\frac{1}{2}} \qquad 5.1$$

where n_e = the number density of electrons.

Using this control over the electron temperature and density, the ion energy and ion flux to the substrate were 'tailored' in an attempt to clarify the role of ions in the argon plasma treatment of polystyrene. The process plasma was characterised using various probe measurements. The data presented in Figure 5.1 shows the effect of applied mesh bias on the electron temperature and electron density (plasma density) of the process plasma. In accordance with results from other workers (*e.g.* Bai *et al.*, 2001; Hong *et al.*, 1999; Kato *et al.*, 1994), three regions can be identified in the graph. At applied mesh biases of 20 V and above, the electron temperature and plasma density remain essentially constant with changes in V_{mesh}. At applied mesh biases between 5 V and 20 V, a large decrease in the electron temperature is apparent. In these conditions, the density decreases until very low electron temperatures are reached, at which secondary ionisation processes occur and cause an increase in the density. For mesh biases of 5 V and less, a very low electron temperature is achieved for all input powers (although it is not affected by mesh bias) and the density decreases further with mesh bias. Here, the ion flux can be changed, without having any effect on the ion energy, by varying the input power. Thus this region is particularly suitable for independent variation of ion flux at constant electron temperature. In Figure 5.2, the spatial variation of T_e and N_e within the process plasma is illustrated. In agreement with Hong *et al.* (1999), the electron temperature remains fairly constant with downstream distance for all the mesh biases investigated. However the plasma density peaks at 15 mm from the mesh and then decreases rapidly from this point, as plasma is lost to the walls through diffusion. The peak may correspond to the mean-free-path for electron impact ionisation of electrons emerging from the mesh, which has been calculated at about 20 mm for these discharge conditions (Liebermann & Lichtenberg, 1994). These results suggest that the ion flux to the substrate can be varied by at least 60 % whilst the ion energy (electron temperature) remains constant. Once again this demonstrates the suitability of this discharge for controlled polymer processing.

The two-stage plasma discharge was utilised in an attempt to investigate the effects of ion energy and flux on the surface modification of polystyrene. The level of oxygen incorporation was ascertained by XPS and possible relations to the processing conditions were identified. Figure 5.3 shows the effect of exposure time

in the process plasma on the level of oxygen incorporation (all other parameters were constant in this experiment). Initially, the oxygen to carbon ratio increases rapidly with treatment time. The rate of oxygen incorporation then decreases, although no saturation level was reached. This could be explained by the kinetics typically observed as such a reaction progresses *i.e.* as the exposure time increases, fewer pristine sites on the surface are available for reaction.

The effect of ion flux was investigated independently from ion energy by two methods. Firstly, by applying a mesh bias of 5 V, the electron temperature (and therefore ion energy) can be kept constant and low (T_e = 0.3 eV, ion energy ≈ 1.5 eV), whilst operating the main plasma at different input powers can change the plasma density, and therefore ion flux (Figure 5.1). From the data it appears that increasing the ion flux in this manner caused a significant increase in the concentration of oxygen detected in the polystyrene surface by XPS (Figure 5.4). The second method of controlling the ion flux is by simple variation of the substrate position in relation to the main plasma source. Figure 5.2 suggests that the electron temperature remains relatively constant with distance from the mesh, whereas the plasma density decreases rapidly beyond 15 mm. The effect of the corresponding change in ion flux on the surface modification of polystyrene is evident in Figure 5.5, which suggests an initially rapid decrease in the oxygen to carbon ratio with distance that flattens beyond 50 mm.

Investigation of the effect of ion energy at constant ion flux was more complex. The electron temperature can be controlled by changing the mesh bias or by changing the input power. However, changing either of these parameters also changes the plasma density, and hence the ion flux. Therefore, in order to achieve different ion energies without changing the ion flux, manipulation of three parameters *i.e.* mesh bias, input power and gas pressure is necessary. Figure 5.6 would indicate that ion energy does exert an effect on the level of surface modification of polystyrene; the oxygen to carbon ratio decreases as the ion energy increases. However, varying three parameters simultaneously is not an ideal experimental situation and it is possible that the chemistry of the plasma is significantly different at each data point.

In order to continue investigations into the influence of ion energy and ion flux on the surface modification of polystyrene, the double-mesh system described in Section 2.4 was designed. This arrangement allows independent variation of the ion energy and ion flux in the process plasma by changing the mesh biases alone. The results of polymer processing experiments using this double-mesh discharge are presented and discussed in Section 5.3.

5.2.4 Conclusions

The stated aims of this Chapter were:

- to develop an argon plasma treatment system in which independent control over the ion energy and flux could be achieved
- to use this 'tailored' plasma to investigate the role of ions in the surface modification of polystyrene

In relation to these aims, the following conclusions may be extracted from the results and discussion presented above:

- Independent control over ion energy and flux to the substrate can be achieved by use of a single biased mesh to separate the main plasma from the process plasma.
- Many variables must be changed simultaneously in order to achieve such control in the single-meshed discharge; this may change the nature of the plasma and thus prevents the relation of changes in ion flux and energy to changes in the modification of the polymer surface.

5.3 Treatment in a Double-Meshed Discharge

5.3.1 Characterisation of the Plasma

The single-meshed discharge described above was improved by introducing a second biased mesh. This double-meshed arrangement allows independent variation of the ion energy and ion flux in the process plasma by changing only the applied mesh biases. The electron temperature, plasma density, plasma potential and ion flux were measured using electrical probes for various applied mesh biases at constant input power, gas pressure and distance from the mesh. The effects of V_{mesh1} and V_{mesh2} on the intrinsic parameters were investigated by initially by keeping V_{mesh1} constant whilst varying V_{mesh2} and then *vice versa*. Control over these intrinsic plasma properties was achieved using the mesh biases, as demonstrated with the examples of electron temperature and plasma density in Figure 5.7.

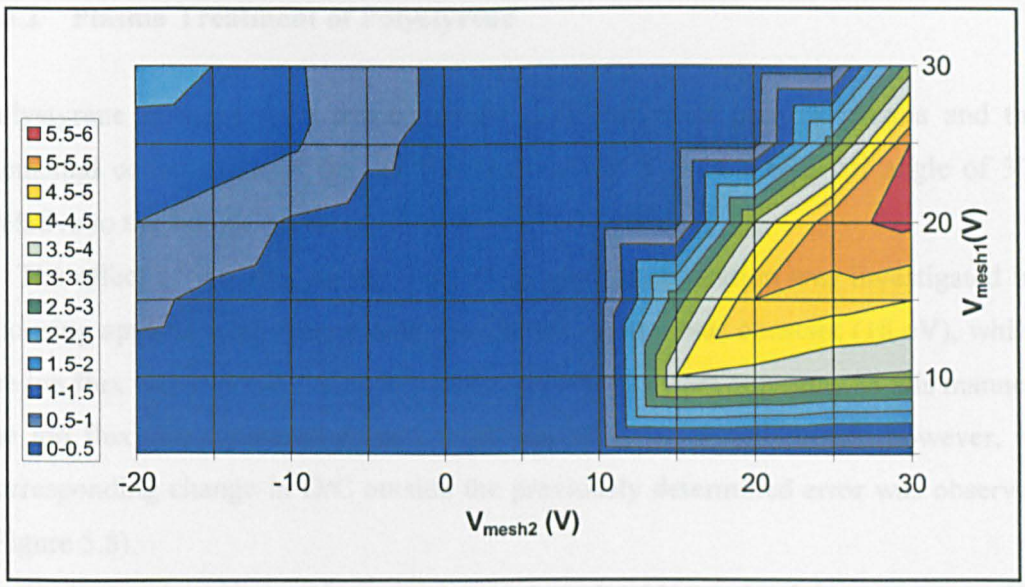

Figure 5.7a: Contour plot of electron temperature, T_e (eV), in the process plasma with variation of V_{mesh1} and V_{mesh2}. All measurements were recorded at 15 mm from mesh 2. Gas pressure = 20 mTorr, input power = 20 W.

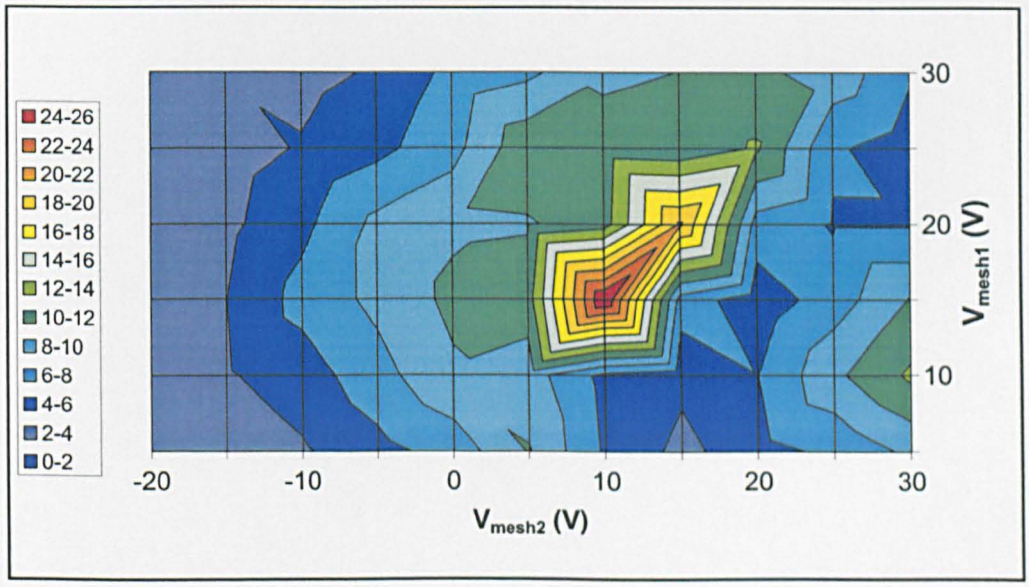

Figure 5.7b: Contour plot of plasma density, N_e (10^{14} m^{-3}), in the process plasma with variation of V_{mesh1} and V_{mesh2}. All measurements were recorded at 15 mm from mesh 2. Gas pressure = 20 mTorr, input power = 20 W.

5.3.2 Plasma Treatment of Polystyrene

Polystyrene samples were treated in the double-meshed process plasma and the elemental composition of the surface analysed by XPS at a take off angle of 30° (relative to the sample surface).

The effect of ion flux on the level of oxygen incorporation was investigated by choosing applied mesh biases such that the ion energy was constant (18 eV), whilst the ion flux was variable. All other global parameters were constant. In this manner, the ion flux was increased from 2 x 10^{18} $m^{-2}s^{-1}$ to 5.1 x 10^{18} $m^{-2}s^{-1}$; however, no corresponding change in O/C outside the previously determined error was observed (Figure 5.8).

Similarly, the effect of ion energy was examined by maintaining a constant ion flux of 3 x 10^{18} $m^{-2}s^{-1}$, whilst varying the ion energy from 1.3 eV to 25 eV. Again, all other global parameters were constant. This large variation in ion energy had no discernable effect on the level of oxygen incorporation into the polystyrene surface (Figure 5.9).

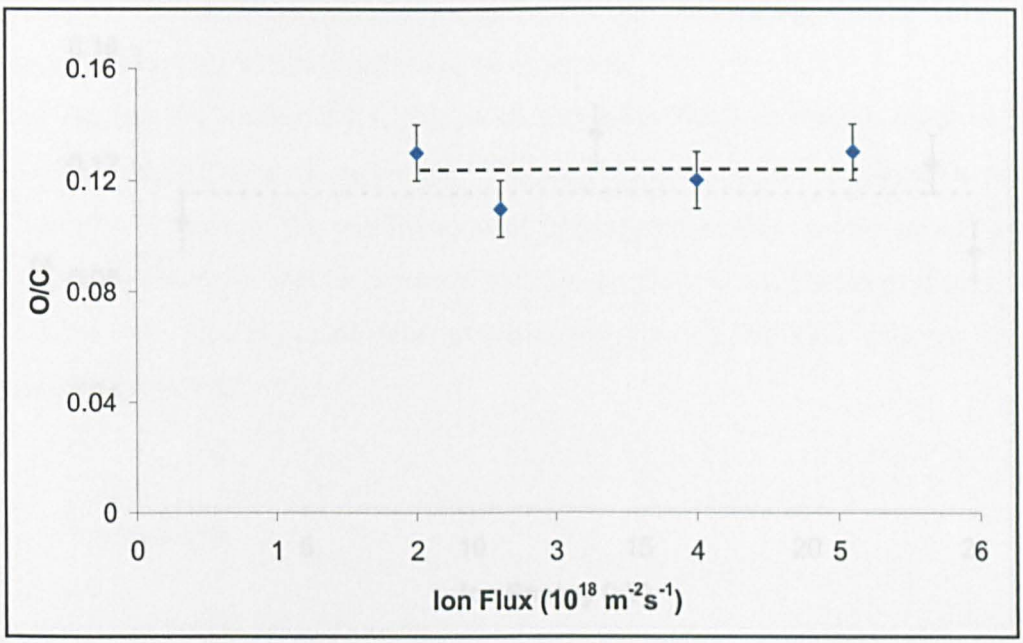

Figure 5.8: Effect of ion flux, at constant ion energy of 18 eV, on the oxygen/carbon ratio of plasma treated polystyrene. Gas pressure = 20 mTorr, input power = 20 W, exposure time = 90 s, sample position = 15 mm from mesh 2. Error bars are the standard deviation calculated in Section 5.1.

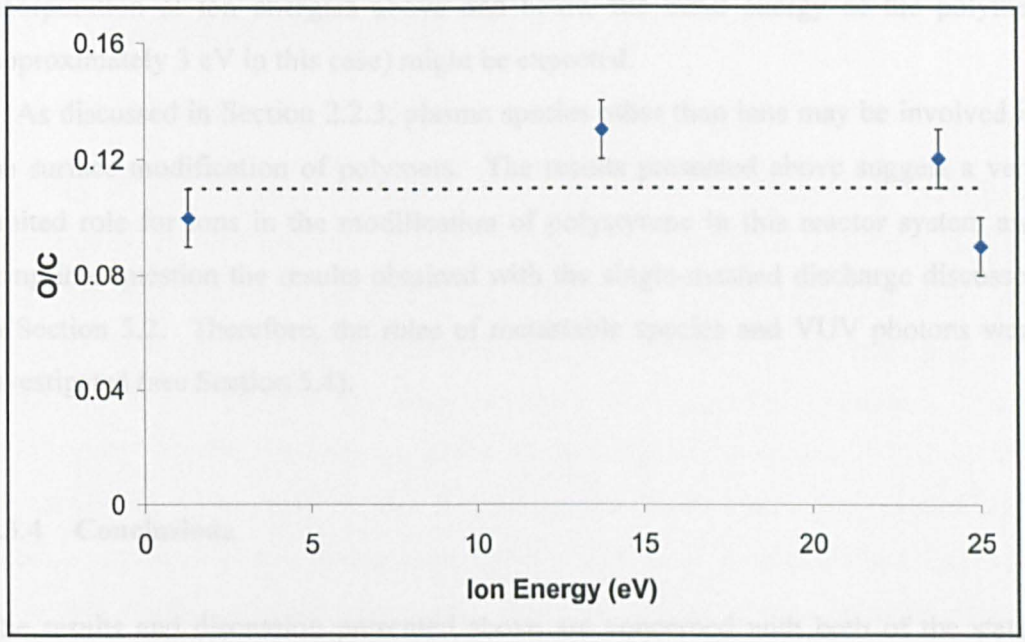

Figure 5.9: Effect of ion energy, at constant ion flux of 3 x 10^{18} $m^{-2}s^{-1}$, on the oxygen/carbon ratio of plasma treated polystyrene. Gas pressure = 20 mTorr, input power = 20 W, exposure time = 90 s, sample position = 15 mm from mesh 2. Error bars are the standard deviation calculated in Section 5.1.

5.3.3 Discussion

A diffuse process plasma has been separated from the main argon plasma by two DC biased meshes. As illustrated in Figure 5.7, variation of the applied biases has allowed independent control over the ion energy and flux in the processing region, without the need to change any other global plasma parameters. When V_{mesh2} >10 V, the electron temperature is very responsive to changes in both mesh biases, as shown by the many contour lines on the right hand side of Figure 5.7a. However, when V_{mesh2} <10 V, there is a range of mesh biases which result in a very low electron temperature (<0.05 eV). The plasma density is most responsive to V_{mesh1} when V_{mesh2} is in the range 5 V to 20 V (Figure 5.7b). However, Figures 5.8 and 5.9 demonstrate that the level of oxygen incorporation caused by the plasma treatment is not strongly influenced by either of these two variables. If ions were the primary source of modification within the plasma, a significant difference in oxygen

incorporation at ion energies above and below the bond energy of the polymer (approximately 3 eV in this case) might be expected.

As discussed in Section 2.2.3, plasma species other than ions may be involved in the surface modification of polymers. The results presented above suggest a very limited role for ions in the modification of polystyrene in this reactor system and bring into question the results obtained with the single-meshed discharge discussed in Section 5.2. Therefore, the roles of metastable species and VUV photons were investigated (see Section 5.4).

5.3.4 Conclusions

The results and discussion presented above are concerned with both of the stated aims of this Chapter, these being:

- to develop an argon plasma treatment system in which independent control over the ion energy and flux could be achieved
- to use this 'tailored' plasma to investigate the role of ions in the surface modification of polystyrene

Thus, the following conclusions are drawn:

- By use of the double-meshed technique, independent control over the ion flux and the ion energy can be achieved by manipulating only the applied mesh biases.
- In this particular plasma reactor system, the role of ions in the modification of polystyrene is very limited and investigations of the function of other species *i.e.* VUV photons and metastables is justified.

5.4 Treatment with VUV

5.4.1 Characterisation of the Source

The role of VUV photons and metastables species was investigated by excluding ions from the process chamber. Figure 5.10 illustrates how the ion saturation current in the process chamber varies with V_{mesh2}, when V_{mesh1} is held constant at 10 V. At V_{mesh2} = -60V the ion saturation current has fallen almost to zero, indicating that practically no ions are passing through into the process region of the reactor. These 'VUV only' conditions were employed to investigate the role of VUV in the processing of polystyrene in this reactor system. (*N.B.* Uncharged species *e.g.* neutrals, metastables are also present under 'VUV only' conditions and they are taken into account in a later experiment. The term 'whole' plasma refers to plasma in which no attempt to control the types of species has been made.)

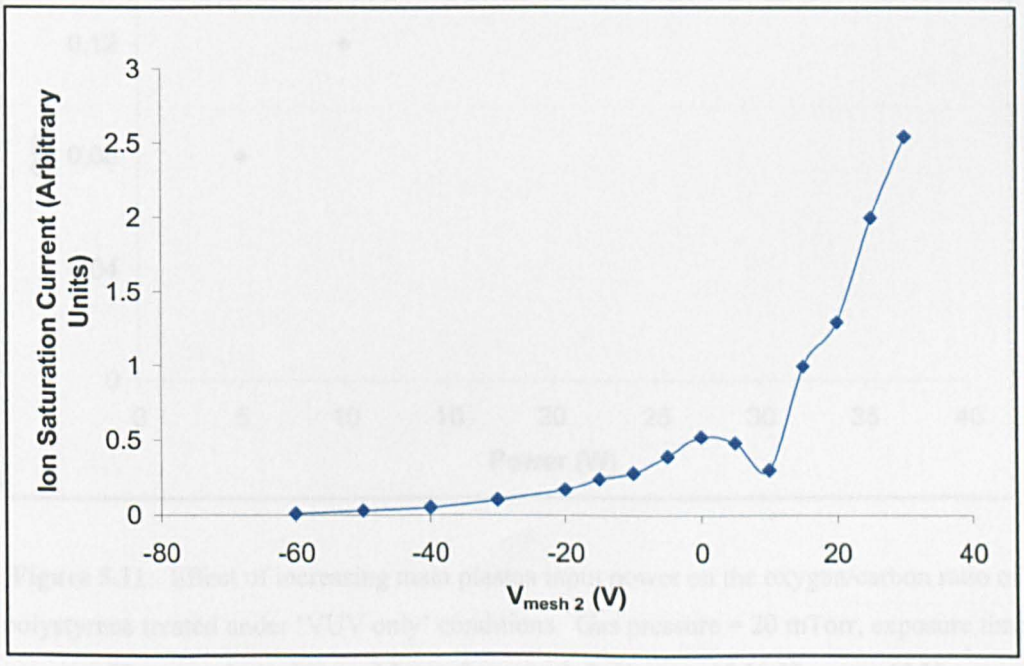

Figure 5.10: Effect of V_{mesh2} on the ion saturation current in the process chamber. V_{mesh1} = 10 V.

5.4.2 Treatment of Polystyrene

By employing the mesh bias conditions described above, polystyrene samples in the process chamber were exposed to the VUV radiation from the main argon plasma. The concentration of oxygen incorporated due to the treatment was measured by XPS at a take of angle of 30° relative to the sample surface.

Changing the input power in the main plasma controlled the VUV flux, which affected the percentage of oxygen incorporated into the PS sample in the process region. The oxygen/carbon ratio increased with input power until a plateau was reached at 20 W (Figure 5.11). Typical XPS widescan spectra for samples treated at 5 W (O/C = 0.08) and 40 W (O/C = 0.14) are presented in Figure 5.12.

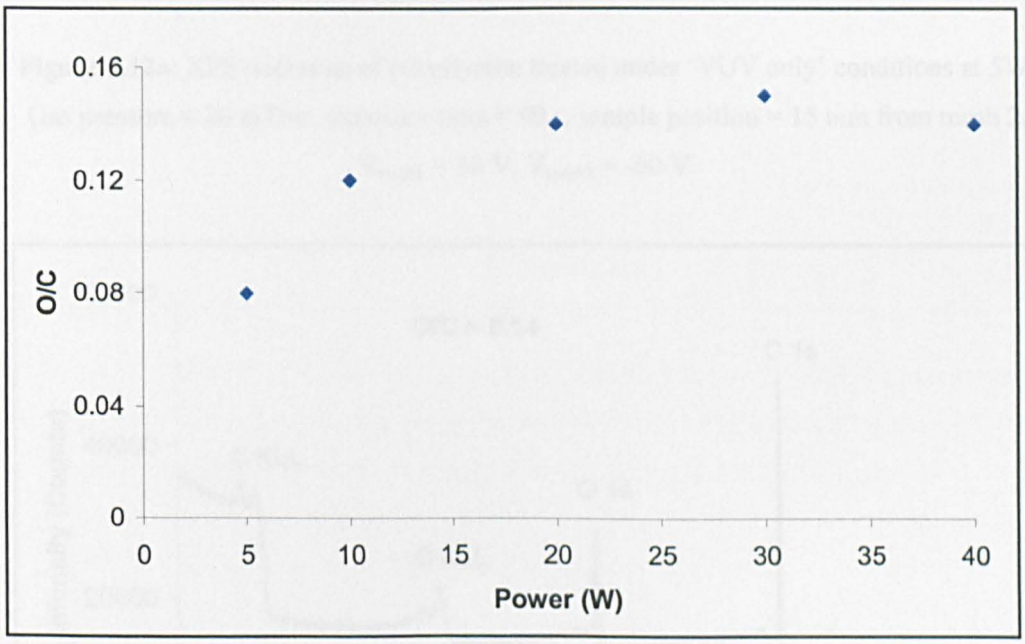

Figure 5.11: Effect of increasing main plasma input power on the oxygen/carbon ratio of polystyrene treated under 'VUV only' conditions. Gas pressure = 20 mTorr, exposure time = 90 s, sample position = 15 mm from mesh 2, V_{mesh1} = 10 V, V_{mesh2} = -60 V.

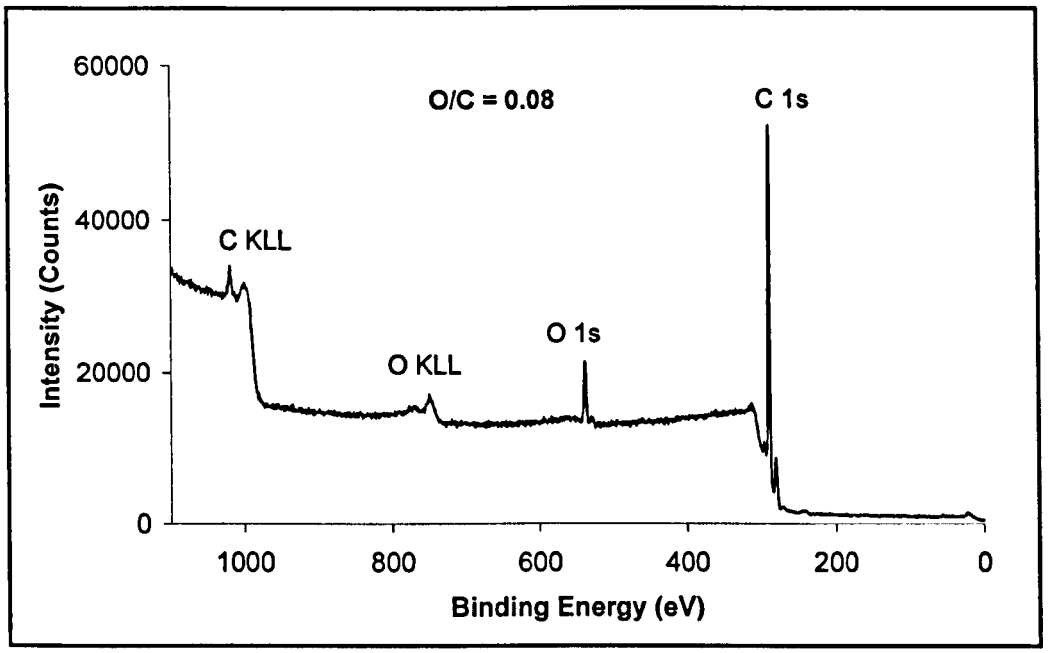

Figure 5.12a: XPS widescan of polystyrene treated under 'VUV only' conditions at 5W. Gas pressure = 20 mTorr, exposure time = 90 s, sample position = 15 mm from mesh 2, V_{mesh1} = 10 V, V_{mesh2} = -60 V.

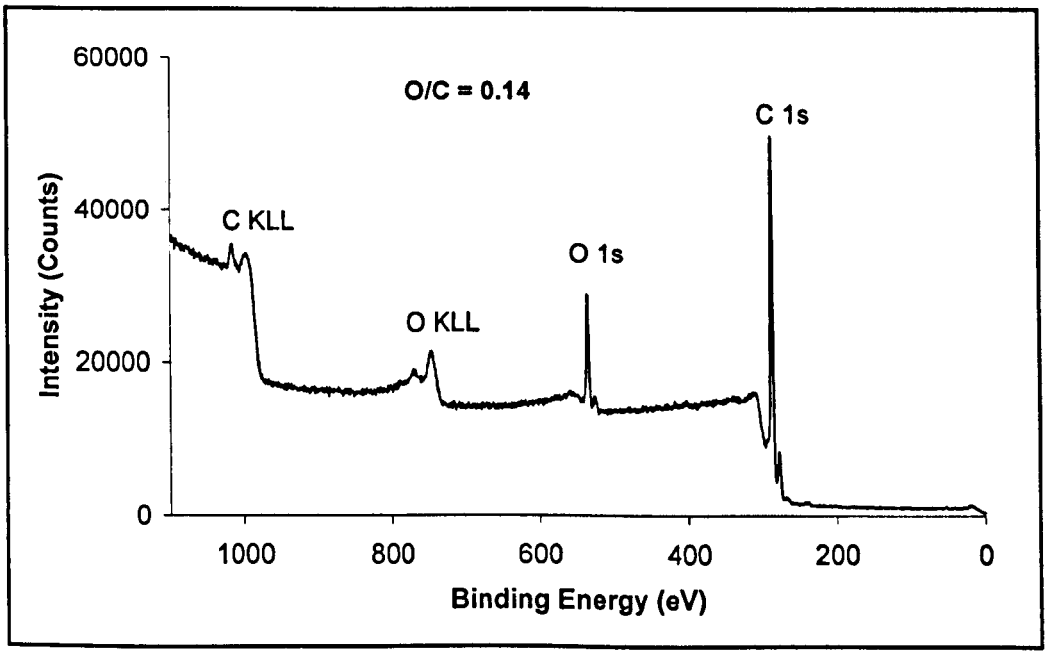

Figure 5.12b: XPS widescan of polystyrene treated under 'VUV only' conditions at 40 W. Gas pressure = 20 mTorr, exposure time = 90 s, sample position = 15 mm from mesh 2, V_{mesh1} = 10 V, V_{mesh2} = -60 V.

The second method of changing the VUV flux to the substrate was simply to vary the distance between the source and the sample. Figure 5.13 shows the decrease in the level of surface modification as the VUV flux is reduced. Typical XPS widescan spectra for samples treated at 15 mm (O/C = 0.13) and 70 mm (O/C = 0.08) are presented in Figure 5.14.

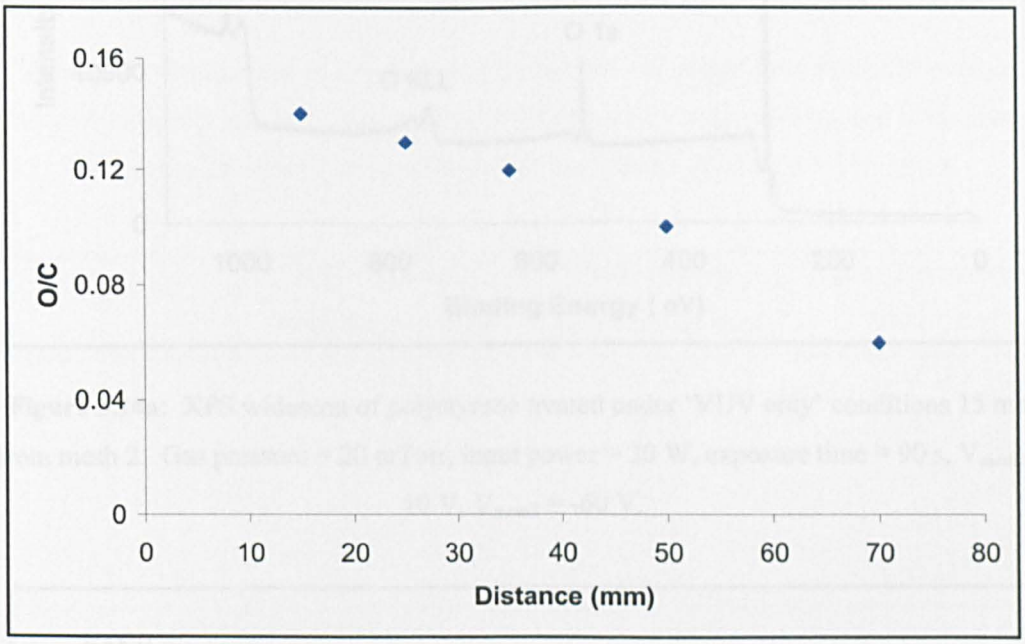

Figure 5.13: Effect of increasing the distance between the source and sample surface on the oxygen/carbon ratio of polystyrene treated under 'VUV only' conditions. Gas pressure = 20 mTorr, input power = 20 W, exposure time = 90 s, V_{mesh1} = 10 V, V_{mesh2} = -60 V.

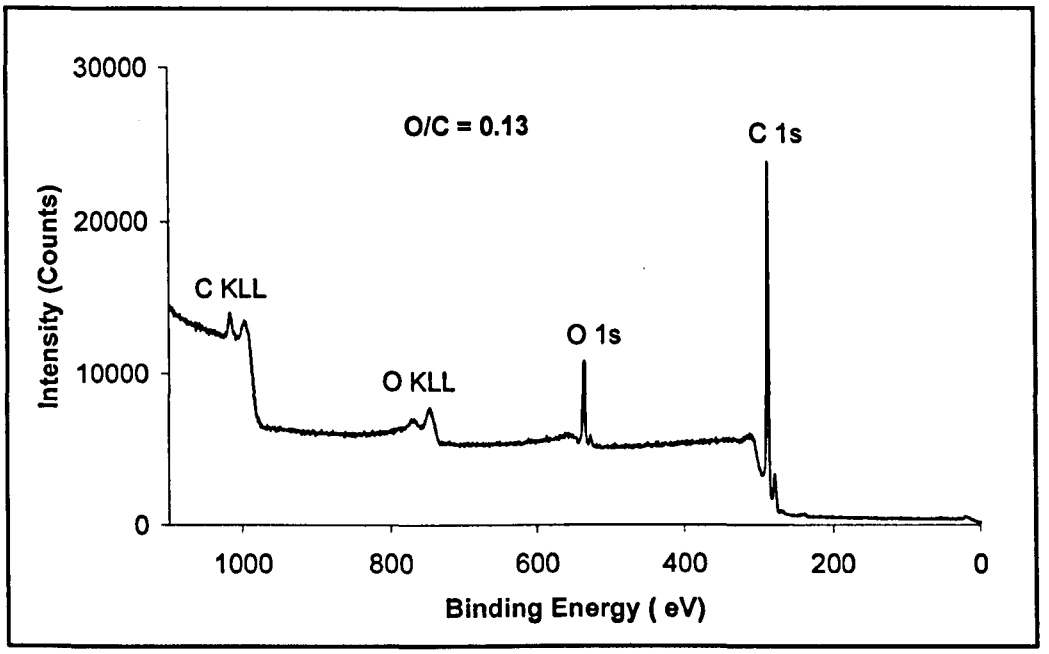

Figure 5.14a: XPS widescan of polystyrene treated under 'VUV only' conditions 15 mm from mesh 2. Gas pressure = 20 mTorr, input power = 20 W, exposure time = 90 s, V_{mesh1} = 10 V, V_{mesh2} = -60 V.

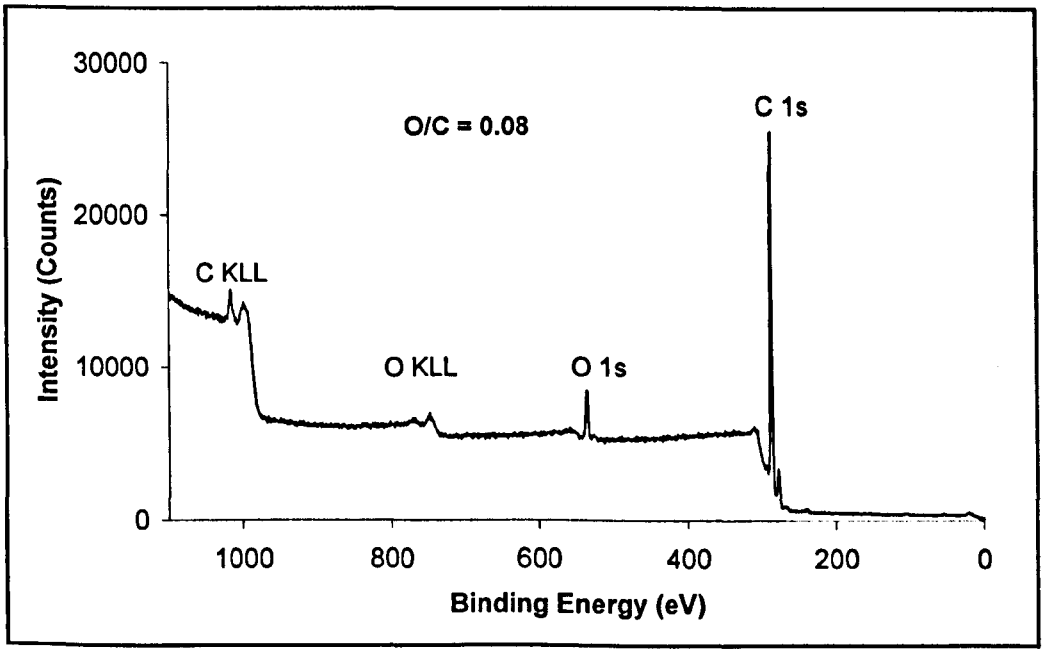

Figure 5.14b: XPS widescan of polystyrene treated under 'VUV only' conditions 70 mm from mesh 2. Gas pressure = 20 mTorr, input power = 20 W, exposure time = 90 s, V_{mesh1} = 10 V, V_{mesh2} = -60 V.

The level of oxygen incorporated into the polymer surface by VUV treatment was compared to that for double-meshed, 'whole' plasma (as discussed in Section 5.3). For samples treated at the same gas pressure (20 mTorr), input power (20 W), exposure time (90 s) and distance from the source (15 mm), the oxygen/carbon ratio was not significantly affected by the presence of ions at either high energy or low energy (Table 5.3).

Table 5.3: Comparison of the oxygen to carbon ratio of polystyrene treated in 'whole' plasma with high and low ion energies (18 eV and 0.5 eV respectively), and in the case where the ions have been excluded from the process chamber ('VUV only').

	Whole Plasma - High Energy Ions	**Whole Plasma - Low Energy Ions**	**Ions Excluded – 'VUV only'**
	0.13	0.12	0.12
	0.12	0.15	0.11
	0.11	0.10	0.13
	0.13	0.10	0.14
		0.10	0.14
Mean	**0.12**	**0.11**	**0.13**
Standard Deviation	**0.01**	**0.02**	**0.01**

To confirm the importance of VUV photons and investigate the roles of neutrals and metastable species, the two biased meshes were replaced with a lithium fluoride window (Figure 5.15). The window allowed only electromagnetic radiation of 104 nm and above to pass through into the process chamber *i.e.* no ions, electrons, neutrals or metastables reached the sample surface – true VUV only conditions. When analysed by XPS, PS samples treated through the window under the same plasma conditions as those in Table 5.3 were found to have an oxygen to carbon ratio of 0.12.

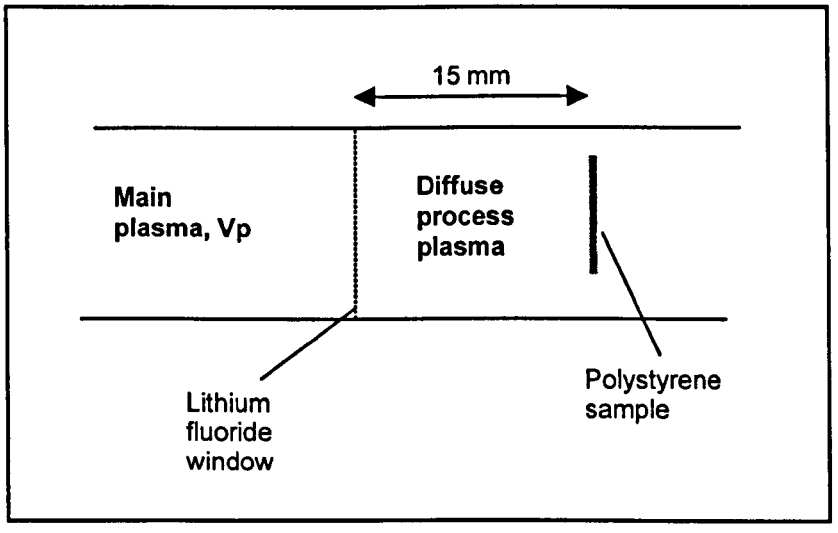

Figure 5.15: Schematic showing separation of plasma by a lithium fluoride window (cut off 104 nm).

The depth of modification of the VUV source was compared to that of 'whole' ion-dominated plasma used by Steele (2000) and Velázquez (2002) in a glass barrel rector. XPS analyses were performed at different take off angles *i.e.* different sampling depths for samples produced in the two reactor systems. Figure 5.16 shows how the level of modification changes with sampling depth in samples treated in a) the ion-dominated 'whole' plasma of Steele and Velázquez and b) the VUV source. The absolute levels of modification are not comparable, but the important feature in these graphs is the ratio between the level of modification at the shallowest and deepest sampling depths. The difference in the level of modification with depth is more pronounced in the ion-dominated plasma sample than the VUV sample.

The surface chemistry of samples prepared in both types of reactor was also compared at one XPS sampling depth. Polystyrene samples with a similar level of modification from each reactor were analysed (O/C = 0.14 for 'VUV only' samples; (O+N)/C = 0.14 for Steele/Velázquez sample). The XPS widescans and C_{1s} narrowscans are presented in Figures 5.17 and 5.18. Although the depth of modification of the two types of treatment is different, the functional group quantification is very similar for samples with the same level of modification (Table 5.4).

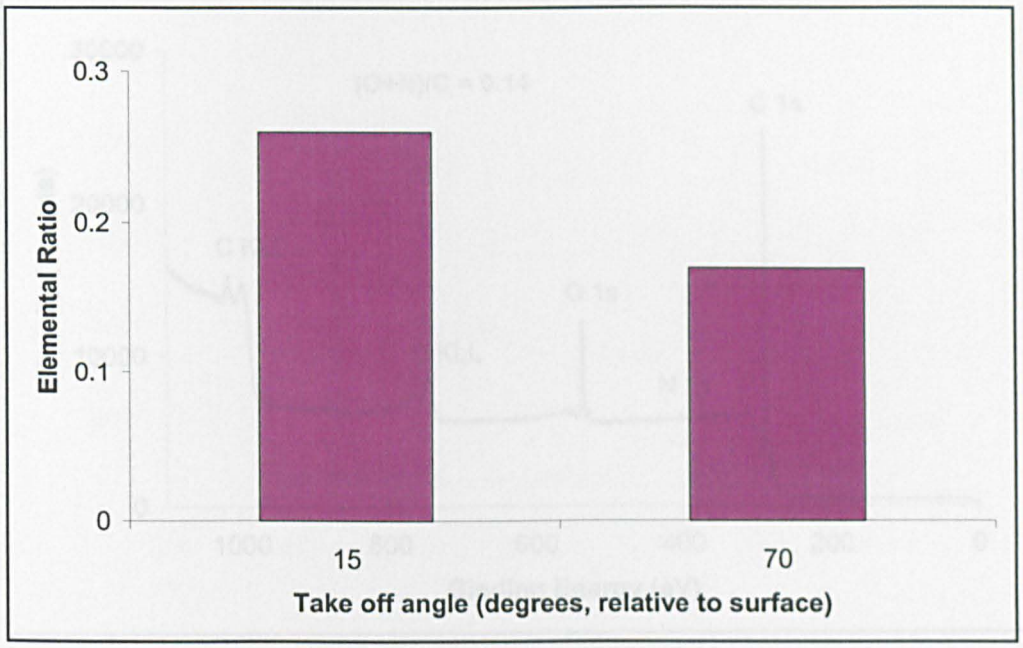

Figure 5.16a: XPS depth profiling for PS treated in the ion-dominated 'whole' plasma source. Data taken from Steele (2000) and Velázquez (2002).

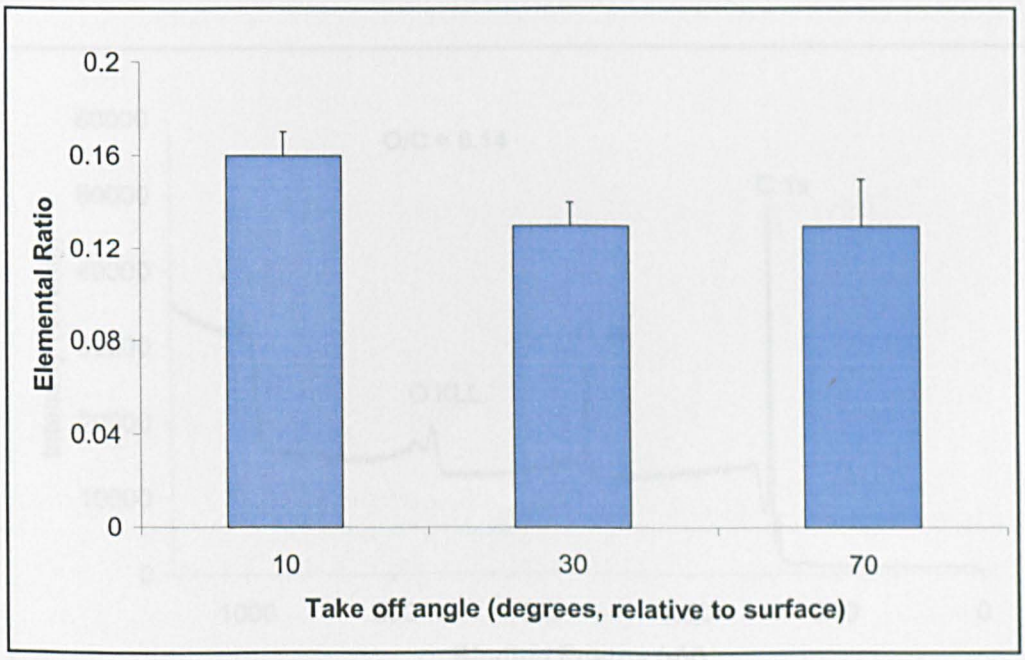

Figure 5.16b: XPS depth profiling for PS treated in the VUV source. Values shown are the mean of five samples; error bars indicate one standard deviation

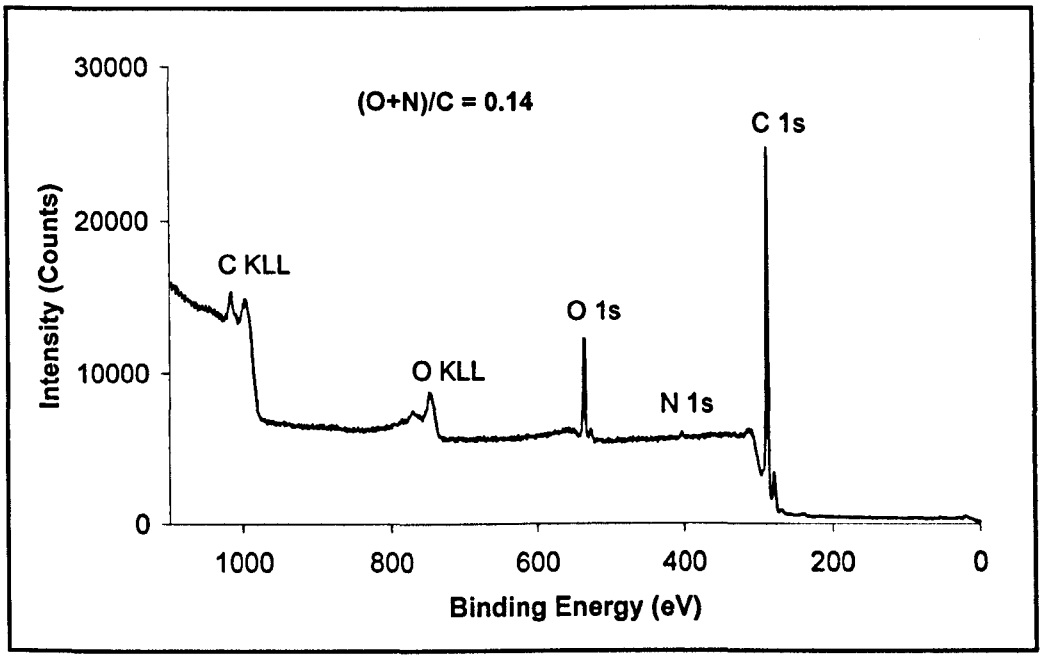

Figure 5.17a: XPS widescan of polystyrene treated with ion-dominated 'whole' plasma in a glass barrel reactor.

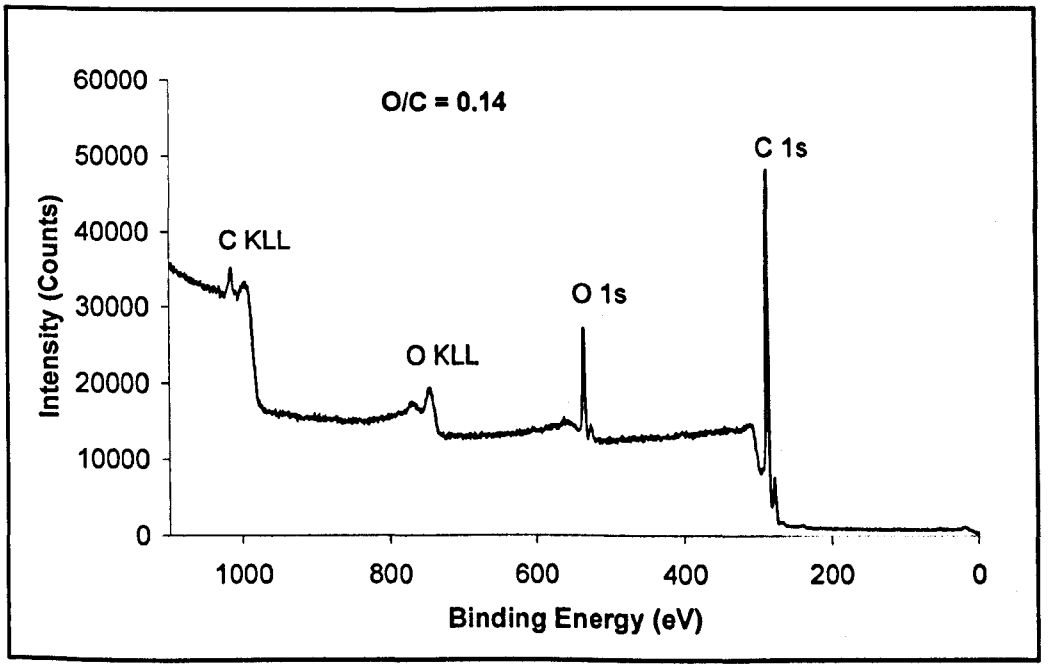

Figure 5.17b: Typical XPS widescan of polystyrene treated under 'VUV only' conditions in the novel plasma source.

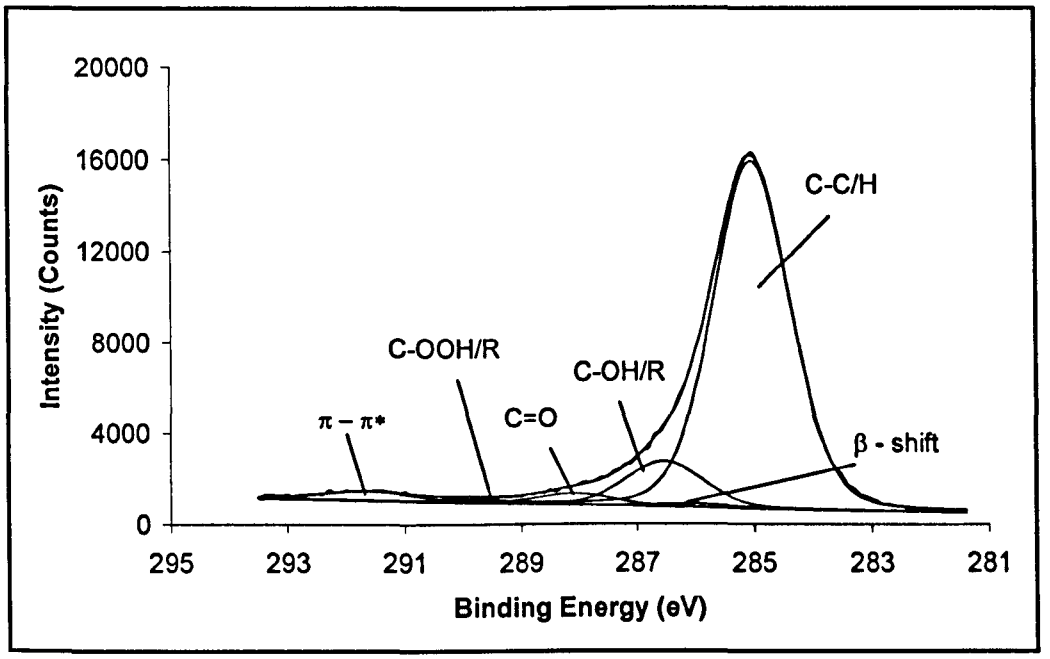

Figure 5.18a: C_{1s} narrowscan of polystyrene treated with ion-dominated 'whole' plasma in a glass barrel reactor.

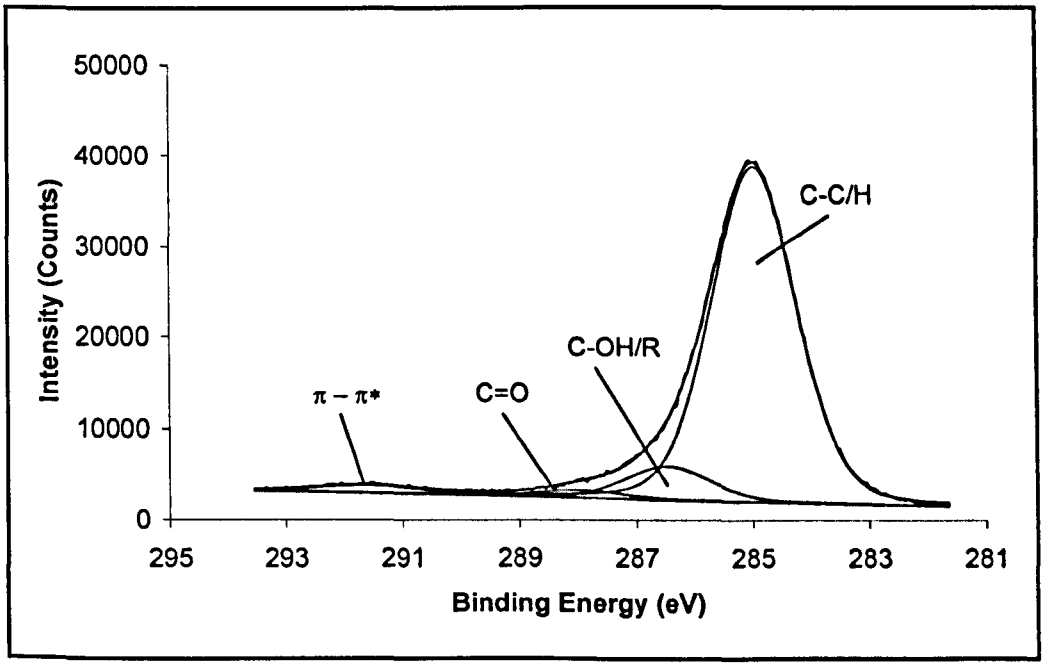

Figure 5.18b: C_{1s} narrowscan of polystyrene treated under 'VUV only' conditions in the novel plasma source.

Table 5.4: Functional group concentrations for PS modified in the ion-dominated barrel reactor and under 'VUV only' conditions. Barrel (O+N/C) = 0.14; VUV O/C = 0.14.

Functional group	Concentration in C_{1s} core level (%)	
	Barrel reactor	'VUV only' source
C-C, C-H	82.1	86.7
β - shift	0.9	0
C-OH/R	10.9	8.7
C=O	2.8	2.0
C-OOH/R	0.9	0
π - π*	2.5	2.6

5.4.3 Discussion

Many previous studies have used nitrogen and hydrogen plasmas as a photon source for the surface treatment of polymers (see Section 2.2.3.2). In this present work, the effects of VUV photons produced in argon plasma are investigated. VUV photons are generated in the main plasma by radiative recombination reactions, such as:

$$e^- + Ar^+ \rightarrow Ar + h\nu$$
$$e^- + Ar^* \rightarrow Ar + h\nu + e^- .$$

The most intense emission lines from argon plasma are the M I at 104.8 nm and 106.7 nm and the M II lines at and 92.0 nm and 93.2 nm. The M I lines are transmitted by the lithium fluoride window (cut-off 104 nm). The energy of these photons is sufficient to cause bond scission within the polystyrene in the process chamber, generating radicals that subsequently react and cause surface modification. Utilising double-mesh conditions that exclude ions from the process chamber (Figure 5.10), the effects of VUV photons, metastables and neutrals in the surface modification of polystyrene were isolated.

XPS analysis of polystyrene treated at different input powers and distances from the meshes revealed that the level of surface modification was dependent on photon

flux. As photon flux increases with input power (Barton *et al.*, 2000), more radical sites are created at higher powers, thus increasing the amount of oxygen incorporated into the surface (Figures 5.11 and 5.12). Similarly, changing the distance between the substrate and the meshes varies the photon flux. Again, the level of surface modification was responsive to changes in photon flux, decreasing with distance (Figures 5.13 and 5.14).

To assess the contribution of VUV photons to surface modification in 'whole' plasma, results from 'VUV only' conditions were compared to those where the ion energy was varied. The level of modification was the same for all these conditions, suggesting (in accordance with the results presented in Section 5.3) that ions make a negligible contribution to surface modification of polystyrene in this novel source (Table 5.3). This suggestion was confirmed by analysis of samples treated through a lithium fluoride window; these had the same level of oxygen incorporation when no species except VUV photons reached the surface. Although the transmission of the window is not known, this suggests that it is approximately the same as the double-mesh arrangement, which has a transmission between 45 % and 20 %. This experiment also revealed that metastables and neutrals contribute little to the modification process. Using a series of vanes, the reverse experiment (where the photons were blocked from the substrate but plasma was allowed to diffuse to it) was attempted, but no ion current was detected in the process region *i.e.* the plasma did not get through either.

Having identified VUV photons as the primary source of modification, a more satisfactory explanation of the single-mesh results presented in Section 5.2 can be provided. These experiments indicated that the level of surface modification could, in fact, be tailored by varying the ion flux and energy. However, as it was assumed that the source was ion-dominated in terms of surface modification, no attempt to control the VUV component of the plasma was made. Thus in the single-mesh experiments, the observed changes in oxygen content correspond to changes in VUV photon flux caused by variation of the input power and/or gas pressure. In controlling the ion flux, for example, the input power or the distance between the source and the sample were varied (Figures 5.4 and 5.5). However, both of these parameters also vary the photon flux. Similarly, when attempting to retain a constant

ion flux whilst controlling the ion energy with the single mesh arrangement, the photon flux would have been variable due to the changes in input power and gas pressure that were necessary to keep the ion flux constant (Figure 5.6 and Table 5.2).

Due to the larger penetration depth of photons (as compared to ions), the modification induced by VUV treatment was more uniformly distributed throughout the XPS sampling depth than that produced in 'whole' plasma treatment by Steele (2000) and Velázquez (2002)(Figure 5.16), although the chemistry of the two surfaces is very similar (Figure 5.18 and Table 5.4). This is significant because surface interactions are mediated by the outermost surface chemistry, not the average chemistry over the XPS sampling depth. The AFM and cell culture results presented in Chapter Six illustrate the different characteristics of two such surfaces, which have similar levels of modification averaged over the XPS sampling depth.

As discussed in Section 2.2.3.2, the reaction times for VUV treatment of polymers are much longer than for conventional 'whole' plasma, typically between 30 and 60 minutes (as opposed to a maximum few minutes for plasma). In some cases the input power to the plasma source is up to 300 W (Hudis & Prescott, 1972; Wilken *et al.*, 1998, 2002). However the exposure times used in this study are up to 90 seconds with a 20 W source to achieve an oxygen to carbon ratio of 0.12. The previous study using the most similar conditions to those employed here is that of Hopkins *et al.* (1996) (Table 5.5).

Table 5.5: Comparison of conditions for argon plasma modification of polystyrene through a LiF window.

	Hopkins *et al.* (1996)	**Present study**
System base pressure	<2 x 10-3 mbar (increased to 0.2 mbar with oxygen for the reaction)	~5 x 10^{-5} Torr
Input power	30 W	20 W
Distance to sample	10 mm	15 mm
O/C	0.2 (toa 60^{O} to surface)	0.12 (toa 30^{O} to surface)
Exposure time	30 minutes	90 seconds

Under these conditions, the novel plasma source described herein appears to produce surfaces modified to a comparable level in a fraction of the time required by Hopkins *et al.* The greatly improved efficiency of this novel plasma source for VUV treatment of polystyrene is unexplained, but potentially very useful in rapid processing of samples.

5.4.4 Conclusions

In considering the above data and interpretation along with a stated aim of this chapter,

- to use a 'tailored' plasma to investigate the role of ions in the surface modification of polystyrene,

the following conclusions are drawn:

- Under certain mesh biases, ions can be excluded from the process chamber.
- The predominant plasma species involved in the surface modification of polystyrene in this reactor system was VUV photons. Metastable species and ions played a negligible role.
- The novel argon plasma source used to generate VUV photons for the treatment of polystyrene is much more efficient than other systems reported in the literature.

Chapter Six

Results II: Cell Culture Substrates

The aims of this section of work were:

- to use VUV treatment of PS to create a surface suitable for culture of BMSC
- to create surface chemical patterns on PS using VUV treatment through patterning grids
- to employ the surface chemical patterns in a pilot study of the effects of geometric constraint on the attachment, growth and differentiation of BMSC

This chapter presents and discusses the results of surface analysis and cell culture experiments performed on bacteriological grade PS (negative control), tissue culture PS (positive control) and VUV treated PS (experimental surface).

X-ray Photoelectron Spectroscopy (XPS) was used to quantify the atomic ratios of elements present, and the carbon-containing functional groups in the surfaces of bacteriological grade PS, TCPS and VUV treated PS. Imaging of condensed water was used as a simple method of visualising surface chemical patterns on the VUV treated PS. The fidelity of the patterns was examined by friction mode atomic force microscopy (FFM) imaging.

Quantitative and qualitative analysis of bone marrow stromal cell (BMSC) proliferation/vitality, alkaline phosphatase production and total collagen production was performed on the three surfaces to ascertain that the experimental surface was suitable as a cell culture substrate. The morphology, alkaline phosphatase production and total collagen production of BMSC cultured on VUV patterned PS was examined qualitatively.

6.1 Surface Analysis of Cell Culture Substrates

6.1.1 X-ray Photoelectron Spectroscopy

XPS was performed as described in Section 4.4.1 at a take off angle of 30° relative to the surface. Samples of tissue culture PS (TCPS) and bacteriological grade PS (BG PS) were obtained from broken-up 24-well plates. To assess the effect of VUV treatment, PS coated coverslips were placed on the bottom of wells of bacteriological grade PS plates and removed after treatment for analysis. The geometry of the plasma reactor (described in Section 4.2) allowed only nine wells on each plate to be treated. Coverslips from different positions within these nine wells were analysed and no significant differences in O/C found.

A typical widescan XP spectrum of bacteriological grade PS is shown in Figure 6.1a. The major peaks are the C_{1s} and the C KLL Auger peak, with very small O_{1s} and O KLL peaks also present. The corresponding narrowscan of the C_{1s} core level (Figure 6.1b) shows the main hydrocarbon peak (corrected to 285 eV to compensate for surface charging effects) and the π - π^* shake-up satellite.

The XPS widescan of TCPS shows carbon and oxygen as the predominant elements present in the surface (Figure 6.2a). Small amounts of nitrogen (1.1 %), sodium (0.3 %) and silicon (1.6 %) are also apparent (Table 6.1). The C_{1s} narrowscan reveals that the carbon exists in three chemical environments: a) bonded to carbon/hydrogen; b) bonded to oxygen in alcohol/ether groups, and c) carbon bonded to oxygen in ketone groups (Table 6.2).

The 'standard' VUV treatment conditions were chosen for production of experimental cell culture surfaces. These conditions are shown in Table 6.3.

Table 6.3: VUV treatment conditions used for production of cell culture substrates. The bottoms of the wells were 35 mm from the mesh unit.

V_{mesh1}	+10 V
V_{mesh2}	-60 V
Exposure Time	180 s
Input Power	20 W
Gas Pressure	20 mTorr

XPS analysis of VUV treated PS shows only carbon and oxygen (Figure 6.3a) present in the surface. The C_{1s} narrowscan (Figure 6.3b) shows carbon in the same three chemical environments as in TCPS, but also exhibits a π - π^* shake-up satellite.

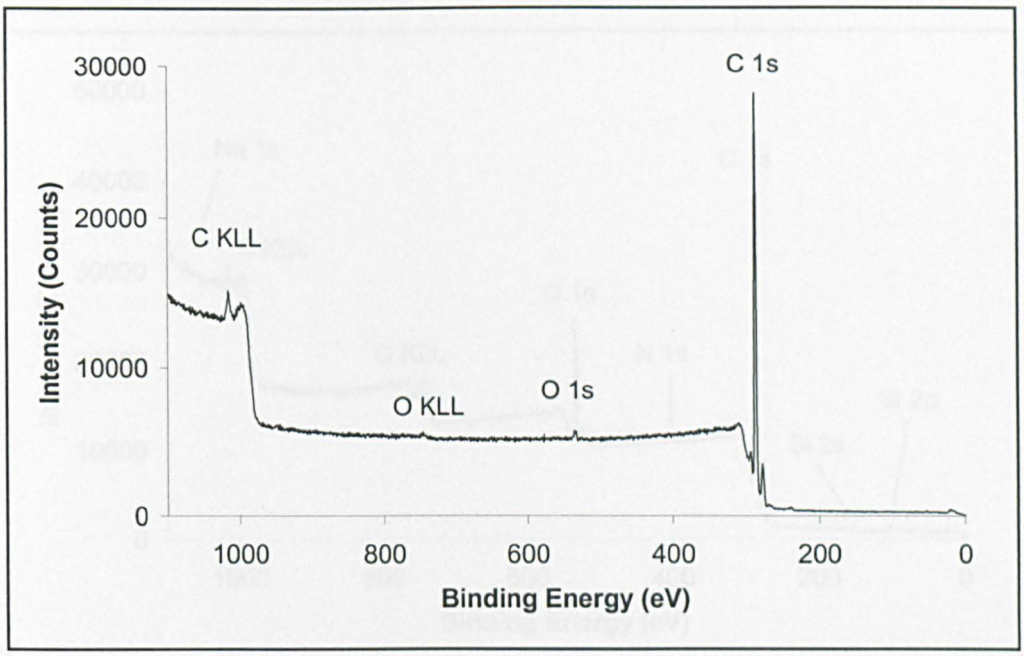

Figure 6.1a: Typical XPS widescan of bacteriological grade PS

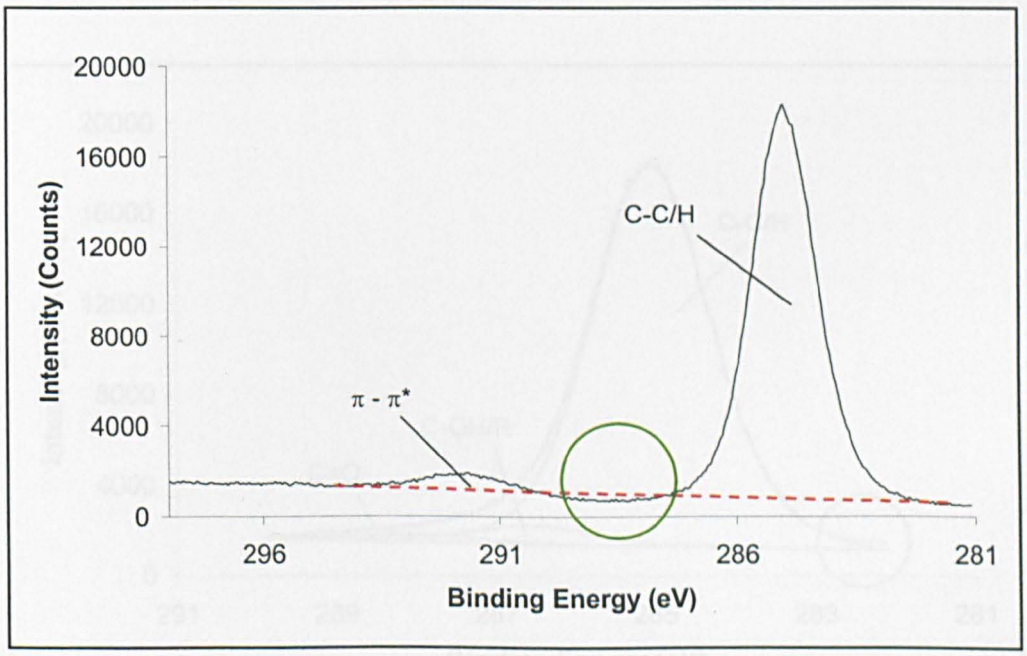

Figure 6.1b: Typical XPS C_{1s} narrowscan of bacteriological grade PS. The green circle indicates where the linear background drawn during peak fitting (dashed red line) crosses above the data envelope (see page 102 for discussion).

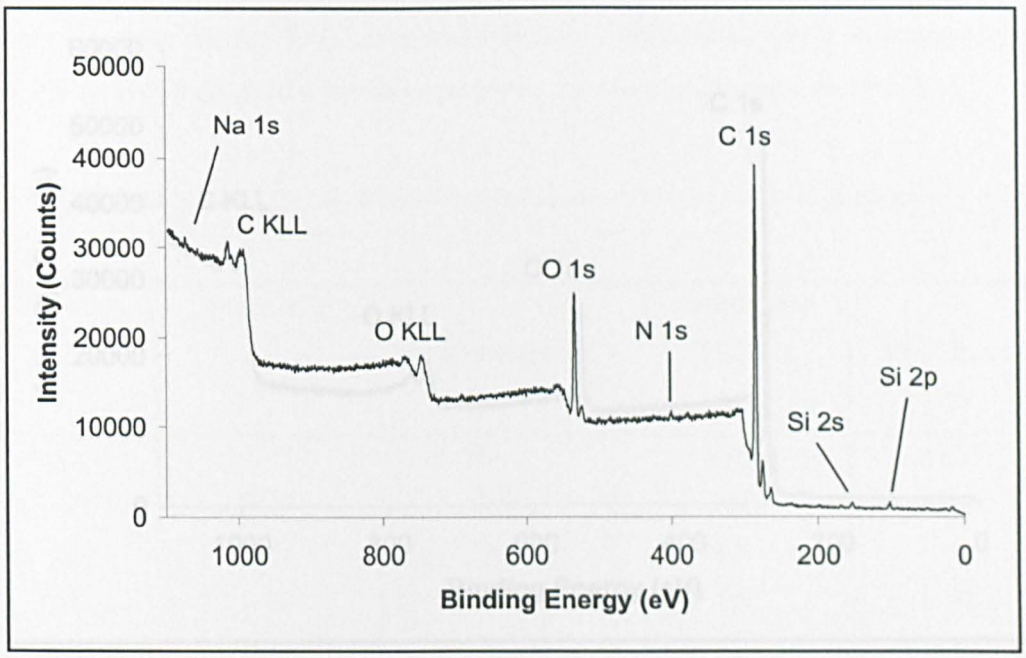

Figure 6.2a: Typical XPS widescan of TCPS

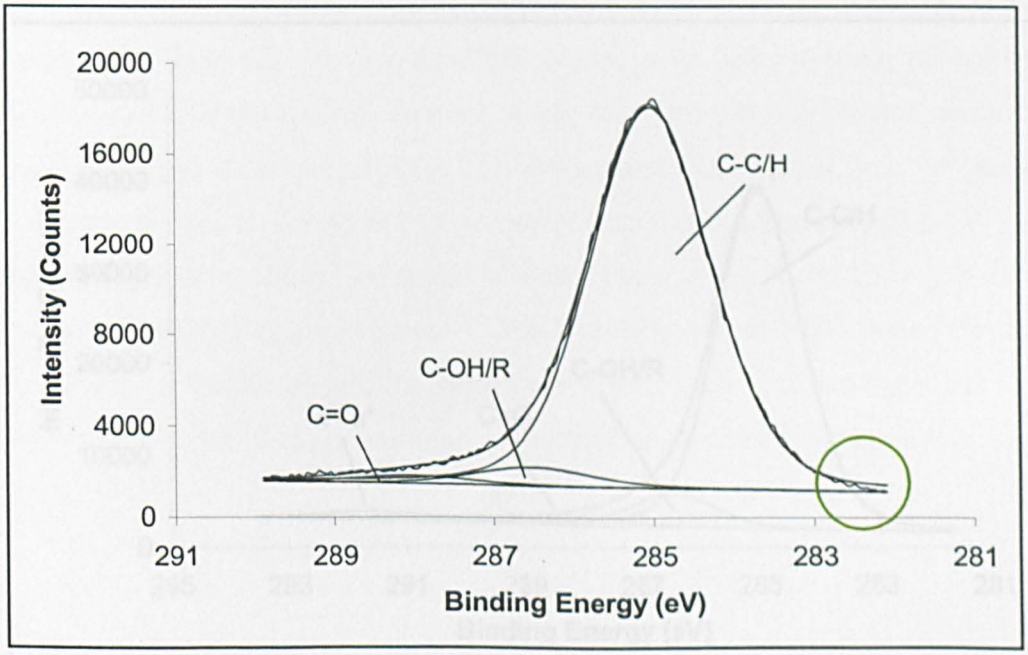

Figure 6.2b: Typical XPS C_{1s} narrowscan of TCPS. The green circle indicates where the peak fit is compromised by the –0.7 eV shift produced by the presence of silicon (see Section 6.1.4 for discussion).

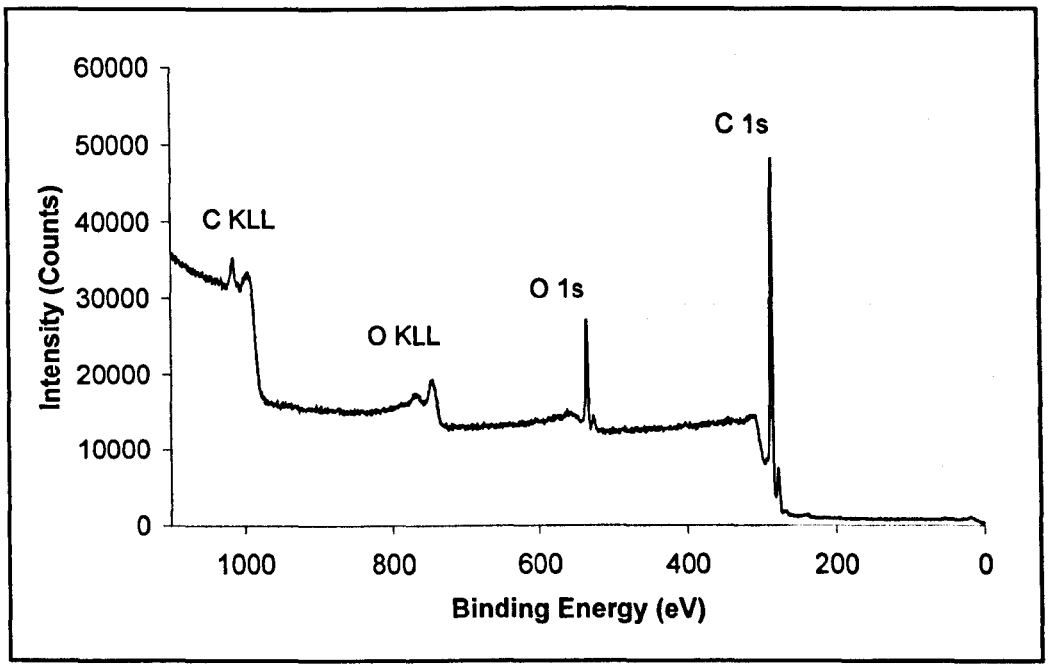

Figure 6.3a: Typical XPS widescan of VUV treated PS

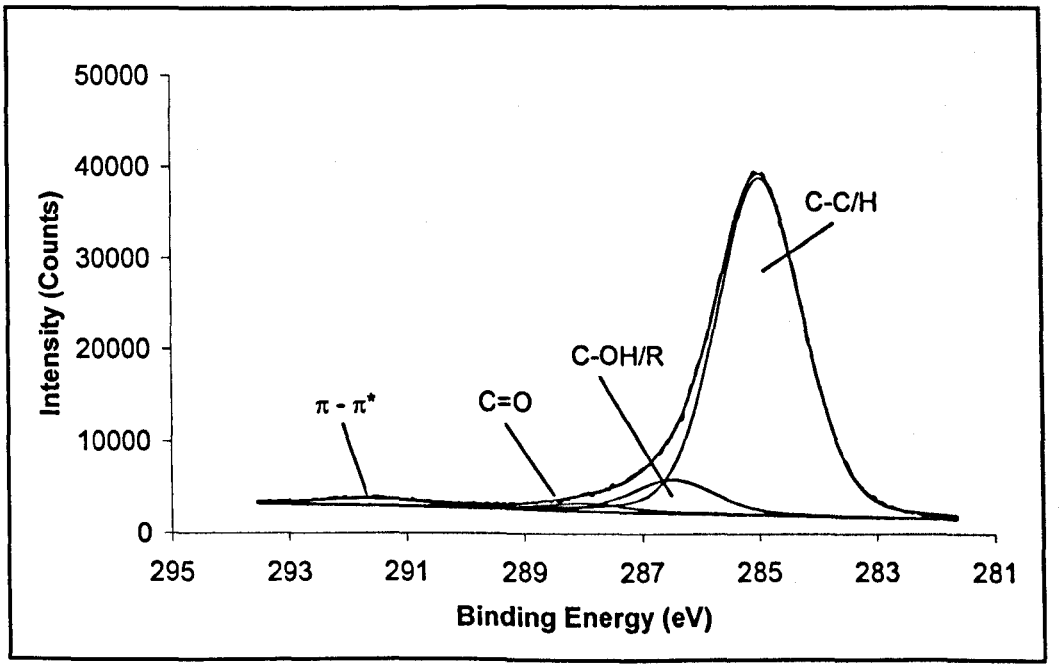

Figure 6.3b: Typical C_{1s} narrowscan of VUV treated PS

The elemental compositions of the three surfaces are compared quantitatively in Table 6.1. The chosen VUV treatment typically introduced slightly less oxygen into the PS surface than did the surface treatment used to manufacture the TCPS.

Table 6.1: Typical elemental quantifications for the three PS surfaces

Element	Sensitivity	Concentration (%)		
		Bacteriological grade PS	TCPS	VUV treated PS
C	1.00	98.3	82.7	87.9
O	2.49	1.7	14.3	12.1
N	1.71	0	1.1	0
Si	1.09	0	1.6	0
Na	8.52	0	0.3	0

The functional group quantification of the C_{1s} core level of the three surfaces is compared in Table 6.2. To overcome the problem with fitting a linear background (as indicated in Figure 6.1b), separate linear backgrounds were drawn under the hydrocarbon and π - π^* peaks of the BG PS spectrum. The area of the π - π^* shake-up satellite is then expressed as a percentage of the hydrocarbon peak (7.2 %). The peak fitting results show that fewer of the carbon atoms in TCPS exist within oxygen-containing functional groups (6.6 %), as compared to VUV treated PS (10.7 %). The π - π^* shake-up satellite, which accounts for 2.6 % of the C_{1s} in the VUV treated PS, indicates that some aromatic character has remained in this surface.

Table 6.2: Typical C_{1s} functional group quantification of TCPS and VUV treated PS surfaces.

Functional group	Concentration in C_{1s} core level (%)	
	TCPS	VUV treated PS
C-C, C-H	93.4	86.7
C-OH/R	4.6	8.7
C=O	2.0	2.0
π - π^*	0	2.6

6.1.2 Condensation patterns

To verify that the patterning procedure was effective, water was condensed onto surface chemical patterns produced by VUV treatment through the grids. The pattern is visualised by the difference in water contact angle between the treated (hydrophilic) areas and untreated PS (hydrophobic). On patterns created using Grid #1 (Figure 6.4a), the difference in surface chemistry is evident across the whole range of features (from 75 μm to 5 μm). However, on patterns produced with Grid #2 (Figure 6.4b), the difference in surface chemistry was apparent only on the larger hydrophilic regions (dimensions in microns: 20 x 20, 28 x 28, 5 x 80, 8 x 50, 10 x 40 and 16 x 50).

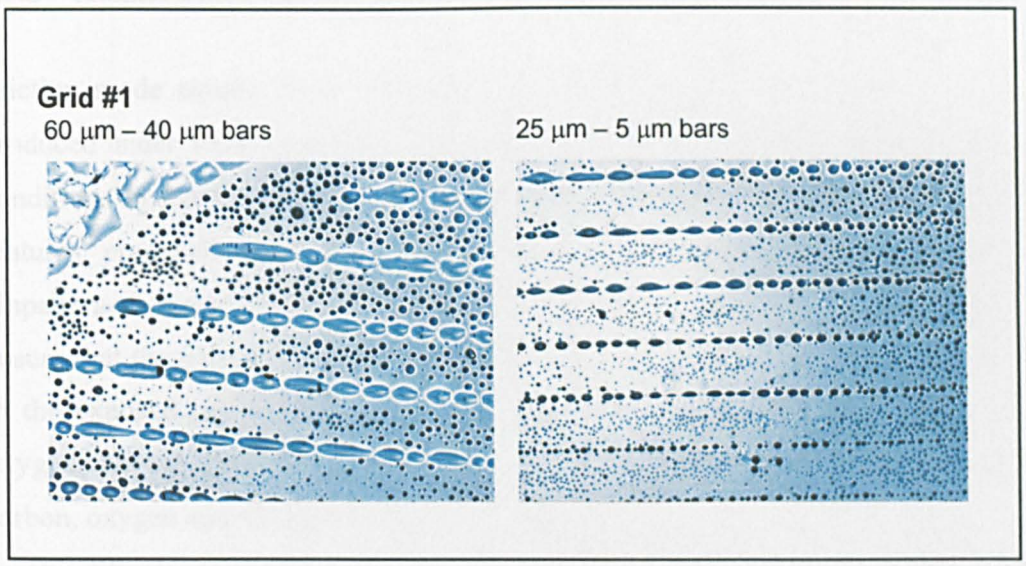

Figure 6.4a: Light microscopy images of water condensed on patterns produced with Grid #1.

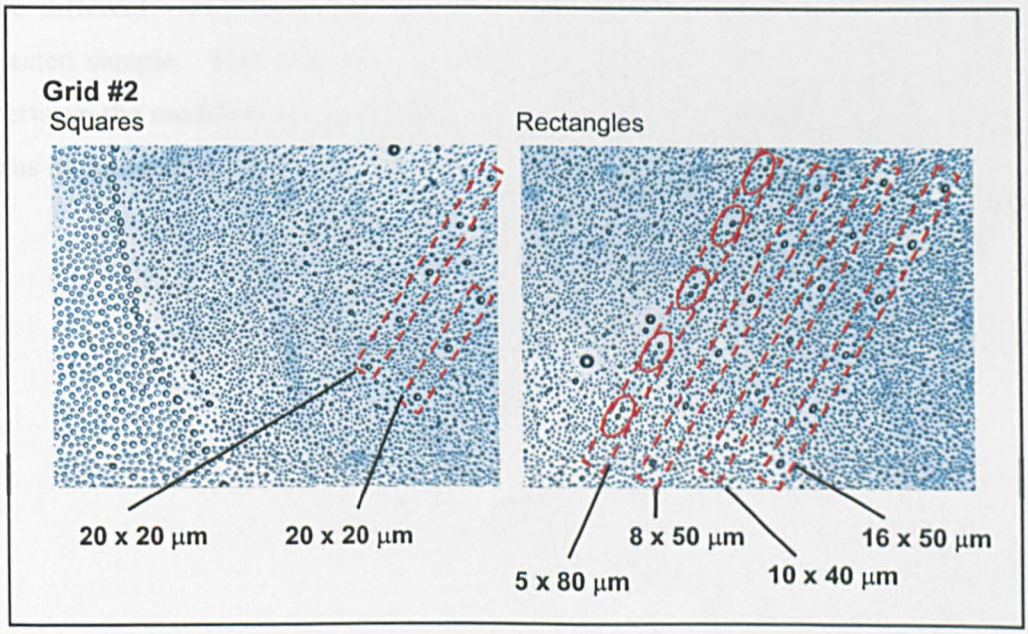

Figure 6.4b: Light microscopy images of water condensed on patterns produced with Grid #2.

6.1.3 Atomic Force Microscopy

Friction mode atomic force microscopy was used to generate images of patterns produced under VUV conditions in the UMIST rig and under ion-dominated plasma conditions in the Sheffield rig. Grid #1 was chosen for these experiments, as the features produced are large enough to be easily located in the instrument. Unpatterned samples produced simultaneously were analysed by XPS to try to ensure that the patterned samples had approximately the same level of modification in the exposed regions. The VUV (UMIST) sample contained only carbon and oxygen, having O/C of 0.27. The plasma treated (Sheffield) sample contained carbon, oxygen and nitrogen, having (O+N)/C of 0.23.

The difference in surface chemistry between the modified and unmodified areas of the polystyrene is reflected in the FFM images by a difference in frictional force (Figure 6.5). VUV treatment appears to have produced sharper edges on the 25 μm hydrophilic bar than plasma treatment. The data scales maximums for the images are different: only 0.1V for the VUV treated sample, but 3.5 V for the plasma treated sample. This indicates that there was less difference in surface chemistry between the modified and unmodified regions in the VUV treated sample than there was in the plasma treated sample.

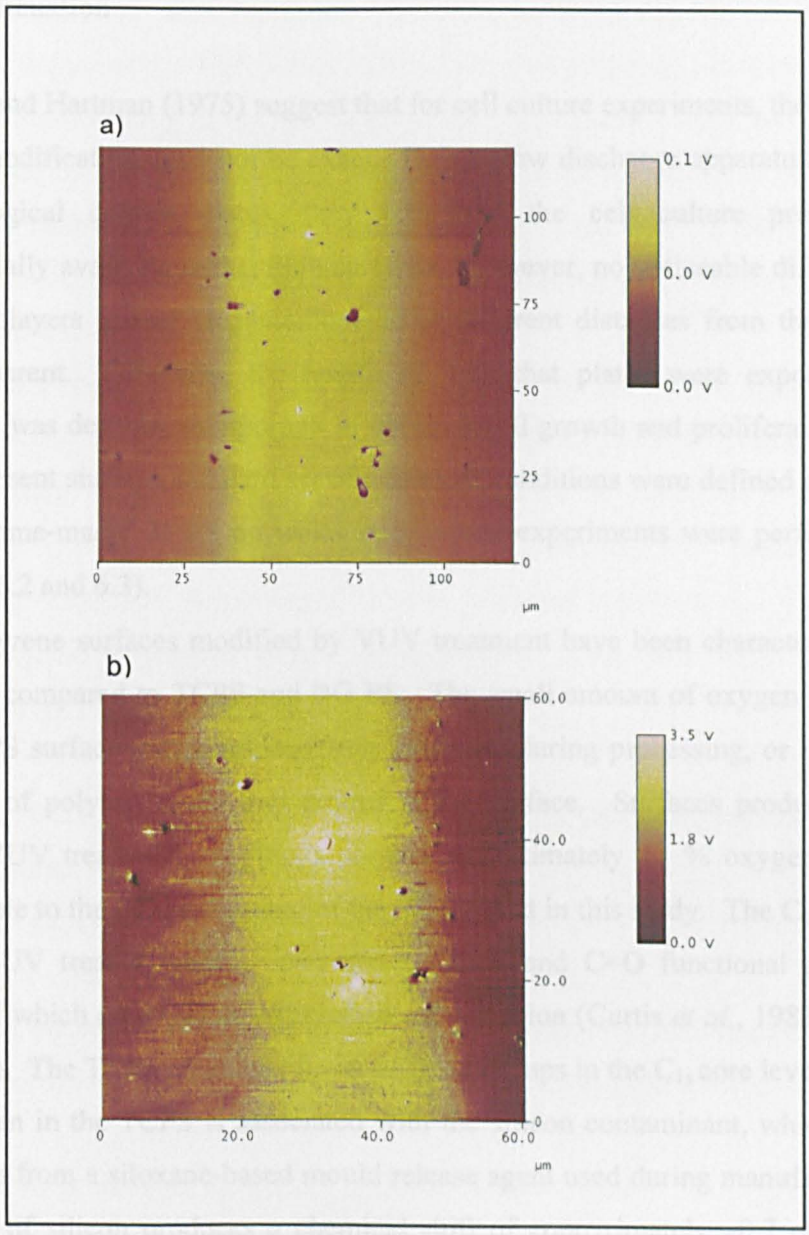

Figure 6.5: Friction force image of 25 µm hydrophilic bar produced by **a)** VUV treatment in the UMIST rig and **b)** ion dominated plasma treatment in the Sheffield rig.

6.1.4 Discussion

Amstein and Hartman (1975) suggest that for cell culture experiments, the process of surface modification need not be exact. Using glow discharge apparatus to modify bacteriological culture plates, they replicated the cell culture properties of commercially available cell culture surfaces. However, no noticeable differences in cell monolayers grown on plates treated at different distances from the electrode were apparent. Similarly, the length of time that plates were exposed to the discharge was deemed unimportant in terms of cell growth and proliferation. Thus, in this present study, a standard set of treatment conditions were defined and used to create 'home-made' TCPS on which cell culture experiments were performed (see Sections 6.2 and 6.3).

Polystyrene surfaces modified by VUV treatment have been characterised using XPS and compared to TCPS and BG PS. The small amount of oxygen detected in the BG PS surface may originate from oxidation during processing, or indicate the presence of polymer chain end groups at the surface. Surfaces produced by the chosen VUV treatment conditions contain approximately 12 % oxygen, which is comparable to the oxygen content of the TCPS used in this study. The C_{1s} core level of the VUV treated surface contained C-OH/R and C=O functional groups, the former of which are reported to enhance cell adhesion (Curtis *et al.*, 1983; France *et al.*, 1998). The TCPS contained fewer of these groups in the C_{1s} core level. Some of the oxygen in the TCPS is associated with the silicon contaminant, which possibly originates from a siloxane-based mould release agent used during manufacture. The presence of silicon produces a chemical shift of approximately –0.7 eV from the hydrocarbon peak in the C_{1s} (Briggs, 1998). This is evident at the low binding energy end of the spectrum shown in Figure 6.2b, where the peak fit is loose. The incorporation of nitrogen also compromises the accuracy of the C_{1s} peak fit, as the differences in chemical shifts produced by alcohol/ether and amine groups or aldehyde/ketone and amide groups are small compared to the spectral resolution of the spectrometer, and thus cannot be individually resolved. The sodium contamination on the TCPS surface would usually be indicative of poor sample handling prior to XPS analysis. However, sodium was detected on all of several

samples analysed. The source of sodium contamination remains unknown, but could possibly be connected with the plastic packaging in which the 24-well plates are received. Alternatively, a high power oxidation treatment during manufacture of the plates may cause etching of the reactor glassware, which could cause silicon and/or sodium contamination on the surface. XPS analysis of several brands of commercial TCPS (not including the brand analysed here) by Daw (1999) did not detect contaminants such as silicon and sodium, but concluded that there is great variability in the surface chemistry of such products.

Patterned surfaces were examined using two techniques. Light microscopy of condensed water was a suitable method for visualising the surface chemical patterns produced using Grid #1 and revealed that features as small as 5 μm were successfully created using VUV treatment. However, the technique was inconclusive when used to investigate patterns produced with Grid #2. The pattern was only visible in regions where the hydrophilic areas were large. Possible explanations for this include:

a) the VUV patterning technique was incapable of producing surface chemical patterns with very small features
b) the patterning grid had not contacted the surface sufficiently to produce a well – defined pattern
c) the water condensation method was not appropriate to visualise the small hydrophilic features widely dispersed on the hydrophobic background

Friction force images of surfaces treated in the UMIST rig (VUV) and the Sheffield rig ('whole' plasma, including ions, photons and metastables) were compared to investigate possible differences in the fidelity of patterns produced by these two methods. In 'whole' plasma processing, the modifying species could arrive at the surface from any angle and potentially "undercut" the grid, blurring the pattern. Bullett (2001) encountered this problem finding that bars deposited through a 75 μm slot in the patterning grid actually measured approximately 98 μm. However, the VUV technique is purely a line-of-sight process, which may result in enhanced pattern fidelity. The FFM results presented in Section 6.1.3 appear to

support this theory, in that the edges of a 25 μm hydrophilic bar (Grid #1) appear to be sharper on the VUV treated sample than on the plasma treated surface.

The difference in data scales for the friction force measurements is indicative of the distribution within the surface of the oxygen detected by XPS. Although both samples had approximately the same level of surface modification, the difference in frictional force between the modified and unmodified regions is less in the VUV treated sample than in the surface treated by 'whole' plasma. This suggests that in the VUV case, the oxygen is distributed more evenly through the XPS sampling depth, whereas for the plasma treated sample it is localised at the surface. This supports the XPS depth profiling results presented in Section 5.4.

The use of grids and plasma-based techniques to create surface chemical patterns on polymeric substrates is well established. However, the features generated are generally similar in size to those in Grid #1. For example, Ohl *et al.* (1999) employed a plasma etching technique to create features ranging from 30 μm to 500 μm; Bullett *et al.* (2001) used plasma deposition to produce 50 μm bars and 75 μm^2 islands. Where smaller features have been created (*e.g.* 5 μm by Mitchell *et al.* (2002) and the 5 μm bars in Grid #1) they have been as part of a continuous pattern rather, than as isolated regions such as in Grid #2 (*e.g.* 7 μm x 7 μm). At this level, both plasma treatment and plasma deposition may be limited in their application. Plasma sheath sizes may become important around small features in the grid, meaning that the ions cannot reach the polymer surface. Any "undercutting" of the grid will be more critical at smaller feature sizes. Moreover, plasma deposition may cause blockage of small slots in the grid as the process progresses. The VUV technique used in this present study is unaffected by these phenomena and so may be advantageous in generating surface chemical patterns on a scale relevant to investigations of cellular constraint. However, problems with the delicate nature of the patterning grids and ensuring their adequate contact with the polymer surface need to be addressed in order to realise the potential of this method.

6.1.5 Conclusions

The results and discussion presented above relate to two of the stated aims of this Chapter:

- to use VUV treatment of PS to create a surface suitable for culture of BMSC
- to create surface chemical patterns on PS using VUV treatment through patterning grids

To this end, the following conclusions may be drawn:

- A substrate with similar surface chemistry to TCPS (the cell culture properties of which are investigated in Section 6.2) can be produced by VUV treatment of PS under the selected conditions.
- Surface chemical patterns can be created on PS by VUV treatment through a grid and visualised by condensing water onto the substrate and imaging under a light microscope.
- The VUV patterning technique can produce hydrophilic bars as small as 5 μm in width using Grid #1; squares of 20 μm x 20 μm and 28 μm x 28 μm and rectangles of 16 μm x 50 μm, 10 μm x 40 μm, 8 μm x 50 μm and 5 μm x 80 μm can be produced using Grid #2.
- The existence of the smaller features of Grid #2 cannot be proved by the condensed water method.
- Poor contact between the patterning grid and the substrate is a major concern in this approach to patterning and cannot be eliminated as the reason for the smaller features of Grid #2 not being evident.
- VUV treatment appears to provide better pattern fidelity than 'whole' plasma and so may have advantages over other plasma-based techniques.

6.2 Cell Culture on Plain Substrates

To ensure that the VUV treated surfaces described above were suitable for cellular patterning experiments, BMSC were cultured on unpatterned VUV treated PS surfaces. The morphology, vitality/proliferation, and production of alkaline phosphatase and total collagen was investigated and compared to that on the TCPS positive control and the bacteriological grade PS negative control.

6.2.1 Cell Morphology

The general cell morphology of BMSC cultures on BG PS, TCPS and VUV treated PS was observed qualitatively. Figure 6.7 shows examples of digital light micrographs of BMSC cultures stained with methylene blue after 9, 12 and 15 days in culture. It is clear that very few cells have attached to the bacteriological grade PS, and those that have, have not been able to spread. However, attachment and spreading on the VUV treated surface is comparable to that on the TCPS positive control.

6.2.2 Cell Proliferation/Vitality

The vitality/proliferation of BMSC cultures on BG PS, TCPS and VUV treated PS was assessed by the Alamar blue assay, as described in Section 4.5.3. Figure 6.8 shows a general upward trend of proliferation on both the positive control TCPS surface and the experimental surface over the 15-day culture period. By comparison, the cells did not proliferate well on the negative control BG PS surface.

As indicated by the ANOVA F-statistics in Table 6.4, significant differences existed between the three surfaces for all time points (99 % confidence level). Post hoc analysis revealed statistically significant differences ($p < 0.01$) between the negative control and the positive control, and also between the experimental surface and the negative control at all time points. However, the mean differences between the positive control and experimental surface were generally smaller, particularly

from five days onwards. This is also evident from examination of Figure 6.8. This trend was found to continue throughout the culture period, with no statistical difference identified between the positive control and experimental surface at 9, 12 and 15 days ($p = 0.322$, 0.014 and 0.986 respectively).

6.2.3 Alkaline Phosphatase Production

Alkaline phosphatase production of BMSC cultures on BG PS, TCPS and VUV treated PS was assessed quantitatively by the assay described in Section 4.5.4. The results presented in Figure 6.9 show a slow increase in alkaline phosphatase production from 9 to 15 days in culture on the TCPS and VUV treated surface. Alkaline phosphatase production on the BG PS was comparatively low.

The ANOVA F-statistics presented in Table 6.5 show significant differences between the three surfaces, which are 99 % certain to be driven by the change in substrate. Again, post hoc analysis illustrated statistically significant differences ($p < 0.01$) between the negative control and the positive control and also between the experimental surface and the negative control at all time points. At the 12-day time point, no significant difference was found in alkaline phosphatase production on the TCPS and VUV treated surfaces ($p = 0.076$). At both the 9 and 15 day time points the differences, although significant, between the TCPS and VUV treated surfaces are much lower than the other comparison tests.

The distribution of alkaline phosphatase in the BMSC cultures is visualised by qualitative staining of naphthol precipitate with Fast Red-TR (as described in Section 4.5.4). Typical micrographs for cultures at 9, 12 and 15 days are presented in Figure 6.10. Very little alkaline phosphatase was detected on the bacteriological grade PS (as confirmed by the quantitative results in Figure 6.9). On TCPS and the experimental surface, the level of staining appears to increase with the culture period and is similar, even if statistically different in some cases.

6.2.4 Total Collagen Production

Total collagen production of BMSC cultures on BG PS, TCPS and VUV treated PS was assessed quantitatively by the assay described in Section 4.5.5. The results presented in Figure 6.11 show a general increase in total collagen production from 9 to 15 days in culture on the TCPS and VUV treated surface. Total collagen production on the BG PS was comparatively low.

Yet again, the ANOVA F-statistics presented in Table 6.6 show significant differences between the three surfaces at the 99 % confidence level. Similarly, the post hoc analysis demonstrated statistically significant differences ($p < 0.01$) between the negative control and the positive control and also between the experimental surface and the negative control at all time points. No statistically significant difference at a 99 % level was identified between total collagen production on TCPS and the VUV treated surface at 9 and 12 days ($p = 0.039$ and 0.368 respectively). At 15 days a significant difference was obtained, although again the mean difference was smaller than those produced by the comparisons involving the negative control.

The production of collagen in the BMSC cultures is visualised by qualitative staining with Sirrius Red (as described in Section 4.5.5). Typical micrographs for cultures at 9, 12 and 15 days are presented in Figure 6.12. Very little collagen was detected on the bacteriological grade PS (as confirmed by the quantitative results in Figure 6.11). The cultures on TCPS and the experimental surface have stained to a similar extent and appear to stain more heavily as the culture period is increased and more collagen is produced.

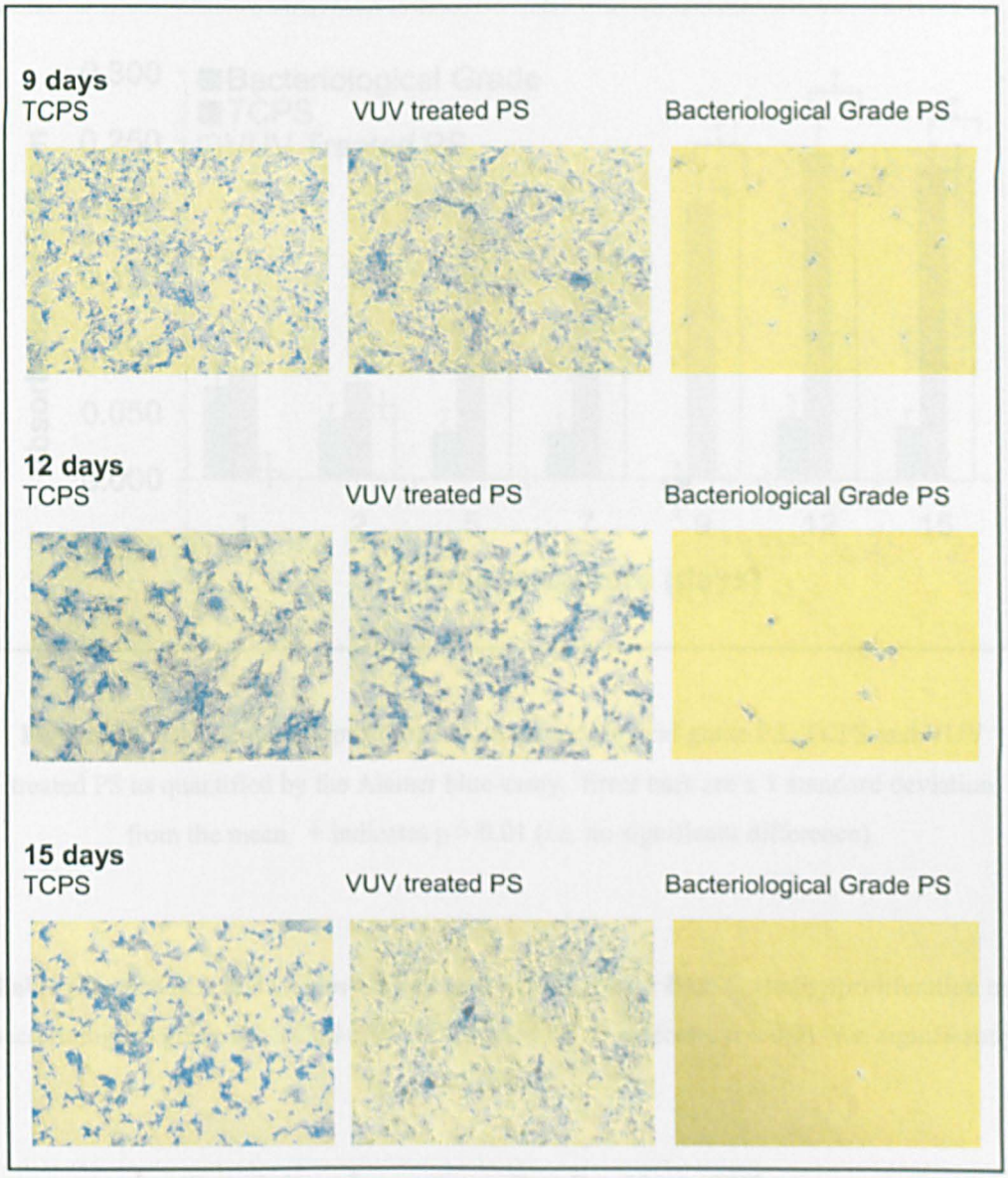

Figure 6.7: BMSC cultures stained with methylene blue after 9, 12 and 15 days in culture. Objective lens = 10x.

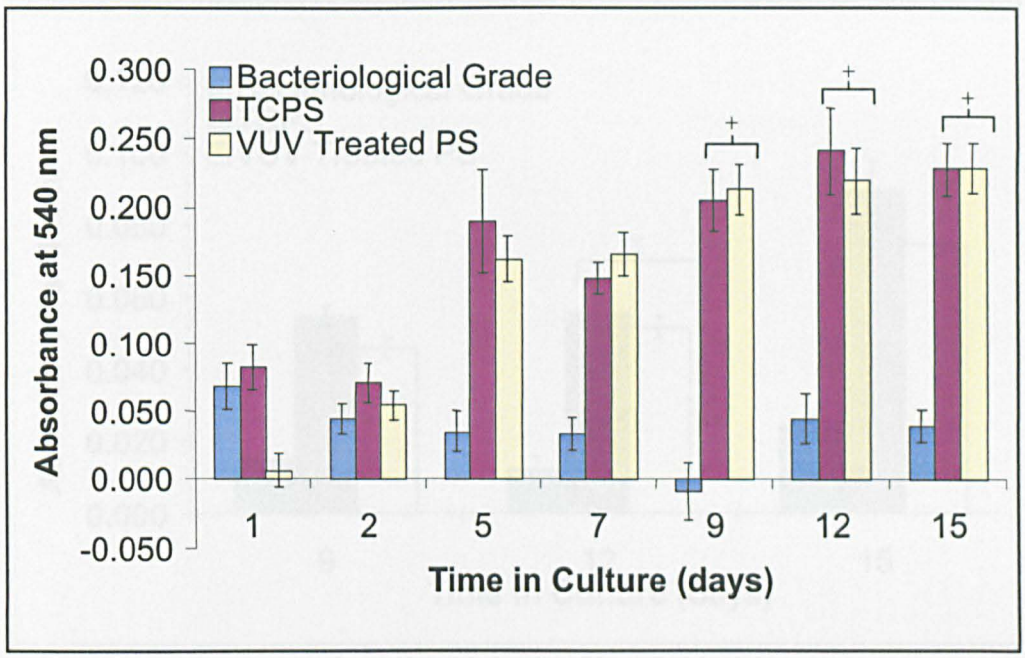

Figure 6.8: BMSC vitality/proliferation on bacteriological grade PS, TCPS and VUV treated PS as quantified by the Alamar blue assay. Error bars are ± 1 standard deviation from the mean. + indicates $p > 0.01$ (*i.e.* no significant difference).

Table 6.4: ANOVA and Games-Howell post hoc results for BMSC vitality/proliferation on bacteriological grade PS, TCPS and VUV treated PS. * indicates $p < 0.01$ (*i.e.* significantly different).

	F-statistic	Post Hoc Means Differences		
		BG-TCPS	BG-Treated	TCPS-Treated
1 day	135.3*	-0.015*	0.063*	0.077*
2 days	36.7*	-0.026*	-0.010*	-0.017*
5 days	307.0*	-0.155*	-0.127*	0.028*
7 days	851.9*	-0.115*	-0.132*	0.017*
9 days	1094.2*	-0. 214*	-0.221*	-0.008
12 days	542.3*	-0.195*	-0.174*	0.021
15 days	153.0*	-0.188*	-0.189*	-0.001

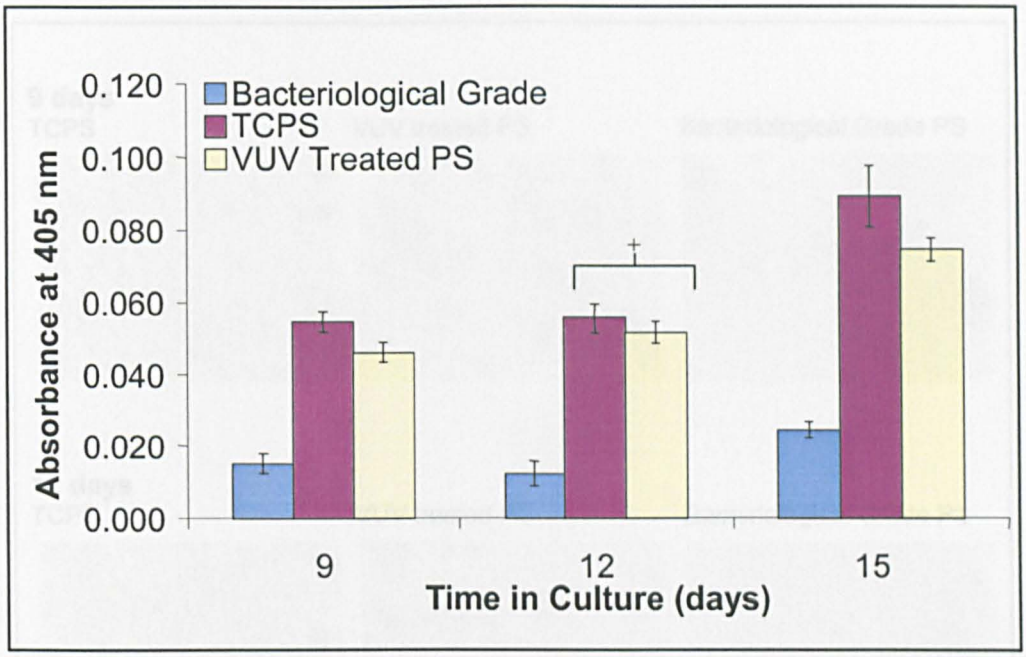

Figure 6.9: Alkaline phosphatase production of BMSC on bacteriological grade PS, TCPS and VUV treated PS. Error bars are ± 1 standard deviation from the mean. + indicates $p > 0.01$ (*i.e.* no significant difference)

Table 6.5: ANOVA and Games-Howell post hoc results for alkaline phosphatase production on bacteriological grade PS, TCPS and VUV treated PS. * indicates $p < 0.01$ (*i.e.* significantly different).

	F-statistic	Post Hoc Means Differences		
		BG-TCPS	BG-Treated	TCPS-Treated
9 days	504.1*	-0.040*	-0.032*	0.008*
12 days	413.6*	-0.043*	-0.039*	0.004
15 days	382.0*	-0.065*	-0.050*	0.015*

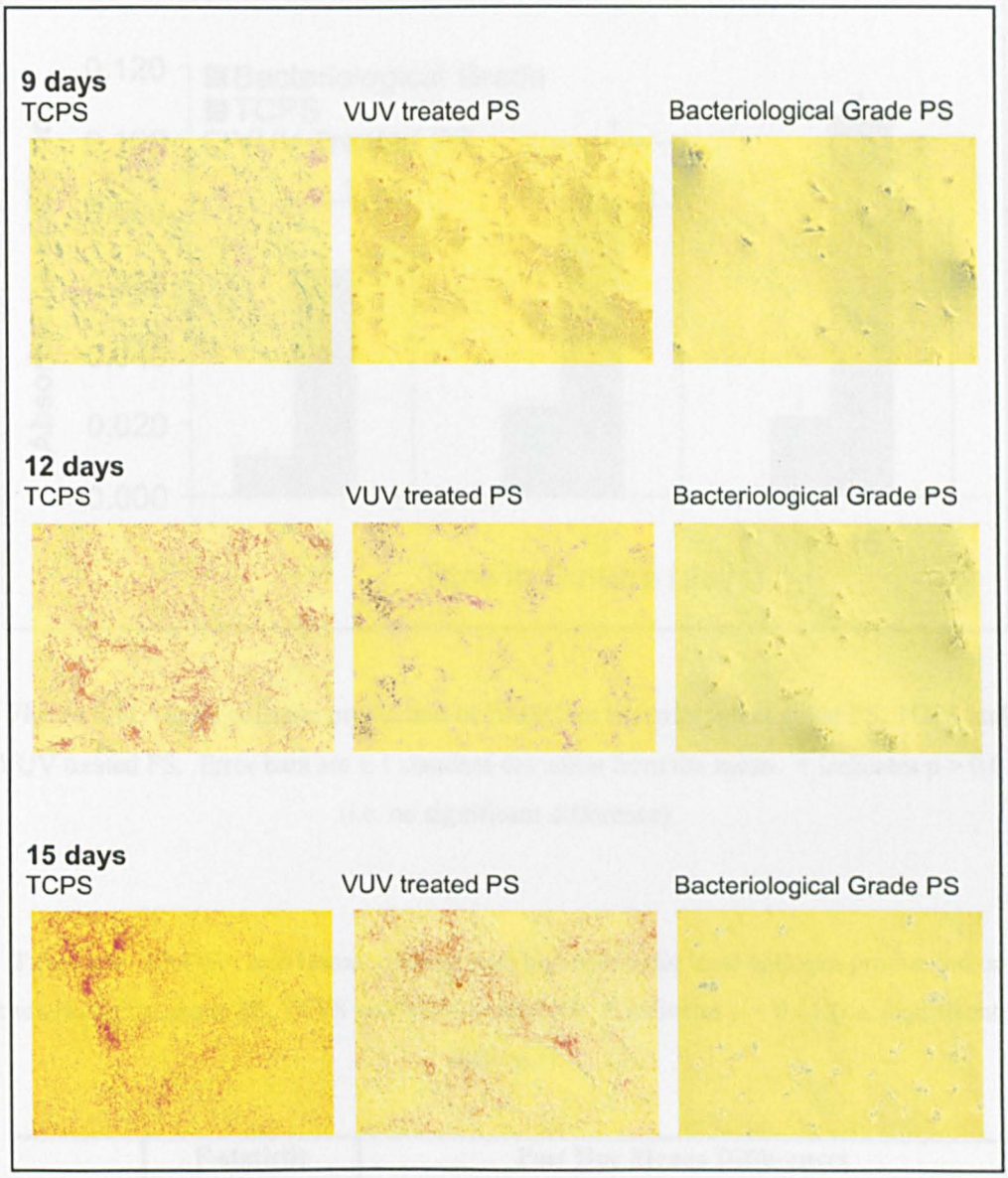

Figure 6.10: BMSC cultures stained for alkaline phosphatase after 9, 12 and 15 days in culture. Objective lens = 10x.

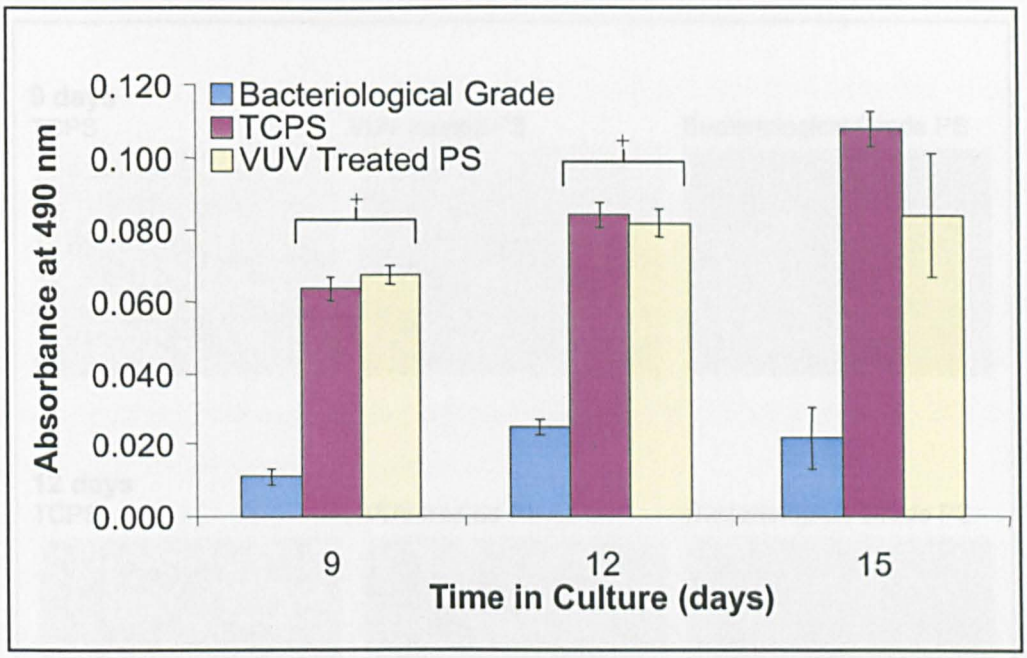

Figure 6.11: Total collagen production of BMSC on bacteriological grade PS, TCPS and VUV treated PS. Error bars are ± 1 standard deviation from the mean. + indicates $p > 0.01$ (*i.e.* no significant difference)

Table 6.6: ANOVA and Games-Howell post hoc results for total collagen production on bacteriological grade PS, TCPS and VUV treated PS. * indicates $p < 0.01$ (*i.e.* significantly different).

	F-statistic	Post Hoc Means Differences		
		BG-TCPS	BG-Treated	TCPS-Treated
9 days	1153.1*	-0.053*	-0.057*	-0.004
12 days	907.0*	-0.059*	-0.057*	0.002
15 days	126.5*	-0.086*	-0.062*	0.024*

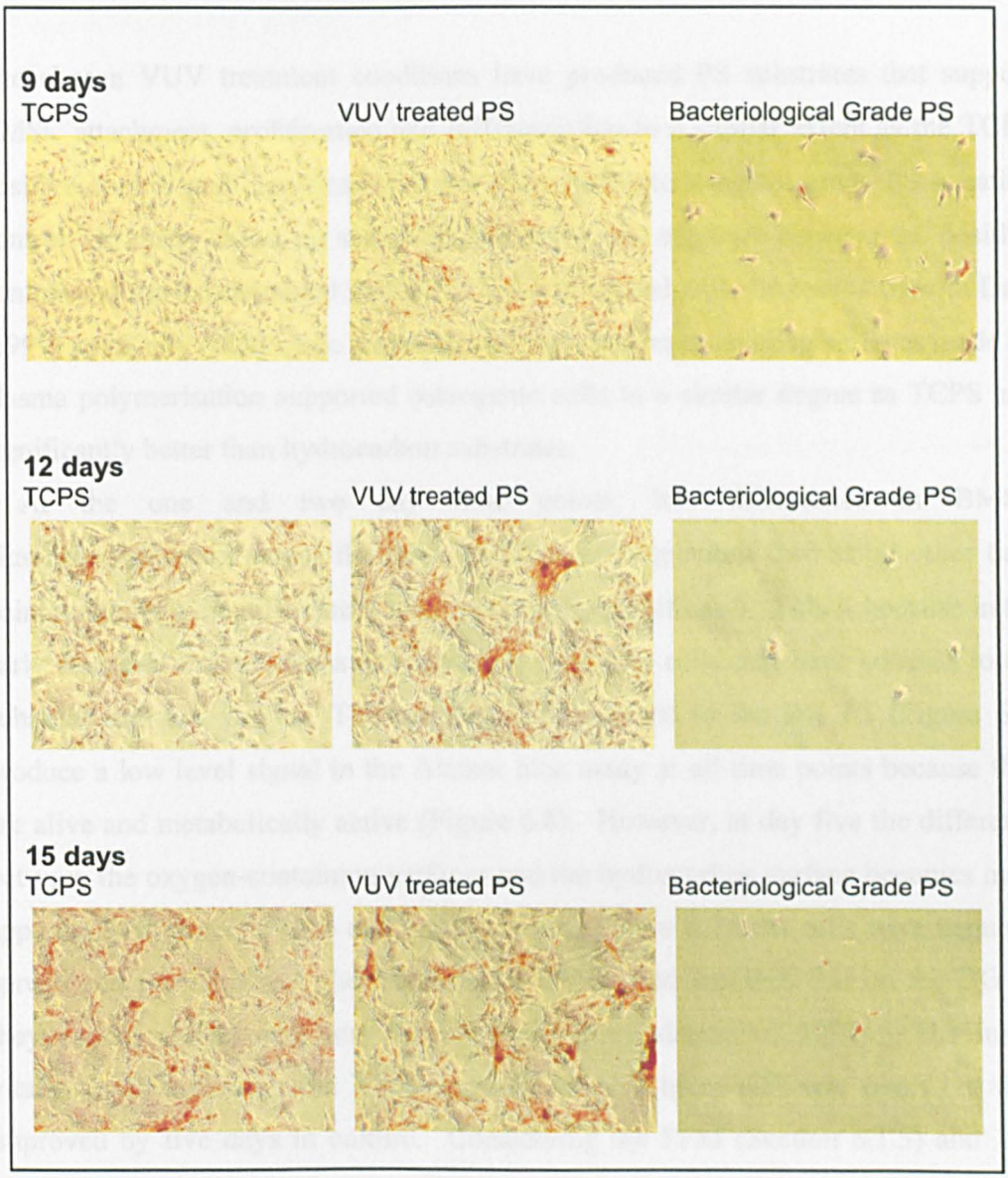

Figure 6.12: BMSC cultures stained for total collagen after 9, 12 and 15 days in culture. Objective lens = 10x.

6.2.5 Discussion

The chosen VUV treatment conditions have produced PS substrates that support BMSC attachment, proliferation and differentiation to a similar extent as the TCPS positive control and significantly better than the bacteriological grade PS negative control. In many cases, no statistical difference was apparent between the positive control and the experimental surface. This is in accord with the results of both Daw (1999) and Kelly (2001) who demonstrated that oxygen-containing surfaces made by plasma polymerisation supported osteogenic cells to a similar degree as TCPS and significantly better than hydrocarbon substrates.

At the one and two day time points, less differences in BMSC vitality/proliferation across the three surfaces were apparent than at all other time points (although the differences were statistically significant). This is because in the early stages of culture, the assay is merely detecting cells that have adhered to the substrate and are viable. The rounded cells adhered to the BG PS (Figure 6.7) produce a low level signal in the Alamar blue assay at all time points because they are alive and metabolically active (Figure 6.8). However, at day five the difference between the oxygen-containing surfaces and the hydrocarbon surface becomes more apparent. As shown by the cell morphologies (Figure 6.7), the cells have begun to spread and proliferate on the TCPS and VUV treated surfaces, but on the BG PS they cannot spread and thus do not proliferate (Maroudas, 1973). The initial vitality/proliferation on the VUV treated surface (Figure 6.8) was poor, but then improved by five days in culture. Considering the FFM (Section 6.1.3) and XPS depth profiling (Section 5.4.2) results, it is likely that the VUV treated surface has less oxygen located at the surface than the does TCPS – despite the two surfaces having a similar oxygen content over the XPS sampling depth. The difference in surface oxygen concentration may affect the amount and conformation of specific proteins adsorbing from serum (Horbett, 1984). Thus, the improvement in cell culture performance of the VUV treated surface over the first five days of the culture period may be associated with a rearrangement of proteins that have adsorbed on to the surface into a more favourable conformation (Horbett, 1984). A similar rearrangement does not take place on the bacteriological grade PS because proteins

adsorb to hydrophobic surfaces irreversibly and therefore cannot reorganise to allow cell spreading (Chinn, 1995).

The decrease in proliferation after nine days is accompanied by the production of alkaline phosphatase and collagen, as described in Section 3.4.1. Due to low attachment and proliferation on the bacteriological grade PS alkaline phosphatase and collagen production were both low on this surface. The level of alkaline phosphatase produced by BMSC on the VUV treated and TCPS surfaces was similar for the three time points, with lower mean differences than for comparisons involving the negative control. Indeed, no statistically significant difference was identified for the 12 day samples. Similarly, total collagen production on the TCPS and VUV treated PS was not significantly different at 9 and 12 days. Although significantly significant, the mean difference between the TCPS and experimental surface at the 15 day time point was very low. In this case, the large variance within the 15 day data set may have skewed the result, producing a false difference. Possible sources of such within-group variance include:

- the number and activity of the cells,
- the level of surface modification and/or presence of contaminants,
- inherent errors in the assay method.

Due to such factors, anomalous results were apparent in each repeat of the experiments (*e.g.* the 9 day measurement in Figure 6.8 and the large variance, indicated by the large error bar, on the 15 day VUV treated surface in Figure 6.11). A larger number of samples for the alkaline phosphatase and collagen assays would have been valuable in identifying such outliers, but the geometry of plasma reactor only allowed VUV treatment of nine wells on each 24-well plate.

6.2.6 Conclusions

The results and discussion presented above relate to one stated aim of this Chapter:

- to use VUV treatment of PS to create a surface suitable for culture of BMSC

Thus, the following conclusions are pertinent:

- The chosen VUV treatment of PS produced a surface suitable for the culture of BMSC, as compared to a TCPS positive control and a BG PS negative control.
- Inherent variability in biological experiments generates the need for many replicates of each surface, the provision of which was limited in this study by the geometry of the processing reactor.

6.3 Cell Culture on Patterned Substrates

6.3.1 Grid #1 Cellular Patterns

BMSC were cultured on chemically patterned VUV treated PS surfaces created using Grid #1. Examples of light microscopy images are presented in Figure 6.13. After 24 hours the cells had adhered preferentially to all of the treated regions, which ranged in width from 75 μm to 5 μm. Images a) and b) clearly show the boundary between the hydrophilic and hydrophobic areas at the rim of the circular grid. After several days in culture, cells that had initially landed on untreated regions of the pattern appear to have migrated to the treated bars, or been removed during media changes. Images c), d), f) and g) demonstrate that the cells produced alkaline phosphatase and collagen whilst their attachment and spreading was restricted to the hydrophilic areas of the pattern. In some wells (*e.g.* image f), the cells did not appear to attach to the bars near the centre of the pattern (5 μm – 10 μm).

6.3.2 Grid #2 Cellular Patterns

On surface chemical patterns created with Grid #2, BMSC attachment was patchy and no cellular pattern was discernable throughout the 15-day culture period (Figure 6.14).

Cellular patterns did not form even when the seeding density of BMSC was increased from 25,000 cells per well to 50,000, 100,000, 200,000 and 400,000 cells per well. This experiment was also performed with a rat osteosarcoma (ROS) cell line, but no patterns were evident at any stage in the culture period for any of the seeding densities tested.

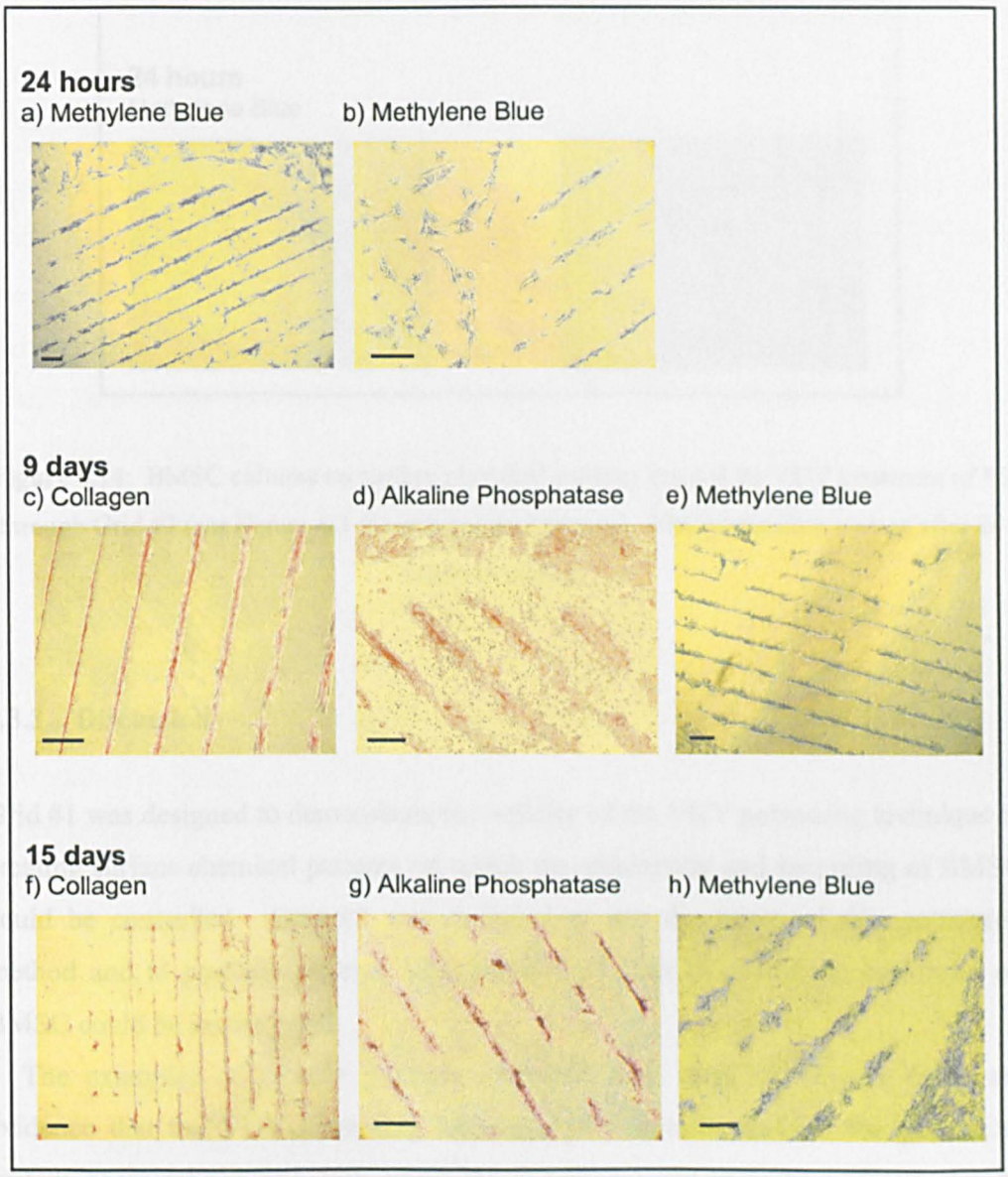

Figure 6.13: BMSC cultures on surface chemical patterns created by VUV treatment of PS thorough Grid #1 (see Figure 4.2 for original grid pattern). Width of bars (left/top to right/bottom of picture): a) 75μm – 10 μm; b) 50 μm – 25 μm; c) 5 μm – 25 μm; d) 40 μm – 60 μm; e) 75μm – 15 μm; f) 5 μm – 75 μm; g) 15 μm – 5 μm; h) 50 μm – 75 μm. Scale bars indicate approximately 200 μm.

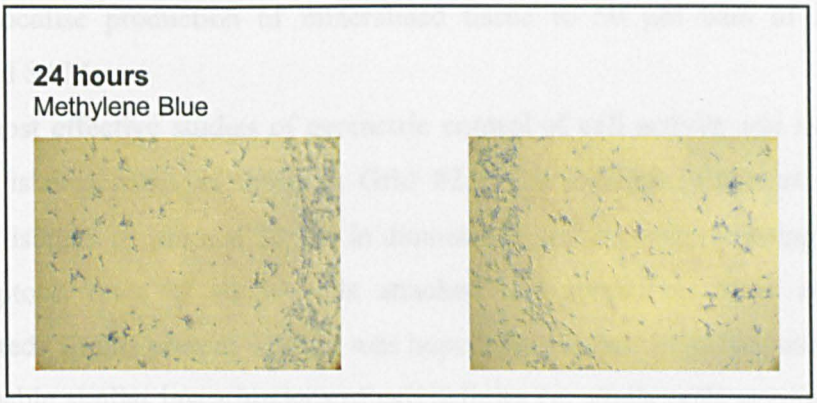

Figure 6.14: BMSC cultures on surface chemical patterns created by VUV treatment of PS through Grid #2 (see Figure 4.3 for original grid pattern). Methylene blue stained after 24 hours in culture.

6.3.3 Discussion

Grid #1 was designed to demonstrate the validity of the VUV patterning technique in creating surface chemical patterns on which the attachment and spreading of BMSC could be controlled. Grid #2 was designed to test the limits of this patterning method and to produce patterns with which the effect of geometric constraint on BMSC could be investigated.

The examples of cellular patterns produced from Grid #1 (Figure 6.13) are evidence that the VUV patterning technique is a suitable method for generating surface chemical patterns with which the attachment and spreading of cells can be controlled. Attachment and spreading was restricted to the areas exposed to the VUV, which ranged from 75 μm to 5 μm in width. In some cases (*e.g.* image 6.13f), the centre of the cellular pattern was less well defined then the larger bars. The condensed water images (Figure 6.4a) prove that the technique is capable of producing these features, therefore the most likely explanation for the lack of definition is insufficient contact between the patterning grid and the substrate where the grid has been bent upwards away from the surface. The production of alkaline phosphatase and the deposition of collagen were restricted to the areas exposed to

the VUV treatment. This is similar to the findings of Healy *et al.* (1996), who were able to localise production of mineralised tissue to 50 μm bars of an amine-terminated SAM.

The most effective studies of geometric control of cell activity use isolated cell adhesive islands, such as those in Grid #2. For example, Chen *et al.* (1997) produced islands 10 μm and 20 μm in diameter by microcontact printing of SAMs. The apoptosis rates of single cells attached and spread on these islands was investigated. In this present work, it was hoped that patterns produced using Grid #2 would enable similar investigations of cell activity *i.e.* single cells would attach and spread on the adhesive islands. However, as illustrated in Figure 6.14, no cellular patterns formed, even on the larger features. This could be because either the pattern was not well defined and/or the cells did not locate the pattern.

Although the condensed water images (Figure 6.4b) were inconclusive for the very small features (*e.g.* 7 μm x 7 μm), the larger features were evident by this method and therefore should have been reproduced in at least some areas. Therefore it is more likely that the cells did not form patterns because they were unable to locate the adhesive regions. This could be due to a number of factors, including:

- Probability – when in suspension the cells are just a few microns in diameter, so the chance of them landing on or near a treated island is very small
- Chemotaxis – cells growing unconstrained on the treated area around the outside of the grid will be sending chemical signals, indicating that they are attached and spreading well, to those that may have landed on the untreated regions

Attempts to increase the probability of cells attaching to the adhesive islands by increasing the seeding density failed, possibly because the number of cells growing unconstrained was also increased. Cell lines are generally more robust and perhaps more capable of attaching to a substrate in smaller groups or even as single cells (Freshney, 1987). Therefore, the seeding density experiment was also performed with ROS cells, but again, no patterns formed.

6.3.4 Conclusions

The results and discussion presented above relate to one stated aim of this Chapter:

- to employ the surface chemical patterns in a pilot study of the effects of geometric constraint on the attachment, growth and differentiation of BMSC

This aim was not achieved due to the problems encountered in creating surface chemical patterns with Grid #2. However, the following conclusions may still be deduced:

- The attachment and spreading of BMSC can be restricted to hydrophilic regions of surface chemical patterns produced using Grid #1, but there is no apparent effect on differentiation other than the localisation of alkaline phosphatase and collagen production.
- For the five seeding densities tested, neither BMSC nor ROS cells form patterns on PS surfaces treated through Grid #2 because either the pattern is not well defined enough and/or the cells cannot locate it.
- The presence of cells in their unconstrained spreading state is a major concern in the design of this experiment.

Chapter Seven

Conclusions and Further Work

Conclusions

A novel, highly manipulable plasma source has been developed and utilised in the manufacture of polystyrene (PS) substrates with surface chemical patterns of controlled chemistry. The resultant surfaces were used to create cellular patterns of bone marrow stromal cells (BMSC).

Conclusions from this study are drawn by revisiting the original project aims stated in Chapter One. These were:

- **to develop an argon plasma treatment system in which independent control over the ion energy and flux could be achieved**

A novel two-stage argon plasma source in which the ion energy and ion flux can be varied independently, by controlling the electron temperature and plasma density has been developed. Such control was possible using a single biased mesh to separate the main plasma from the process region, but multiple global plasma parameters needed to be varied. A double biased mesh system afforded more control over the ion flux and ion energy whilst all other global parameters were kept constant.

- **to use this 'tailored' plasma to investigate the role of ions in the surface modification of polystyrene**

Surface analysis by XPS revealed that oxygen incorporation into the surface of polystyrene treated in this source was independent of ion flux and ion energy. By exclusion of ions from the process chamber, VUV photons were found to be the major source of modification of polystyrene in this reactor system. A control

experiment employing a lithium fluoride window to eliminate all species except VUV photons from the process chamber showed that the role of metastables in this system is also negligible.

- **to use plasma processing of PS to create a surface suitable for culture of BMSC**

Cell culture surfaces manufactured using the VUV source supported the attachment, proliferation and differentiation of primary rat bone marrow stromal cells to a similar degree as commercially available tissue culture plastic.

- **to create surface chemical patterns on PS using a plasma-based patterning technique**

VUV patterning with Grid #1 produced hydrophilic bars of as small as 5 μm in width. These patterns were clearly visualised by condensing water onto the surface. The production of collagen and alkaline phosphatase by BMSC cultured on these patterns was localised to the VUV treated areas of the PS.

- **to employ the surface chemical patterns in a pilot study of the effects of geometric constraint on the attachment, growth and differentiation of BMSC**

Surface chemical patterns produced with Grid #2 were not easily visualised with condensed water. Only the larger features were apparent and BMSC did not form clearly defined patterns on these surfaces. Therefore it was not possible to produce surfaces suitable for the pilot study regarding geometric control of cell behaviour.

Further Work

Further investigations of depth of modification

XPS depth profiling may not reflect the true structure of the modified polymer because a signal from the uppermost layers is always included when analysing deeper into the sample. Investigations with reflectance Infra Red Spectroscopy may provide better comparison of the depth of modification of both traditional argon plasma and the novel plasma source used in this work.

Investigations of the limits of VUV patterning

A more sophisticated method than condensed water is necessary to ascertain whether the smaller features of Grid #2 are actually on the surface or not. This could be achieved by use of imaging XPS or ToF-SIMS.

Improvements to cell culture

When producing samples for use in studies of geometric constraint on cells, it would be beneficial to find a method of preventing cells from growing unconstrained around edges of the pattern and communicating with cells growing on the pattern.

Examination of cytoskeleton in geometrically constrained cells

Florescent labelling of the cytoskeleton in patterned cells would allow visualisation of the effects of geometric confinement.

Analysis of collagen fibres

Electron microscopy of collagen produced by geometrically confined cells to investigate the alignment of fibrils.

References

Alberts, B., Bray, D., Lewis, J., Raff, M., Roberts, K. and Watson, J. D. (1994). Cell Junctions, Cell Adhesion and the Extracellular Matrix. In *Molecular Biology of the Cell*, eds. B. Alberts D. Bray J. Lewis M. Raff K. Roberts and J. D. Watson. New York: Garland.

Amstein, C. F. and Hartman, P. A. (1975). Adaptation of Plastic Surfaces for Tissue Culture by Glow Discharge. *J. Clin. Microbiol.* **2**, 46-54.

Andrade, J. D. and Hlady, V. (1986). Protein Adsorption and Materials Biocompatibility. *Adv. Polymer Sci.* **79**, 1-65.

Ayad, S., Boot-Handford, R. P., Humphries, M. J., Kadler, K. E. and Shuttleworth, C. A. (1998). The Extracellular Matrix Factsbook. San Diego: Academic Press.

Bai, H. K., Hong, J. I., Chung, C. W., Kim, S. S. and Chang, H. Y. (2001). Pressure and Helium Mixing Effects on Plasma Parameters in Temperature Control Using a Grid System. *Phys. Plasmas* **8**, 3498-3501.

Bai, H. K., Hong, J. I., You, S. J., Choi, C. K. and Chang, H. Y. (2002). The Effects of Mixing Molecular Gases on Plasma Parameters in a System with Grid-Controlled Electron Temperature. *Phys. Plasmas* **9**, 1025-1028.

Bale, M. D., Wolfhart, L. A., Tomasini, B. and Sutton, R. C. (1989). Identification of Vitronectin as a Major Plasma Protein Adsorbed on Polymer Surfaces of Different Copolymer Composition. *Blood* **74**, 2698-2706.

Barry, F., Boynton, R. E., Liu, B. and Murphy, J. M. (2001). Chondrogenic Differentiation of Mesenchymal Stem Cells from Bone Marrow: Differentiation-Dependent Gene Expression of Matrix Components. *Exp. Cell Res.* **268**, 189-200.

Barton, D., Bradley, J. W., Gibson, K. J., Steele, D. A. and Short, R. D. (2000). An *in situ* Comparison between VUV Photon Energy and Ion Energy Fluxes to Polymer Surfaces Immersed in RF Plasma. *J. Phys. Chem. B* **104**, 7150-7153.

Barton, D., Bradley, J. W., Steele, D. A. and Short, R. D. (1999). Investigating Radio Frequency Plasmas Used for the Modification of Polymer Surfaces. *J. Phys. Chem. B* **103**, 4423-4430.

Beake, B. D. and Leggett, G. J. (2000). Variation of Frictional Forces in Air with the Compositions of Heterogeneous Organic Surfaces. *Langmuir* **16**, 735-739.

Bentley, K. L. and Klebe, R. J. (1985). Fibronectin Binding Properties of Bacteriologic Petri Plates and Tissue Culture Dishes. *J. Biomed. Mater. Res.* **19**, 757-769.

Ben-Ze'ev, A. (1991). Animal Cell Shape Changes and Gene Expression. *BioEssays* **13**, 207-212.

Beumer, G. J., van Blitterswijk, C. A. and Ponec, M. (1994). The Use of Gas Plasma Treatment to Improve the Cell-Substrate Properties of a Skin Substitute Made of Poly(ether)/Poly(ester) Coploymers. *J. Mater. Sci. - Mater. Med.* **5**, 1-6.

Bhatia, S. N., Yarmush, M. L. and Toner, M. (1997). Controlling Cell Interactions by Micropatterning in Co-Cultures: Hepatocytes and 3T3 Fibroblasts. *J. Biomed. Mater. Res.* **34**, 189-199.

Briggs, D. (1998). Surface Analysis of Polymers by XPS and Static SIMS. Cambridge: Cambridge University Press.

Brown, A. F. and Lackie, J. M. (1981). Fibronectin and Collagen Inhibit Cell-Substratum Adhesion of Neutrophil Granulocytes. *Exp. Cell Res.* **136**, 225-231.

Bullett, N. A. (2001). Plasma Polymer Deposition and Chemical Micropatterning for the Control of Attachment and Spatial Distribution of Proteins. PhD. Thesis, *Department of Engineering Materials*, University of Sheffield.

Bullett, N. A., Short, R. D., O'Leary, T., Beck, A. J., Douglas, C. W. I., Cambray-Deakin, M., Fletcher, I. W., Roberts, A. and Blomfield, C. (2001). Direct Imaging of Plasma-Polymerized Chemical Micropatterns. *Surf. Interface Anal.* **31**, 1074-1076.

Callen, B. W., Sodhi, R. N. S., Shelton, R. M. and Davies, J. E. (1993). Behaviour of Primary Bone Cells on Characterized Polystyrene Surfaces. *J. Biomed. Mater. Res.* **27**, 851-859.

Cassiman, J. J., Marynen, P., Brugmans, M., van Leuven, F. and van den Berghe, H. (1981). Role of the Alpha-2-M Receptor in Attachment and Spreading of Human Fibroblasts. *Cell Biol. Int. Rep.* **5**, 901-911.

Chandy, T., Das, G. S., Wilson, R. F. and Rao, G. H. R. (2000). Use of Plasma Glow for Surface-Engineering Biomolecules to Enhance Bloodcompatibility of Dacron and PTFE Vascular Prosthesis. *Biomaterials* **21**, 699-712.

Chapman, B. (1980). Glow Discharge Processes - Sputtering and Plasma Etching. New York: John Wiley & Sons Inc.

Chehroudi, B., Gould, T. R. L. and Brunette, D. M. (1992). The Role of Connective Tissue in Inhibiting Epithelial Downgrowth on Titanium-Coated Percutaneous Implants. *J. Biomed. Mater. Res.* **26**, 493-515.

Chen, C. S., Mrksich, M., Huang, S., Whitesides, G. M. and Ingber, D. E. (1997). Geometric Control of Cell Life and Death. *Science* **276**, 1425-1428.

Chen, C. S., Mrksich, M., Huang, S., Whitesides, G. M. and Ingber, D. E. (1998). Micropatterned Surfaces for Control of Cell Shape, Position, and Function. *Biotechnol. Prog.* **14**, 356-363.

Chinn, J. A. (1995). Biomaterials: Protein-Surface Interactions. In *The Biomedical Engineering Handbook*, (ed. J. D. Bronzino). Boca Raton: CRC Press.

Chiu, D. T., Jeon, N. L., Huang, S., Kane, R., Wargo, C. J., Choi, I. S., Ingber, D. E. and Whitesides, G. M. (2000). Patterned Deposition of Cells and Proteins onto Surfaces by Using Three-Dimensional Microfluidic Systems. *Proc. Natl. Acad. Sci. USA* **97**, 2408-2413.

Chu, P. K., Chen, J. Y., Wang, L. P. and Huang, N. (2002). Plasma-Surface Modification of Biomaterials. *Materials Science and Engineering* **R36**, 143-206.

Clark, D. T. and Dilks, A. (1977). ESCA Applied to Polymers. XV. RF Glow-Discharge Modification of Polymers, Studied by Means of ESCA in Terms of a Direct and Radiative Energy-Transfer Model. *J. Polym. Sci., Polym. Chem. Ed.* **15**, 2321-2345.

Clark, D. T. and Dilks, A. (1978). ESCA Applied to Polymers XVIII. RF Glow Discharge Modification of Polymers in Helium, Neon, Argon and Krypton. *J. Polym. Sci., Polym. Chem. Ed.* **16**, 911-936.

Clark, D. T. and Dilks, A. (1980). An Investigation of the Vacuum UV Spectra of Inductively Coupled RF Plasmas Excited in Inert Gases as a Function of Some of the Operating Parameters. *J. Polym. Sci., Polym. Chem. Ed.* **18**, 1233-1246.

Clark, P., Connolly, P., Curtis, A. S. G., Dow, J. A. T. and Wilkinson, C. D. W. (1990). Topographical Control of Cell Behaviour: II. Multiple Grooved Substrata. *Development* **108**, 635-644.

Clark, P., Connolly, P., Curtis, A. S. G., Dow, J. A. T. and Wilkinson, C. D. W. (1991). Cell Guidance by Ultrafine Topography *in Vitro*. *J. Cell Sci.* **99**, 73-77.

Cooper, E., Wiggs, R., Hutt, D. A., Parker, L., Leggett, G. J. and Parker, T. L. (1997). Rates of Attachment of Fibroblasts to Self-Assembled Monolayers Formed by the Adsorption of Alkylthiols onto Gold Surfaces. *J. Mater. Chem.* **7**, 435-441.

Corbin, G. A., Cohen, R. E. and Baddour, R. F. (1985). Surface Fluorination of Polymers in a Glow Discharge Plasma: Photochemistry. *Macromolecules* **18**, 98-103.

Curtis, A. S. G., Forrester, J. V., McInnes, C. and Lawrie, F. (1983). Adhesion of Cells to Polystyrene Surfaces. *J. Cell Biol.* **97**, 1500-1506.

Curtis, A. S. G. and McMurray, H. (1986). Conditions for Fibroblast Adhesion without Fibronectin. *J. Cell Sci.* **86**, 25-33.

Dai, L., Griesser, H. J. and Mau, A. W. H. (1997). Surface Modification by Plasma Etching and Plasma Patterning. *J. Phys. Chem. B* **101**, 9548-9554.

Daw, R. (1999). Plasma Co-Polymer Surfaces of Acrylic Acid/Octa-1,7-Diene: Surface Characterisation and Behaviour of Osteoblast-Like Cells. PhD. Thesis, *Department of Engineering Materials and Department of Clinical Dentistry*, University of Sheffield.

Dedhar, S., Ruoslahti, E. and Pierschbacher, M. D. (1987). A Cell Surface Receptor Complex for Collagen Type I Recognises the Arg-Gly-Asp Sequence. *J. Cell Biol.* **104**, 585-593.

Dhayal, M., Forder, D., Parry, K., Short, R. D., Barton, D. and Bradley, J. W. (2003). Tailored Plasmas for Applications in the Surface Treatment of Materials. *Surface Coatings Technology* **162**, 294-300.

Evans, M. D. M. and Steele, J. G. (1997). Multiple Attachment Mechanisms of Corneal Epithelial Cells to a Polymer - Cells Can Attach in the Absence of Exogenous Adhesion Proteins through a Mechanism That Requires Microtubules. *Exp. Cell Res.* **233**, 88-98.

Fabrizius-Homan, D. J. and Cooper, S. L. (1991). Competitive Adsorption of Vitronectin with Albumin, Fibrinogen and Fibronectin on Polymeric Biomaterials. *J. Biomed. Mater. Res.* **25**, 953-971.

Favre-Quattropani, L., Groening, P., Ramseyer, D. and Schlapbach, L. (2000). The Protection of Metallic Archaeological Objects Using Plasma Polymer Coatings. *Surface Coatings Technology* **125**, 377-382.

Ferri, K. F., Jacotot, E., Leduc, P., Geuskens, M., Ingber, D. E. and Kroemer, G. (2000). Apoptosis of Syncytia Induced by the HIV-1-Envelope Glycoprotein Complex: Influence of Cell Shape and Size. *Exp. Cell Res.* **261**, 119-126.

Foerch, R., McIntyre, N. S. and Hunter, D. (1990). Oxidation of Polyethylene Surfaces by Remote Plasma Discharge: A Comparison Study with Alternative Oxidation Methods. *J. Polym. Sci., Polym. Chem. Ed.* **28**, 193-204.

Folch, A., Jo, B., Hurtado, O., Beebe, D. J. and Toner, M. (2000). Microfabricated Elastomeric Stencils for Micropatterning Cell Cultures. *J. Biomed. Mater. Res.* **52**, 346-353.

Folch, A. and Toner, M. (1998). Cellular Micropatterns on Biocompatible Materials. *Biotechnol. Prog.* **14**, 388-392.

France, R. M. and Short, R. D. (1997). Plasma Treatment of Polymers: Effects of Energy Transfer from an Argon Plasma on the Surface Chemistry of Poly(Styrene), Low Density Poly(ethylene), Poly(propylene) and Poly(ethylene terephthalate). *J. Chem. Soc., Faraday Trans.* **93**, 3173-3178.

France, R. M., Short, R. D., Duval, E., Jones, F. R., Dawson, R. A. and MacNeil, S. (1998). Plasma Co-Polymerisation of Allyl Alcohol/1,7-Octadiene: Surface Characterisation and Attachment of Human Keratinocytes. *Chem. Mater.* **10**, 1176-1183.

Freidenstein, A. J., Gorskaja, J. F. and Kulagina, N. N. (1976). Fibroblast Precursors in Normal and Irradiated Mouse Hematopoietic Organs. *Exp. Hematol.* **4**, 267-274.

Freshney, R. I. (1987). Culture of Animal Cells (a Manual of Basic Technique). New York: Wiley-Liss.

Gengenbach, T. R., Chatelier, R. C. and Griesser, H. J. (1994). Characterisation of the Ageing of Plasma-Deposited Polymer Films: Global Analysis of X-Ray Photoelectron Spectroscopy Data. *Surf. Interface Anal.* **24**, 271-281.

Gerenser, L. J. (1987). X-Ray Photoemission Study of Plasma Modified Polyethylene Surfaces. *J. Adhesion Sci.Technol.* **1**, 265-352.

Gerenser, L. J. (1993). XPS Studies of *in Situ* Plasma-Modified Polymer Surfaces. *J. Adhesion Sci.Technol.* **7**, 1019-1040.

Ginsberg, M., Pierschbacher, M. D., Ruoslahti, E., Marguerie, G. and Plow, E. (1985). Inhibition of Fibronectin Binding to Platelets by Proteolytic Fragments and Synthetic Peptides Which Support Fibroblast Adhesion. *J. Biol. Chem.*, 3931-3936.

Grill, A. (1993). Cold Plasma in Materials Fabrication. Piscataway, NJ: IEEE Press.

Grill, A. and Itzhak, D. (1983). Nitriding of AISI M2 Tool Steel in an Inductive RF Plasma. *Thin Solid Films* **101**, 219-222.

Grinnell, F. and Feld, M. J. (1982). Fibronectin Adsorption on Hydrophilic and Hydrophobic Surfaces Detected by Antibody Binding and Analysed During Cell Adhesion in Serum Containing Medium. *J. Biol. Chem.* **257**, 4888-4893.

Haverstick, D. M., Cowan, J. F., Yamada, K. M. and Santoro, S. A. (1985). Inhibition of Platelet Adhesion to Fibronectin, Fibrinogen and Von Willebrand Factor Substrates by a Synthetic Tetrapeptide Derived from the Cell Binding Domain of Fibronectin. *Blood* **66**, 946-953.

Hayman, E. G., Pierschbacher, M. D. and Ruoslahti, E. (1985a). Detachment of Cells from Culture Substrate by Soluble Fibronectin Peptides. *J. Cell Biol.* **100**, 1948-1954.

Hayman, E. G., Pierschbacher, M. D., Suzuki, S. and Ruoslahti, E. (1985b). Vitronectin - a Major Cell Attachment-Promoting Protein in Foetal Bovine Serum. *Exp. Cell Res.* **160**, 245-258.

Healy, K. E., Lom, B. and Hockberger, P. E. (1994). Spatial Distribution of Mammalian Cells Dictated by Material Surface Chemistry. *Biotechnol. Bioeng.* **43**, 792-800.

Healy, K. E., Thomas, C. H., Rezania, A., Kim, J. E., McKeown, P. J., Lom, B. and Hockberger, P. E. (1996). Kinetics of Bone Cell Organization and Mineralization on Materials with Patterned Surface Chemistry. *Biomaterials* **17**, 195-208.

Holländer, A., Klemberg-Sapieha, J. E. and Wertheimer, M. R. (1994). Vacuum-Ultraviolet-Induced Oxidation of Polyethylene. *Macromolecules* **27**, 2893-2895.

Holländer, A., Klemberg-Sapieha, J. E. and Wertheimer, M. R. (1995). Polymer Oxidation Induced by Vacuum-Ultraviolet Emission. *Surface Coatings Technology* **74-75**, 55-58.

Hong, J. I., Seo, S. H., Kim, S. S., Yoon, N. S., Chang, C. S. and Chang, H. Y. (1999). Electron Temperature Control with Grid Bias Inductively Coupled Argon Plasma. *Phys. Plasmas* **6**, 1017-1028.

Hopkins, J., Wheale, S. H. and Badyal, J. P. S. (1996). Synergistic Oxidation at the Plasma/Polymer Interface. *J. Phys. Chem.* **100**, 14062-14066.

Horbett, T. A. (1984). Mass Action Effects on Competitive Adsorption of Fibrinogen from Haemoglobin Solutions and from Plasma. *Thromb. Haemostas.* **51**, 174-187.

Huang, S., Chen, C. S. and Ingber, D. E. (1998). Control of Cyclin D1 P27 KIP1 and Cell Cycle Progression in Human Capillary Endothelialcells by Cell Shape and Cytoskeletal Tension. *Mol. Biol. Cell* **9**, 3179-3193.

Huang, S. and Ingber, D. E. (2000). Shape-Dependent Control of Cell Growth, Differentiation, and Apoptosis: Switching between Attractors in Cell Regulatory Networks. *Exp. Cell Res.* **261**, 91-103.

Hudis, M. (1972). Surface Crosslinking of Polyethylene Using a Hydrogen Glow Discharge. *J. App. Polym. Sci.* **16**, 2397-2415.

Hudis, M. and Prescott, L. E. (1972). Surface Crosslinking of Polyethylene Produced by the Ultraviolet Radiation from a Hydrogen Glow Discharge. *Polym. Lett.* **10**, 179-183.

Inagaki, N. and Yasuda, H. (1981). Adhesion of Glow Discharge Polymers to Metals and Polymers. *J. App. Polym. Sci.* **26**, 3333-3341.

Ingber, D. E. (1990). Fibronectin Controls Capillary Endothelial Growth by Modulating Cell Shape. *Proc. Natl. Acad. Sci. USA* **87**, 3579-3583.

Ingber, D. E. (1998). In Search of Cellular Control: Signal Transduction in Context. *J. Cell Biochem. Suppl.* **30/31**, 232-237.

Ingber, D. E. and Folkman, J. (1989). Mechanochemical Switching between Growth and Differentiation During Fibroblast Growth Factor-Stimulated Angiogenesis in Vitro: Role of Extracellular Matrix. *J. Cell Biol.* **109**, 317-330.

Ingber, D. E., Prusty, D., Frangione, J., Cragoe, E. J. J., Lechene, C. and Schwartz, M. (1990). Control of Intracellular pH and Growth by Fibronectin in Capillary Endothelial Cells. *J. Cell Biol.* **110**, 1803-1812.

Kato, K., Iizuka, S. and Sato, N. (1994). Electron-Temperature Control for Plasmas Passing through a Negatively Biased Grid. *Appl. Phys. Lett.* **65**, 816-818.

Kato, S., Ando, J. and Matsuda, T. (2001). mRNA Expression on Shape-Engineered Endothelial Cells: Adhesion Molecules ICAM-1 and VCAM-1. *J. Biomed. Mater. Res.* **54**, 366-372.

Kelly, J. M. (2001). Osteoblast Response to Oxygen Functionalised Plasma Polymer Surfaces. PhD. Thesis, *Department of Engineering Materials*, University of Sheffield.

Kleinfeld, D., Kahler, K. H. and Hockberger, P. E. (1988). Controlled Outgrowth of Dissociated Neurons on Patterned Substrates. *J. Neurosci.* **8**, 4098-4120.

Kühn, G., Weidner, S., Decker, R., Ghode, A. and Friedrich, J. (1999). Selective Surface Funtionalization of Polyolefins by Plasma Treatment Followed by Chemical Reduction. *Surface Coatings Technology* **116/119**, 796-801.

Kumar, A. and Whitesides, G. M. (1993). Features of Gold Having Micrometer to Centimeter Dimensions Can Be Formed through a Combination of Stamping with an Elastomeric Stamp and an Alkanethiol "Ink" Followed by Chemical Etching. *Appl. Phys. Lett.* **63**, 2002-2004.

LaRocca, P. (1996). Technical Brief: Tissue Culture Surface Treatments. In *The Cell/Line*, vol. 6, pp. 1-2.

Latkany, R., Tsuk, A., Sheu, M.-S., Loh, I.-H. and Trinkaus-Randall, V. (1997). Plasma Surface Modification of Artificial Corneas for Optimal Endothelialization. *J. Biomed. Mater. Res.* **36**, 29-37.

Le, Q. T., Pireaux, J. J. and Caudano, R. (1997). XPS Study of the PET Film Surface Modified by CO_2 Plasma: Effects of the Plasma Parameters and Ageing. *J. Adhesion Sci.Technol.* **11**, 735-751.

Lee, J., Sugioka, K. and Toyoda, K. (1994). Micropatterning of Cultured Cells on Polystyrene Surface by Using an Excimer Laser. *Appl. Phys. Lett.* **65**, 400-402.

Lee, S.-D., Hsiue, G.-H., Chang, P. C.-T. and Kao, C.-Y. (1996a). Plasma-Induced Grafted Polymerization of Acrylic Acid and Subsequent Grafting of Collagen onto Polymer Film as Biomaterials. *Biomaterials* **17**, 1599-1608.

Lee, S.-D., Hsiue, G.-H., Kao, C.-Y. and Chang, P. C.-T. (1996b). Artificial Cornea: Surface Modification F Silicone Rubber Membrane by Raft Polymerization of pHEMA Via Glow Discharge. *Biomaterials* **17**, 587-595.

Lewandowska, K., Pergament, E., Sukenik, C. N. and Culp, L. A. (1992). Cell-Type-Specific Adhesion Mechanisms Mediated by Fibronectin Adsorbed to Cheimcally Derivatised Substrata. *J. Biomed. Mater. Res.* **26**, 1343-1363.

Liebermann, M. A. and Lichtenberg, A. J. (1994). Principles of Plasma Discharges and Materials Processing. New York: Wiley.

Lin, T. J., Antonelli, J. A., Yang, D. J., Yasuda, H. K. and Wang, F. T. (1997). Plasma Treatment of Automotive Steel for Corrosion Protection - a Dry Energetic Process for Coatings. *Progress in Organic Coatings* **31**, 351-361.

Lub, J., van Vroonhoven, F. C. B. M. and Bruninx, E. (1989). Interaction of Nitrogen and Ammonia Plasmas with Polystyrene and Polycarbonate Studied by X-Ray Photoelectron Spectroscopy, Neutron Activation Analysis and Static Secondary Ion Mass Spectrometry. *Polymer* **30**, 40-44.

Maroudas, N. G. (1973). Growth of Fibroblasts on Linear and Planar Anchorages of Limiting Dimensions. *Exp. Cell Res.* **81**, 104-110.

Mirenghi, L., Ramires, P. A., Pentassuglia, R. E., Rotolo, P. and Romito, A. (2000). Growth of Human Endothelial Cells on Plasma-Treated Polyethyleneterephthalate Surfaces. *J. Mater. Sci. - Mater. Med.* **11**, 327-331.

Mitchell, S. A., Emmison, N. and Shard, A. G. (2002). Spatial Control of Cell Attachment Using Plasma Micropatterned Polymers. *Surf. Interface Anal.* **33**, 742-747.

Momose, Y., Tamura, Y., Ogino, M. and Okazaki, S. (1992). Chemical Reactivity between Teflon® Surfaces Subjected to Argon Plasma Treatment and Atmospheric Oxygen. *J. Vac. Sci. Technol. A* **10**, 229-238.

Morra, M., Occhiello, E. and Garbassi, F. (1990). Surface Characterization of Plasma-Treated PTFE. *Surf. Interface Anal.* **16**, 412-417.

Moss, S. J., Jolly, A. M. and Tighe, B. J. (1986). Plasma Oxidation of Polymers. *Plasma Chem., Plasma Proc.* **6**, 401-416.

Mrksich, M., Chen, C. S., Xia, Y., Dike, L. E., Ingber, D. E. and Whitesides, G. M. (1996). Controlling Cell Attachment on Contoured Surfaces with Self-Assembled Monolayers of Alkanethiolates on Gold. *Proc. Natl. Acad. Sci. USA* **93**, 10775-10778.

Nakayama, Y., Takahagi, T., Soeda, F., Hatada, K., Nagaoka, S., Suzuki, J. and Ishitani, A. (1988). XPS Analysis of NH_3 Plasma-Treated Polystyrene Films Utilising Gas Phase Chemical Modification. *J. Polym. Sci., Polym. Chem. Ed.* **26**, 559-572.

Occhiello, E., Morra, M., Morini, G., Garbassi, F. and Humphrey, P. (1991). Oxygen-Plasma-Treated Polypropylene Interfaces with Air, Water and Epoxy Resins: Part 1. Air and Water. *J. App. Polym. Sci.* **42**, 551-559.

Ohl, A. and Schroder, K. (1999). Plasma-Induced Chemical Micropatterning for Cell Culturing Applications: A Brief Review. *Surface Coatings Technology* **116-119**.

Ohl, A., Schroder, K., Keller, D., Meyer-Plath, A., Bienert, H., Husen, B. and Rune, G. M. (1999). Chemical Micropatterning of Polymeric Cell Culture Substrates Using Low-Pressure Hydrogen Gas Discharge Plasmas. *J. Mater. Sci. - Mater. Med.* **10**, 747-754.

Okell, S., Henshaw, T., Farrow, G., Aindow, M. and Jones, C. (1995). Effects of Low-Power Plasma Treatment on Polyethylene Surfaces. *Surf. Interface Anal.* **23**, 319-327.

Oldberg, A., Franzen, A. and Heingard, D. (1986). Cloning and Sequence Analysis of Rat Sialoprotein (Osteopontin) cDNA Reveals an Arg-Gly-Asp Cell-Binding Sequence. *Proc. Natl. Acad. Sci. USA* **83**, 8819-8823.

Ostuni, E., Kane, R., Chen, C. S., Ingber, D. E. and Whitesides, G. M. (2000). Patterning Mammalian Cells Using Elastomeric Membranes. *Langmuir* **16**, 7811-7819.

Owen, M. (1988). Marrow Stromal Cells. *J. Cell Sci. Suppl.* **10**, 63-76.

Ozdemir, M., Yurteri, C. U. and Sadikoglu, H. (1999). Physical Polymer Surface Modification Methods and Applications in Food Packaging Polymers. *Crit. Rev. Food Sci.* **39**, 457-477.

Peel, S. A. F., Sodhi, R. N., Duc, T. M. and Davies, J. E. (1992). Polymer Surface Modification Causes Change in Phenotypic Expression of Primary Bone Cells. *Mat. Res. Soc. Symp. Proc* **252**, 71-77.

Pierschbacher, M. D. and Ruoslahti, E. (1984). Cell Attachment Activity of Fibronectin Can Be Duplicated by Small Synthetic Fragments of the Molecule. *Nature* **309**, 30-33.

Piglowski, J., Gancarz, I., Staniszewska-Kus, J., Paluch, D., Szymonowicz, M. and Konieczny, A. (1994). Influence of Plasma Modification on Biological Properties of Poly(ethylene terephthalate). *Biomaterials* **15**, 909-916.

Pittenger, M. F. (1998). Adipogenic Differentiation of Human Mesenchymal Stem Cells. United States: Osiris Therapeutics, Inc.

Pittenger, M. F., Mackay, A. M., Beck, S. C., Jaiswal, R. K., Douglas, R., Mosca, J. D., Moorman, M. A., Simonetti, D. W., Craig, S. and Marshak, D. R. (1999). Multilineage Potential of Adult Human Mesenchymal Stem Cells. *Science* **284**, 143-147.

Plow, E., Pierschbacher, M. D., Ruoslahti, E., Gartner, G. A. and Ginsberg, M. H. (1985). The Effect of Arg-Gly-Asp-Containing Peptides on Fibrinogen and Von Willebrand Factor Binding to Platelets. *Proc. Natl. Acad. Sci. USA* **82**, 8057-8061.

Pringle, S. D., Joss, V. S. and Jones, C. (1996). Ammonia Plasma Treatment of PTFE under Known Plasma Conditions. *Surf. Interface Anal.* **24**, 821-829.

Prockop, D. J. (1997). Marrow Stromal Cells as Stem Cells for Nonhaematopoietic Tissues. *Science* **276**, 71-74.

Ratner, B. D., Chilkoti, A. and Lopez, G. P. (1990). Plasma Deposition and Treatment for Biomaterial Applications. In *Plasma Deposition, Treatment and Etching of Polymers*, (ed. R. d'Agostino), pp. 463-516: Academic Press, Inc.

Roth, J. R. (1995). Industrial Plasma Engineering, Vol. 1: Principles. Bristol: IOP Publishing.

Rovensky, Y. A., Slavnaja, I. L. and Vasiliev, J. M. (1971). Behaviour of Fibroblast-Like Cells on Grooved Surfaces. *Exp. Cell Res.* **65**, 193-201.

Ruoslahti, E. (1996). RGD and Other Recognition Sequences for Integrins. *Annu. Rev. Cell Dev. Biol.* **12**, 697-715.

Ruoslahti, E. and Pierschbacher, M. D. (1987). New Perspectives in Cell Adhesion: RGD and Integrins. *Science* **238**, 491-497.

Schonhorn, H. and Hansen, R. H. (1967). Surface Treatment of Polymers for Adhesive Bonding. *J. App. Polym. Sci.* **11**, 1461-1474.

Schwarzenbach, W., Derouard, J. and Sadeghi, N. (2001). Treatment of Organic Polymer Surfaces by CF_4 Plasmas: Etching by Flourine Atoms and Influence of Vacuum Ultraviolet Radiation. *J. App. Physics* **90**, 5491-5496.

Scotchford, C. A., Cooper, E., Leggett, G. J. and Downes, S. (1998). Growth of Human Osteoblast-Like Cells on Alkanethiol on Gold Self-Assembled Monolayers: The Effect of Surface Chemistry. *J. Biomed. Mater. Res.* **41**, 431-442.

Shard, A. G. and Badyal, J. P. S. (1991a). Plasma Oxidation Versus Photooxidation of Polystyrene. *J. Phys. Chem.* **95**, 9436-9438.

Shard, A. G. and Badyal, J. P. S. (1991b). Plasma Versus Ultraviolet Enhanced Oxidation of Polyethylene. *Polym. Commun.* **32**, 217-219.

Singhvi, R., Stephanopoulos, G. N. and Wang, D. I. C. (1994a). Review: Effects of Substratum Morphology on Cell Physiology. *Biotechnol. Bioeng.* **43**, 764-771.

Singhvi, R., Stephanopoulos, G. N., Wang, D. I. C., Kumar, A., Lopez, G. P., Whitesides, G. M. and Ingber, D. E. (1994b). Engineering Cell Shape and Function. *Science* **264**, 696-698.

Steele, D. A. (2000). Radio Frequency Plasma Used for the Surface Modification of Polymers: A Physical and Chemical Investigation. PhD. Thesis, *Department of Engineering Materials*, University of Sheffield.

Steele, J. G., Dalton, B. A., Johnson, G. and Underwood, P. A. (1993). Polystyrene Affects Vitronectin Activity: An Explanation for Cell Attachment to Tissue Culture Polystyrene but Not to Unmodified Polystyrene. *J. Biomed. Mater. Res.* **27**, 927-940.

Steele, J. G., Johnson, G., Norris, W. D. and Underwood, P. A. (1991). Adhesion and Growth of Cultured Human Endothelial Cells on Perfluorosulphonate: Role of Vitronectin and Fibronectin in Cell Attachment. *Biomaterials* **12**, 531-539.

Steele, J. G., Johnson, G. and Underwood, P. A. (1992). Role of Serum Vitronectin and Fibronectin Adhesion of Fibroblasts Following Seeding onto Tissue Culture Polystyrene. *J. Biomed. Mater. Res.* **26**, 861-884.

Suzuki, M., Kishida, A., Iwata, H. and Ikada, Y. (1986). Graft Copolymerization of Acrylamide onto a Polyethylene Surface Pretreated with a Glow Discharge. *Macromolecules* **19**, 1804-1808.

Thomas, C. H., McFarland, C. D., Jenkins, M. L., Rezania, A., Steele, J. G. and Healy, K. E. (1997). The Role of Vitronectin in the Attachment and Spatial Distribution of

Bone-Derived Cells on Materials with Patterned Surface Chemistry. *J. Biomed. Mater. Res.* **37**, 81-93.

Unhjem, O. and Prydz, H. (1973). Interference of Serum and Serum Components with the Attachment of Hela 71 Cells to the Surface of Plastic Culture Vessels. *Exp. Cell Res.* **83**, 418-421.

Vargo, T. G., Thompson, P. M., Gerenser, L. J., Valentini, R. F., Aebischer, P., Hook, D. J. and Gardella, J. A., Jr. (1992). Monolayer Chemical Lithography and Characterization of Fluoropolymer Films. *Langmuir* **8**, 130-134.

Velázquez, M. G. N. (2002). Argon Plasma Treatment of Polymers. PhD. Thesis, *Department of Engineering Materials*, University of Sheffield.

Wakitani, S., Saito, T. and Caplan, A. I. (1995). Myogenic Cells Derived from Rat Bone Marrow Mesenchymal Stem Cells Exposed to 5-Azacytidine. *Muscle Nerve* **18**, 1417-1426.

Ward, R. J. and Wood, B. J. (1992). A Comparison of Experimental and Theoretically Derived Sensitivity Factors for XPS. *Surf. Interface Anal.* **18**, 679-684.

Wells, R. K., Ryan, M. E. and Badyal, J. P. S. (1993). Modeling of Non-Isothermal Glow Discharge Modification of PTFE Using Low Energy Ion Beams. *J. Phys. Chem.* **97**, 12879-12881.

Westerdahl, C. A. L., Hall, J. R., Schramm, E. C. and Levi, D. W. (1974). Gas Plasma Effects on Polymer Surfaces. *J. Colloid. Interf. Sci.* **47**, 610-620.

Wilken, R., Holländer, A. and Behnisch, J. (1998). Nitric Oxide Radical Trapping Analysis on Vacuum-Ultraviolet Treated Polymers. *Macromolecules* **31**, 7613-7617.

Wilken, R., Holländer, A. and Behnisch, J. (2002). Vacuum Ultraviolet Photolysis of Polyethylene, Polypropylene and Polystyrene. *Plasmas and Polymers* **7**, 19-39.

Wonnacott, T. H. and Wonnacott, R. J. (1990). Introductory Statistics: John Wiley & Sons, Inc.

Wood, A. (1988). Contact Guidance on Microfabricated Substrata: The Response of Teleost Fin Mesenchyme Cells to Repeating Topographical Patterns. *J. Cell Sci.* **90**, 667-681.

Yang, Y., Relan, N. K., Przywara, D. A. and Schuger, L. (1999). Embryonic Mesenchymal Cells Share the Potential for Smooth Muscle Differentiation: Myogenesis Is Controlled by the Cell's Shape. *Development* **126**, 3027-3033.

Yasuda, H., Marsh, H. C., Brandt, E. S. and Reilley, C. N. (1977). ESCA Study of Polymer Surfaces Treated by Plasma. *J. Polym. Sci., Polym. Chem. Ed.* **15**, 991-1019.

Yoo, J. G., Barthel, T. S., Nishimura, K., Solchaga, L., Caplan, A. I., Goldberg, V. and Johnstone, B. (1998). The Chondrogenic Potential of Human Bone-Marrow-Derived Mesenchymal Progenitor Cells. *J. Bone Joint Surg.* **80A**, 1745-1757.

Youxian, D., Griesser, H. J., Man, A. W.-H., Schmidt, R. and Liesegang, J. (1991). Surface Modification of Poly(tetrafluoroethylene) by Gas Plasma Treatment. *Polymer* **32**, 1126-1130.

Zhang, S., Yan, L., Altman, M., Lassle, M., Nugent, H., Frankel, F., Lauffenburger, D. A., Whitesides, G. M. and Rich, A. (1999). Biological Surface Engineering: A Simple System for Cell Pattern Formation. *Biomaterials* **20**, 1213-1220.

Appendix One

X-ray Photoelectron Spectroscopy

Principles of XPS

X-ray Photoelectron Spectroscopy (XPS) is an ultra-high vacuum technique routinely used to acquire chemical information from the top 5-10 nm of solid material surfaces. The technique relies on the photoemission of electrons from the sample surface during irradiation with X-rays.

Soft X-ray generation is by bombardment of a target anode (usually aluminium or magnesium) with high-energy electrons from a heated filament. The sample surface is then flooded with the resulting X-rays of known energy, which may be absorbed by core level electrons of atoms in the ground state. These electrons are then ejected from the core level as *photoelectrons*, which have binding energies that are characteristic of the parent element and also the chemical environment in which that element is present. This photoemission process is illustrated in Figure A1.1.

The photoelectrons are collected and analysed by their energy, E_k, which is given by:

$$E_k = h\nu - E_b - \Phi_{SP} \qquad \text{A1.1}$$

where

$h\nu$ = the X-ray photon energy,

E_b = the binding energy of the photoemitted electrons,

Φ_{SP} = an experimentally determined work function of the spectrometer, which accounts for energy losses within the instrument.

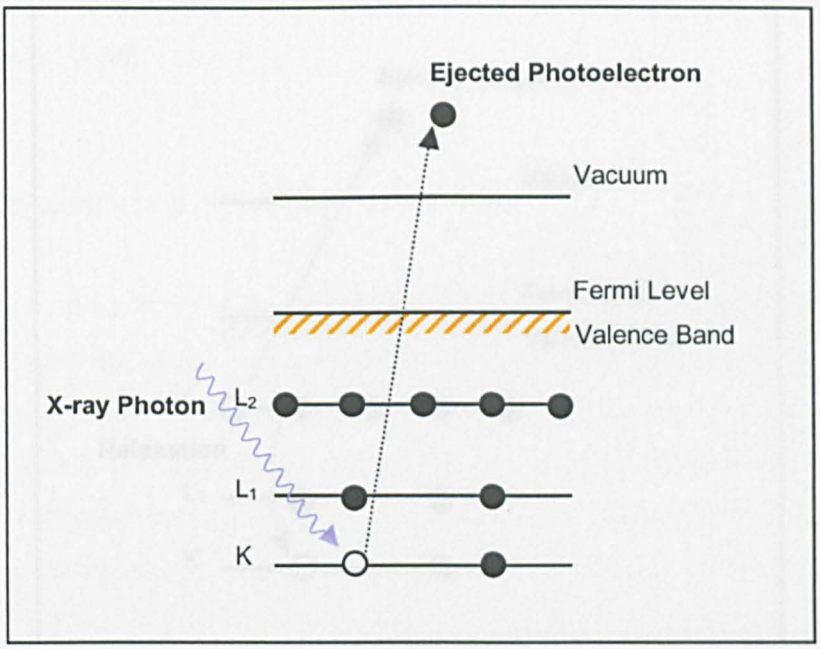

Figure A1.1: Schematic of the X-ray Photoelectron emission process (adapted from Briggs, 1998).

Using Equation A1.1, the binding energy of the photoelectrons is calculated and a spectrum of intensity (counts) against binding energy is produced. Thus a characteristic peak in intensity appears at the binding energy corresponding to each of the different core levels present in the sample surface. Only photoelectrons that have escaped without losing energy contribute to these peaks; photoelectrons that lose energy through inelastic scattering form the background of the spectrum.

Once the photoelectron has been emitted, the atom is left in an energetically unstable state due to the gap in the lowest electron shell. To fill this gap, a higher energy electron relaxes down to the lower shell. The excess energy of this electron may be transferred to a second electron from the higher shell, which is then emitted as an Auger electron (Figure A1.2). Auger Electron Spectroscopy is a surface analytical technique in it's own right, which provides elemental analysis. However, as XPS delivers both elemental information *and* chemical state analysis, Auger peaks in the XP spectrum are regarded as artefacts.

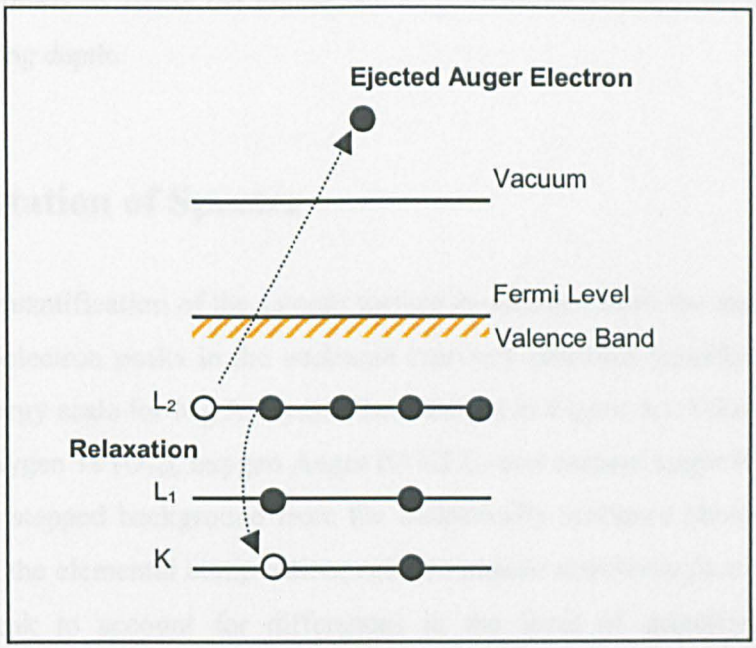

Figure A1.2: Schematic of the Auger emission process (adapted from Briggs, 1998) .

Although X-rays may penetrate many microns into the surface being analysed, only photoelectrons that can escape from the sample without undergoing inelastic collisions contribute to the characteristic peaks of the parent element. The average sampling depth, d, is related to the attenuation length of the photoelectrons within the sample material and the take off angle at which they are detected by:

$$d = 3\lambda_{AL} \sin\theta \qquad \text{A1.2}$$

where

λ_{AL} = the attenuation length of the photoelectrons,

θ = the electron take off angle relative to the surface.

Thus, changing the angle at which the electrons are detected, θ, varies the average sampling depth. For example, if C_{1s} photoelectrons in a polymeric matrix have an attenuation length of ~2.5 nm (Briggs, 1998) then varying θ from 10° to 70° changes the sampling depth from 1.3 nm to 7.0 nm. This method has been used in Section

5.4 of this thesis to assess the uniformity of plasma-induced modification over the XPS sampling depth.

Interpretation of Spectra

Elemental quantification of the sample surface is obtained from the areas of the core level photoelectron peaks in the *widescan* (survey) spectrum (usually 0 – 1100 eV binding energy scale for Mg X-rays). The example in Figure A1.3 shows the carbon 1s (C_{1s}), oxygen 1s (O_{1s}), oxygen Auger (O KLL) and carbon Auger (C KLL) peaks against the stepped background from the inelastically scattered photoelectrons. In calculating the elemental composition, *relative atomic sensitivity factors* are applied to each peak to account for differences in the level of detection of different photoelectrons. For example, the cross-section for photoemission is different for each atomic orbital and depends on the energy of the impacting X-rays; the escape depth and kinetic energy of photoelectrons depends on the material from which they originate. Usually carbon is set at the arbitrary sensitivity factor of 1, and values for other elements are determined relative to this. Theoretical tables of sensitivity factors are available although due to spectrometer variations, experimentally determined values are more accurate (Ward & Wood, 1992). Therefore empirically derived sensitivity factors, obtained from analysis of a set of polymer standards of known structure, have been used in this thesis.

The elemental composition having been established by the widescan spectrum, chemical state information can be gathered to determine what type of functional groups the component elements are present in. This is done by "zooming in" on core level peaks to perform a high-resolution scan over a much smaller range of binding energies *i.e.* a *narrowscan* spectrum. The narrowscan photoelectron peak is generally composed of a number of overlapping peaks arising from the different chemical environments in which the corresponding core level electrons are present (Figure A1.4). These peaks have slightly different binding energies due to differences in the electronegativity of different functional groups (known as the *chemical shift* effect). Taking into account the type of functional groups that are

likely to be present given the sample, the component peaks are fitted to the narrowscan spectrum using a peak-fitting program.

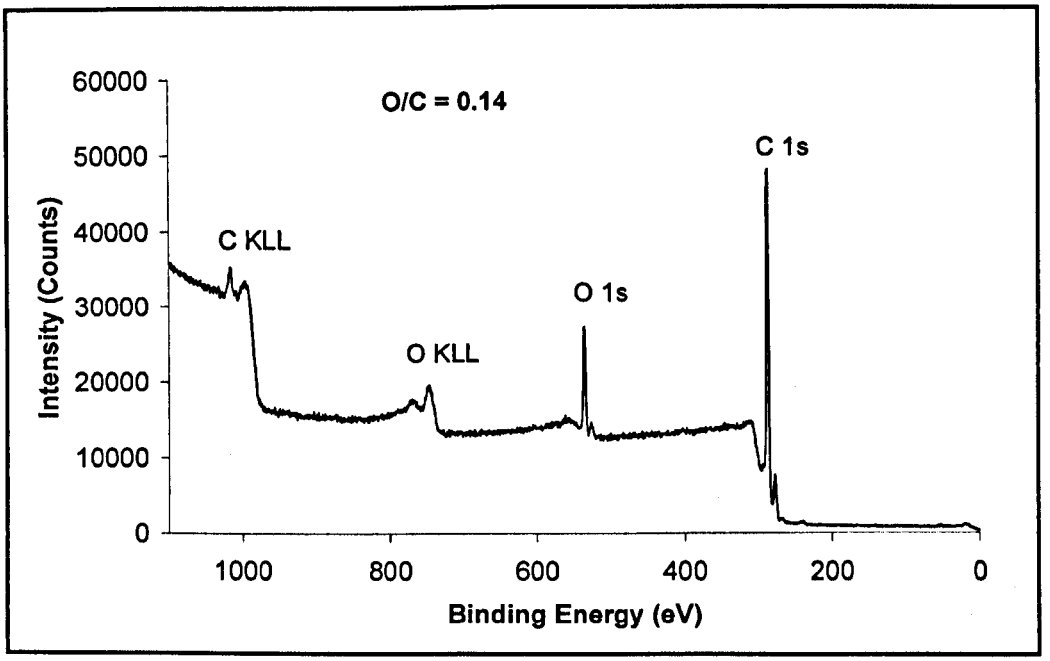

Figure A1.3: XPS widescan spectrum of plasma treated polystyrene. Sensitivity factor for oxygen (relative to carbon at 1) = 2.52.

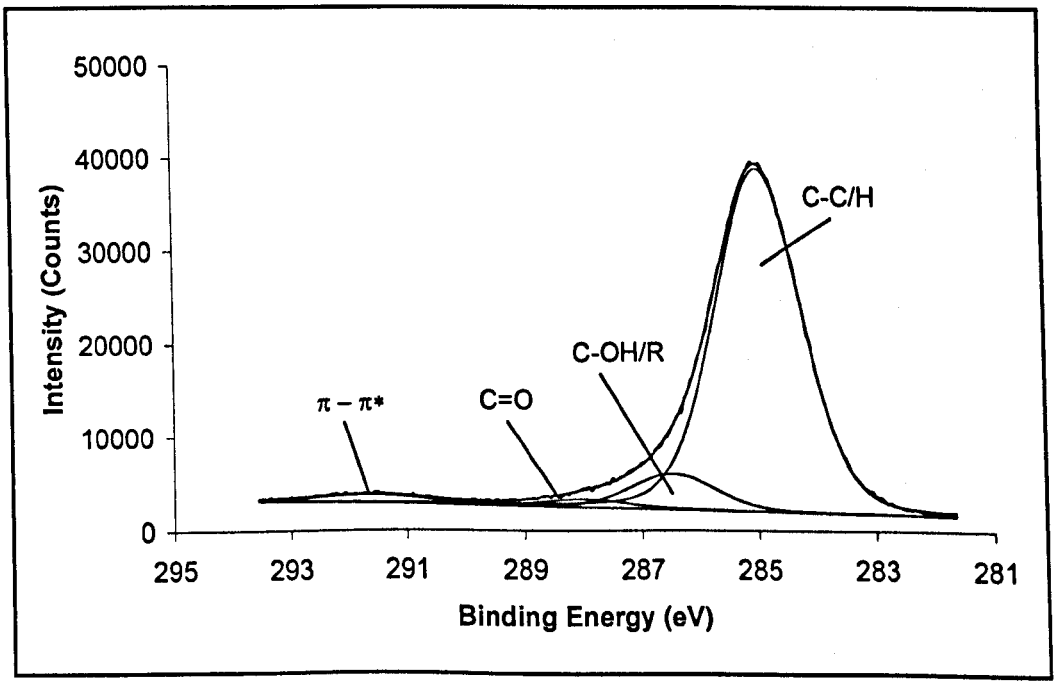

Figure A1.4: C1s narrowscan fitted with component peaks.

Appendix Two

Friction Force Microscopy

Principles of FFM

Friction Force Microscopy (FFM) is a surface analysis technique based on the principles of Atomic Force Microscopy (AFM). AFM is commonly used to generate topographical images of a surface. However, friction force data is easily gathered simultaneously and can give indications of differences in surface chemistry.

AFM instrumentation consists of a micromachined silicon/amorphous silicon nitride tip (typical radius 50 – 100 Å), attached to a flexible cantilever of the same material and an optical deflection detector system (Figure A2.1). In simple 'contact' mode, the tip is scanned across the surface in an x-y direction. A laser beam is reflected off the back surface of the cantilever and to strike a photodiode, which detects changes in the z-direction (*i.e.* topography) as small as 1 Å. The signals are processed and converted to an image. AFM can also be conducted in 'tapping' mode, where the tip is in intermittent contact with the surface to minimise disruption of the substrate caused by dragging the tip across the surface in contact mode.

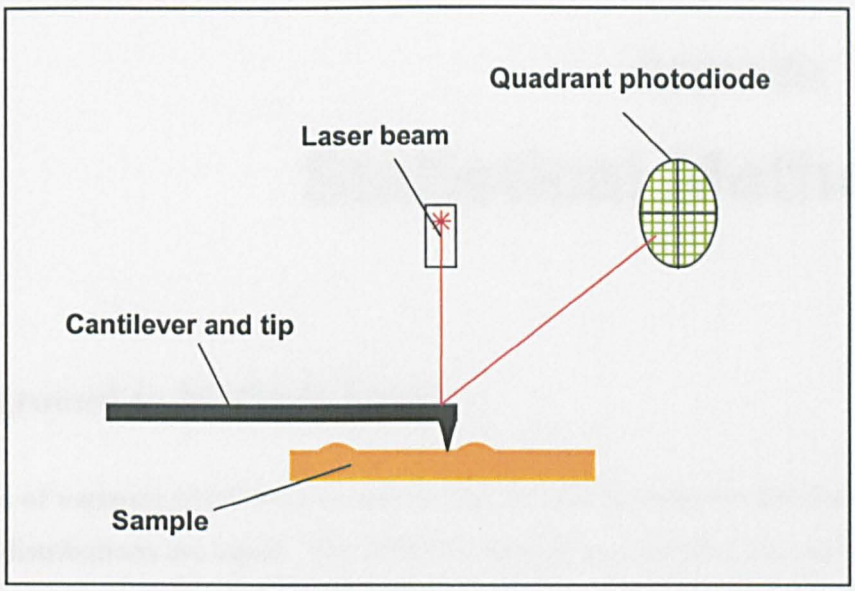

Figure A2.1: Schematic of a typical AFM system. In FFM, lateral deflection of the cantilever resulting from frictional forces is measured in addition to the deflection normal to the surface caused by topography.

In FFM, the lateral deflections of the cantilever in contact mode are measured. For flat surfaces, these lateral deflections are largely influenced by the strength of frictional forces between the tip and the surface and can be related to surface chemistry (Beake & Leggett, 2000).

Appendix Three

Statistical Methods

Background to Methods Used

Analysis of variance (ANOVA) is used to test the null hypothesis that the means of several distributions are equal. The ANOVA procedure examines the variances of a quantitative dependent variable for three or more categories of an independent variable. Thus, ANOVA is essentially an extension of the two-sample t test. ANOVA assumes that the means of the dependant variable are obtained from normally distributed continuous data, where the variance of each distribution is approximately equal. A Homogeneity of Variance test can be used to assess the equality of variances across the categories.

In addition to determining that differences exist among the means, it is often valuable to ascertain which of the means differ, and to what extent. Post hoc multiple comparisons tests are used to examine mean differences between each pair of categories of the independent variable (for more details on these procedures see Wonnacott & Wonnacott, 1990). The Games-Howell post hoc procedure is a widely used multiple comparisons test which does not assume equality of variance.

Interpretation of Results

The result of the ANOVA test is the F-statistic, which is the ratio of the mean squares of the between group variability and the within group variability. The F-statistic therefore shows whether explained variability (driven by controlled changes in the independent variable) or inherent variability ('natural' variation within groups) is the dominant factor in differences between groups. A high F-statistic shows that the between group variability is dominant and that changes produced by the

independent variable are significantly altering the dependant variable. The *p*-value (or significance value) indicates the confidence with which the difference between the independent variable categories can be expressed. A *p*-value below 0.01 indicates that there is a statistical difference between the means of the groups and that 99 % certainty can be expressed that this difference is driven by the change in independent variable. A *p*-value above 0.01 indicates that there is no statistical difference between the two means.

Some difference between the groups can be explained by the assumptions of the ANOVA test not being fully met. The Test of Homogeneity of Variances produces a Levene Statistic, which indicates whether there are equal variances between the groups. The Levene Statistic is important because large differences in within-group variability across the categories biases the F-statistic ratio determined by ANOVA. When the significance level of the Levene statistic is below 0.01, at a 99 % confidence level, the variances are deemed not to be equal across the groups and this should be taken into account when interpreting the ANOVA results. Where this is the case, the F-statistic is effectively reduced because the within-group variance is often higher. Therefore, when the ANOVA is compromised in this manner, it is less likely to identify significant differences between the groups.

Post hoc multiple comparisons examine the mean differences between each pair of categories in turn. As described above for ANOVA, the *p*-value (significance level) produced expresses the likelihood that the difference between the means could occur by chance alone.

Example

In Section 6.2, ANOVA and post hoc tests were performed to investigate differences in cell activity on three different surfaces at several time points. To illustrate the use of these techniques, the following example uses data from the 15-day cell vitality/proliferation (Alamar blue) assay carried out on cells cultured on BG PS, TCPS and VUV treated PS. The data taken to produce the summary tables in Section 6.2 are highlighted in red. The dependent variable is the measured optical absorbance and the independent variable is the type of surface, which falls into three

categories: BG, TCPS and Treated. The whole procedure was repeated for each time point (one, two, five, seven, nine, 12 and 15 days) of each of the three assays performed (vitality/proliferation, alkaline phosphatase and total collagen).

The first step is to produce a set of descriptive statistics for each data set, including the mean and standard deviation and number of samples (N) (Table A3.1). This verifies the suitability of the data for the ANOVA test.

Table A3.1: Descriptive statistics of the data set for cell vitality/proliferation at 15 days.

Descriptives

15d AB

	N	Mean	Std. Deviation	Std. Error	95% Confidence Interval for Mean		Minimum	Maximum
					Lower Bound	Upper Bound		
BG	30	.0395	.01217	.00222	.0350	.0440	.02	.07
TCPS	30	.2273	.01884	.00344	.2203	.2344	.20	.26
Treated	27	.2281	.01834	.00353	.2209	.2354	.21	.28
Total	87	.1628	.09147	.00981	.1433	.1823	.02	.28

The ANOVA test is then used to investigate differences between cell vitality/proliferation on the three different surfaces and also within the data for each individual surface. The results in Table A3.2 show a low mean square difference within groups and a high mean square difference between groups. Therefore the F-statistic is high, showing that the cell vitality/proliferation at 15 days is not the same on all three surfaces. This statement can be expressed with 99 % confidence, as indicated by the significance value being below 0.01.

Table A3.2: ANOVA results of the data set for cell vitality/proliferation at 15 days. indicates $p < 0.01$.

ANOVA

15d AB

	Sum of Squares	df	Mean Square	F	Sig.
Between Groups	.696	2	.348	1252.959*	.000
Within Groups	.023	84	.000		
Total	.720	86			

The Test of Homogeneity of Variances then checks the significance of the Levene Statistic in order to establish whether the assumption of roughly equal within-group variance that the ANOVA relies on has been satisfied. Table A3.3 shows a Levene statistic of 0.029, which is above 0.01 and is thus not significant at a 99 % level. Therefore in this example, the ANOVA F-statistic has not been compromised by large and unequal within-group variance.

Table A3.3: Test of Homogeneity of Variances results of the data set for cell vitality/proliferation at 15 days.

Test of Homogeneity of Variances

15d AB

Levene Statistic	df1	df2	Sig.
3.698	2	84	.029

Having established by the ANOVA procedure that differences in the vitality/proliferation of cells cultured on the three surfaces exist, the next step is to identify between which surfaces these differences lie. The post hoc test performs the following comparisons of vitality/proliferation: BG PS with TCPS; BG PS with Treated; TCPS with Treated. The results of these multiple comparisons are presented in Table A3.4.

Table A3.4: Games-Howell multiple comparisons results of the data set for cell vitality/proliferation at 15 days. * indicates $p < 0.01$.

Multiple Comparisons

15d AB
Games-Howell

		Mean Difference (I-J)	Std. Error	Sig.	95% Confidence Interval	
(I)	(J)				Lower Bound	Upper Bound
BG	TCPS	-.1878*	.00410	.000	-.1977	-.1779
	Treated	-.1886*	.00417	.000	-.1987	-.1785
TCPS	BG	.1878*	.00410	.000	.1779	.1977
	Treated	-.0008	.00493	.986	-.0127	.0111
Treated	BG	.1886*	.00417	.000	.1785	.1987
	TCPS	.0008	.00493	.986	-.0111	.0127

In this example, the difference between BG PS and TCPS is statistically significant at the 99 % level (indicated by $p < 0.01$), as is the difference between BG PS and the VUV treated surface (again $p < 0.01$). However, the difference between TCPS and the VUV treated surface is not statistically significant at the 99 % level ($p = 0.986$). Thus we can conclude from the post hoc test that, in terms of cell vitality/proliferation at 15 days, the performance of the experimental surface (VUV treated) is statistically better than the negative control (BG PS) and statistically no different from the positive control (TCPS).